INVESTIGATION OF SEPARATION STRATEGIES FOR BIOANALYTICAL METHODS: CHROMATOGRAPHY, ION MOBILITY AND MASS SPECTROMETRY

By

James N. Dodds

Dissertation

Submitted to the Faculty of the

Graduate School of Vanderbilt University

in partial fulfillment of the requirements

for the degree of

DOCTOR OF PHILOSOPHY

in

Chemistry

May 11, 2018

Nashville, TN

Approved:

John A. McLean, Ph.D.

David E. Cliffel, Ph.D.

Steven D. Townsend, Ph.D.

Erin C. Rericha, Ph.D.

To my friends, family, and coworkers,

who have me helped along the way and have been there always.

ACKNOWLEDGEMENTS

I would like to thank my dissertation advisor Dr. John. A. McLean first and foremost for providing me with the opportunity to join the McLean research group and pursue my passion of exploring bioanalytical applications of mass spectrometry. I have been very fortunate in this opportunity to develop my scientific skills in a setting of cutting edge analytical instrumentation and mentorship which are hallmarks of our research team. Thank you for your mentorship, expertise, and patience throughout this process.

I would like to thank my dissertation committee members, Dr. David E. Cliffel, Steven D. Townsend, and Erin C. Rericha for their time and diligence throughout this process. I have appreciated your feedback along the way at each of our meetings, and I am especially grateful for the differences in perspective that each of you have provided, as it is very easy to get stuck in our own microcosm in our respective research fields.

I would also like to acknowledge Dr. Jody C. May for timeless hours of editing and mentorship for the past five years. I know that time is precious for everyone, and that makes your sacrifice all the more meaningful. I am deeply grateful for all of your training and advice and I know I am a better scientist for it.

I also want to acknowledge my colleagues in the McLean research group for helping me with presentations, proof reading papers, and enduring countless hours of troubleshooting both professional and personal problems both inside and outside of the lab. I hope that each of you know how much you mean to me, and I only wish the best for you all as you finish your time in the lab and move on to other phases in life.

I would also like to thank my family and my friends who have provided support for me over these past five years. I know that most of the time my spent rambling on about scientific ideas might not have been the most interesting discussions, but I appreciate you listening just the same.

Lastly, I would like to acknowledge the funding sources for this research: the Vanderbilt Institute of Chemical Biology, the College of Arts and Sciences, the Vanderbilt Institute for Integrative Biosystems Research and Education, the Center for Innovative Technology, the National Institutes of Health (NIH Grant R01GM099218) and under Assistance Agreement No. 83573601 awarded by the U.S. Environmental Protection Agency. This work has not been formally reviewed by EPA. The views expressed in this document are solely those of the authors and do not necessarily reflect those of the Agency. EPA does not endorse any products or commercial services mentioned in this publication. Furthermore, the content is solely the responsibility of the authors and does not necessarily represent the official views of the funding agencies and organizations.

TABLE OF CONTENTS

Page

DEDICATION……ii

ACKNOWLEDGMENTS.....iii

LIST OF TABLES.....x

LIST OF FIGURES…… xi

LIST OF ABBREVIATIONS…….. xiii

Chapters

Introduction.....1

State of the Field and Personal Contributions.....1

1. Chiral Separation Strategies in Mass Spectrometry: Integration of Chromatography, Electrophoresis, and Gas-Phase Mobility.....4

1.1. Introduction.....4

1.2. Chromatography and Mass Spectrometry.....7

1.2.1. Liquid Chromatography.....10

1.3. Electrophoresis-Mass Spectrometry 13

1.3.1. Isomer Separations by IM-MS.....18

1.4. Conclusions.....23

1.5. Acknowledgements.....24

1.6. References.....24

2. Isomeric and Conformational Analysis of Small Drug and Drug-Like Molecules by Ion Mobility-Mass Spectrometry (IM-MS).....30

2.1. Introduction.....30

2.1.1. Isomers.....31

2.2. Instrumentation and Theory.....34

2.2.1. Drift Tube Ion Mobility.....36

2.2.2. Traveling Wave Ion Mobility.....37

2.3. Current Work in Isomer Structural Separations.....38

2.3.1. Separation of Constitutional Isomers.....38

2.3.2. Separation of Conformational Isomers.....41

2.4. Materials.....44

2.5. Methods.....46

2.5.1. Preparing the Instrument.....47

2.5.2. Data Acquisition.....48

2.5.3. Data Workup.....49

2.6. Acknowledgements.....50

2.7. References.....51

3. Assessing Ion Mobility Resolving Power Theory for Broadscale Mobility Analysis with a High Precision Uniform Field Ion Mobility-Mass Spectrometer.....56

3.1. Introduction.....56

3.2. Experimental 59
3.2.1. Uniform Field IM-MS Instrument 60
3.2.2. Analytical Precision 62
3.3. Data Acquisition and Analysis 63
3.3.1. Semi-Empirical Fitting Procedure 64
3.4. Results and Discussion 64
3.4.1. Factors affecting semi-empirical coefficients 64
3.4.2. Empirical Correlation of Theoretical Resolving Power 68
3.4.3. Broadscale Validity of Semi-Empirical Results 75
3.5. Conclusions 77
3.6. Acknowledgments 79
3.7. References 79

4. Investigation of the Complete Suite of the Leucine and Isoleucine Isomers: Towards Prediction of Ion Mobility Separation Capabilities 82

4.1. Introduction 82
4.2. Experimental Methods 84
4.2.1. Preparation of Standards 84
4.2.2. Experimental Parameters 84
4.2.3. Collision Cross Section Measurements 87
4.3. Results and Discussion 87
4.3.1. Isomer Classifications and Separations 87

4.3.2. Peak Shape Modeling and Ion Mobility 89
4.3.3. Resolving Power and Separations.....92
4.4. Conclusions.....98
4.5. Acknowledgements.....100
4.6. References.....101

5. Correlating Resolving Power, Resolution, and Collision Cross Section: Unifying Cross-Platform Assessment of Separation Efficiency in Ion Mobility Spectrometry.....106

5.1. Introduction.....106
5.2. Experimental Methods.....110
5.2.1. Chemical Standards 110
5.2.2. Instrumentation and Methods 111
5.2.3. Selection of Published Spectra.....111
5.2.4. Evaluation of Separation Efficiency 112
5.3. Results and Discussion 113
5.3.1. Gaussian Distributions.....113
5.3.2. CCS-Based Resolving Power 113
5.3.3. Cross-Platform Assessment 115
5.3.4. Traveling Wave Resolving Power 117
5.3.5. Cross-Platform Assessment of Separation Capabilities.....119
5.3.6. How Much Resolving Power is Necessary.....122
5.3.6.1. Mass Analysis 122

5.3.6.2. Ion Mobility Analysis 124
5.3.7. Ion Mobility-Mass Spectrometry 124
5.4. Conclusions 125
5.5. Acknowledgements 126
5.6. References 127

APPENDIX

A. References of Adaption for Chapters 134
B. Supplementary Materials for Chapter II 135
C. Supplementary Materials for Chapter III 138
D. Supplementary Materials for Chapter IV 151
E. Supplementary Materials for Chapter V 159

LIST OF TABLES

Table Page

3.1. Summary of Results from Semi-Empirical Fitting 65

4.1. Predicted Resolving Power for Leucine Isomer Separations 99

5.1. Various Ion Mobility Techniques and Dispersive Dimensions 107

5.2. Separation Parameters for Published Ion Mobility Separations 116

LIST OF FIGURES

Figure Page

1.1. Increasing Structural Complexity for One Molecular Formula 6

1.2. Three Point Model for Chiral Separations 8

1.3. Mechanisms of Chiral Separations 12

1.4. Instrument Schematic for Agilent 6560 16

1.5. Timescale of Analytical Separations 17

1.6. Skeletal Structure and Separation of Leucine Isomers 19

1.7. Desmopressin Structure and Chiral IM-MS Separation 21

2.1. Structures of Acetaminophen Constitutional Isomers 32

2.2. Block Diagrams of Drift Tube and Traveling Wave Instrumentation 35

2.3. Skeletal Structure and Separation of Leucine Isomers 40

2.4. Complexity of Carbohydrate Isomers 43

2.5. Drift Time Profiles for Thalidomide Chiral Isomers 45

3.1. Instrument Schematic for Agilent 6560 61

3.2. Resolving Power Curves as a Function of Gate Width 69

3.3. 3D Resolving Power Curves for Experimental and Theoretical Models 72

3.4. Resolving Power as a Function of Reduced Mobility 74

3.5. Resolving Power Curves as a function of Drift Gas Composition 76

4.1. Isomer Classification Hierarchy 86

4.2. Skeletal Structure and Separation of Leucine Isomers 88

4.3. Theoretical Resolution as a Function of Resolving Power and Concentration 91

4.4. Plot of Increasing Separation as a Function of Resolving Power 95

4.5. Experimental and Theoretical Separations of Leucine Isomers 97

5.1. Selected Ion Mobility Separations from Literature Publications 114

5.2. Ion Mobility Separations as a Function of Resolving Power and CCS 120

5.3. Biological Separation of Peptides from Ion Mobility and Mass Spectrometry 123

LIST OF ABBREVIATIONS

CCS	Collision Cross Section
µs	Microsecond
3D	Three-Dimensional
ACN	Acetonitrile
MeOH	Methanol
MS	Mass Spectrometry
ms	Millisecond
MS/MS	Tandem Mass Spectrometry
IM	Ion Mobility
eV	Electron Volt
GC	Gas Chromatography
LC	Liquid Chromatography
HILIC	Hydrophilic Interaction Liquid Chromatography
CE	Capillary Electrophoresis
TLC	Thin Layer Chromatography
CID	Collision Induced Disassociation
ETD	Electron Transfer Disassociation

DT	Drift Time
FWHM	Full Width at Half Maximum Height
R_p	Resolving Power
R_{p-p}	Two-Peak Resolution
ΔCCS%	Percent Difference in Cross Section
ESI	Electrospray Ionization
MALDI	Matrix-Assisted Laser Desorption Ionization
IM-MS	Ion Mobility-Mass Spectrometry
m/z	Mass-To-Charge Ratio
ppb	Parts Per Billion
ppm	Parts Per Million
TOF	Time of Flight Mass Spectrometer
QTOF	Quadrupole-Time of Flight
TWIMS	Traveling Wave Ion Mobility Spectrometry
DTIMS	Drift Tube Ion Mobility Spectrometry
UPLC	Ultra-Performance Liquid Chromatography
SFC	Supercritical Fluid Chromatography

INTRODUCTION

STATE OF THE FIELD AND PERSONAL CONTRIBUTIONS

The field of mass spectrometry has been developing rapidly after its initial debut in the second half of the previous century.[1] The separation capacity of instrumentation in MS has increased by orders of magnitude in comparison to initial devices developed in the previous century, and new platforms are being developed each year. While mass spectrometry is still enjoying steady growth in the analytical community, several intrinsic challenges remain in the analysis of complex samples. Specifically, the analysis and characterization of isomeric species in complex biological matrices remains a distinct issue of paramount importance for downstream metabolic pathway analysis. To address the challenge these isomeric species present, many orthogonal separation techniques have been developed to separate isomeric compounds prior to mass analysis. These techniques include, but are not limited to, gas and liquid chromatography, capillary electrophoresis, and ion mobility spectrometry.

As ion mobility spectrometry is a gas phase separation which takes place in the millisecond timescale, this technique is rapidly growing in popularity in the analytical community, specifically studies related to mass spectrometry.[2] Currently, two of the most popular instrument platforms in IM-MS are time-dispersive methods, namely drift tube and traveling wave ion mobility spectrometers, which are currently marketed by Agilent Technologies and Waters Corporation, respectively. While these two instrument vendors have been very successful in terms of marketing their new platforms, new instruments are being commercialized each year. As a result of the rapidly expanding market for ion mobility technology, other instrument manufacturers are developing additional strategies to improve the separation capacity of ion mobility spectrometry,

including high pressure separations and ion trapping devices (Tofwerks and Bruker, respectively).[3] The more recent additions to the ion mobility field achieve an increased capacity for separation by extending the effective path length in which the gas phase analytes are able to interact with the drift gas, which operates as a pseudo stationary phase in these devices. In this manner, the emerging ion mobility platforms can be seen in analogous fashion to advances in liquid chromatography with smaller particle diameter or increased column length. My initial ion mobility studies illustrated exciting separation potential for constitutional isomers related to amino acids (see Chapter 4), while stereoisomers proved to be more challenging to separate using ion mobility. While these results were somewhat expected in that existing chromatography methods illustrate similar characteristics, these studies did show that ion mobility could provide a comparable level of separation efficiency in comparison to condensed phase methods with orders of magnitude less analysis time. More massive chiral compounds did illustrate some propensity for separation based on macromolecular rearrangement, which is imperative in the production of pharmaceuticals. These studies are covered in detail in Chapters 1 and 2, and to our knowledge represent one of the few ion mobility studies which provides chiral recognition (separation of diastereomers) in an achiral drift gas environment.

With so many new devices launched on the market in the past decade, establishing a common metric to gauge each platform is imperative in the field to avoid ambiguity with regard to instrument performance. Using this lens as an objective, my graduate studies have largely been devoted towards characterizing the fundamental separation performance of both ion mobility spectrometers in my laboratory as well as those devices just emerging on the market. While an expanded account of these studies are provided in Chapters 4 and 5 of this work, briefly an ensemble of literature was collected throughout the ion mobility field and the instrument

performance of each platform was characterized in terms of efficiency of instrumentation (resolving power, R_p) and difficulty of separation (percent difference in CCS, or %CCSΔ). Using the metrics established throughout my graduate studies, the works compiled in this dissertation were able to definitively demonstrate that the new devices operate with a level of separation efficiency increased by almost an order of magnitude over the previous generation of instruments, even those released only a decade ago. Using these emerging platforms allows researchers to characterize complex mixtures of isomeric species previously inseparable by the previous generation of instruments, which provides an additional level of selectivity for identification of unknown compounds. These advances will push the ion mobility field to the forefront of the mass spectrometry community, increasing the peak capacity of existing workflows and generating further confidence in establishing collision cross section libraries for untargeted analysis.

References

1. Griffiths, J. A brief history of mass spectrometry. *Anal. Chem.* **2008**, *80*, 5678-5683.
2. May, J. C., and McLean, J. A. *Anal. Chem.* **2015**, *8*, 1422-1436.
3. Dodds, J. N.; May, J. C.; and McLean, J. A. *Anal. Chem.* **2017**, *89*, 12176-12184.

CHAPTER 1

CHIRAL SEPARATION STRATEGIES IN MASS SPECTROMETRY: INTEGRATION OF CHROMATOGRAPHY, ELECTROPHORESIS, AND GAS-PHASE MOBILITY

1.1. Introduction

As chiral molecules by definition are characterized by rotation of plane polarized light, it may initially seem odd that many analytical studies have utilized mass spectrometry (MS), a non-spectroscopic technique, to analyze chiral systems. As the biological function of compounds is derived from molecular structure, many mass spectrometry studies specifically focus on what structural forms of the analyte contribute to an observed phenotype.[1] Modern mass spectrometers are highly selective, often able to identify small molecule analytes (< 200 Da) based solely on accurate mass measurement to a level of better than 2 ppm in mass error (0.0002%) and approach unambiguous molecular formula determination at 100 ppb.[2] However, mass spectrometry is intrinsically a "chiral blind" experiment, wherein the mass measurement has no inherent differentiation towards the chirality of the molecule detected. For these reasons chiral recognition by MS is typically obtained by condensed phase-separation techniques which we focus on in this chapter.

Mass spectrometers separate and detect analyte ions by means of their mass-to-charge ratio, which can be subsequently deconvoluted to the corresponding neutral analyte mass. For identification of unknowns, the molecular mass is typically screened against a compound database (*e.g.* PubChem, Metlin, etc.) in order to determine the most probable molecular formula of the analyte.[3] However, as the molecular mass increases, so does the potential structural complexity of the system and the likelihood of detecting multiple isomeric species possessing a shared molecular

formula.[4] For example, as shown in Figure 1.1, as molecular mass increases from 150-400 Da the number of corresponding entries catalogued in the PubChem database for each molecular formula increases dramatically.

As the number of potential isomers increases for a single molecular formula, separation and identification of unique structures becomes increasingly challenging. The implementation of various fragmentation techniques (*e.g.* CID, ETD) in tandem MS/MS methods has been very successful in providing an approach toward differentiating constitutional isomers (compounds with differing molecular scaffolds) either by variations in observed fragment ion masses or bond disassociation energies.[5,6] However, more structurally similar stereoisomers (chiral isomers) predominantly fragment with similar fragmentation patterns, and hence are difficult to differentiate through tandem MS/MS approaches. In order to overcome the challenge of differentiating isomers by MS, other analytical techniques are commonly utilized prior to mass analysis. These methods include capillary electrophoresis (CE),[7] gas chromatography (GC),[8] liquid chromatography (LC),[9] supercritical fluid chromatography (SFC),[10] electrochemical sensing[11] and more recently ion mobility (IM).[12] As liquid chromatography is the most frequently used method of chromatographic separation, we will initially focus on typical LC strategies and mechanics and then devote the remaining chapter on the emerging role of ion mobility in isomer separations.

Regardless of the chosen analytical approach to chiral selectivity, it is thought that the general mechanics of chiral separations are related on a molecular level to the so called "three-point model" known as Pirkle's Rule (see Figure 1.2 A).[13,14] In order to distinguish chiral molecules in a chromatographic system, both isomers must interact with the chiral selector in such a manner that one analyte interacts more strongly with the chiral selector than the other and hence is more retained. Theory advocating for the three-point model suggests that at the heart of chiral

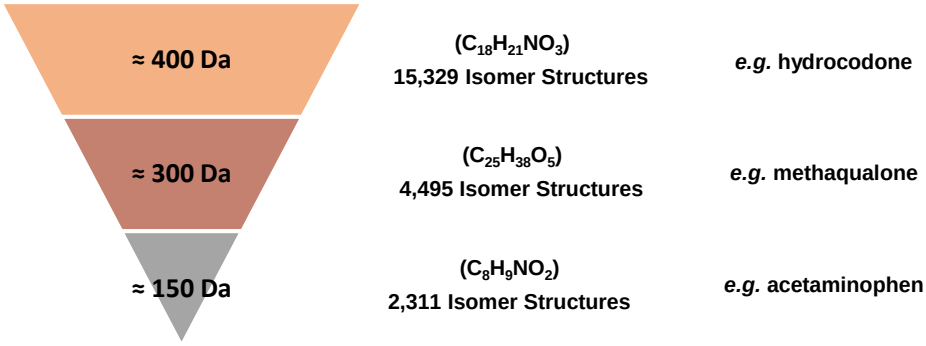

Figure 1.1. Illustration of increasing structural isomer complexity within a given molecular formula which scales as a function of the molecular mass. Example formulae corresponding to a given mass is provided for relative example.

recognition is a three-point interaction between the substituents in a chiral molecule in the analyte and the structure of chiral selector (*e.g.* stationary phase) which preferentially retains one stereochemistry of the analyte (Analyte 1, Figure 1.2 A). This preferred mechanism of retention is based on the stereochemistry at the chiral center and of the subsequent neighboring atoms which interact stronger with the chiral selector in one enantiomer form compared to the other (for example by hydrogen bonding), leading to enantioselectivity in chiral separations. This selective binding requires multiple interactions, thus chiral separations have been most successfully implemented in the condensed phase, where the collision frequency is high, such as in LC or SFC separations.

1.2. Chromatography and Mass Spectrometry

Although the specific origins of chromatography are still debated, several literature sources attribute the foundation of chromatography to Russian scientist Mikhail Tsvet[15-17] who published his first work detailing the separation of chlorophyll pigments in green plants in the early 1900s.[18] Tsvet's observations relating analyte adsorption (with what is now called the stationary phase) to the importance of solvent composition (later termed the mobile phase) established the framework for our current understanding of chromatographic techniques. Later work from Martin and Synge further developed the study of partition chromatography, and for their efforts they were jointly awarded the Nobel Prize in 1952.[19] Chromatography methods continued to increase in popularity and with the introduction of analytical mass spectrometry the two techniques were combined in the 1950s to provide orthogonal separation methods based on polarity discrimination and mass analysis.[20] In the separation of complex analytical mixtures, typically the chromatographic separation is performed prior to mass analysis, which serves as the detector. In this way, the

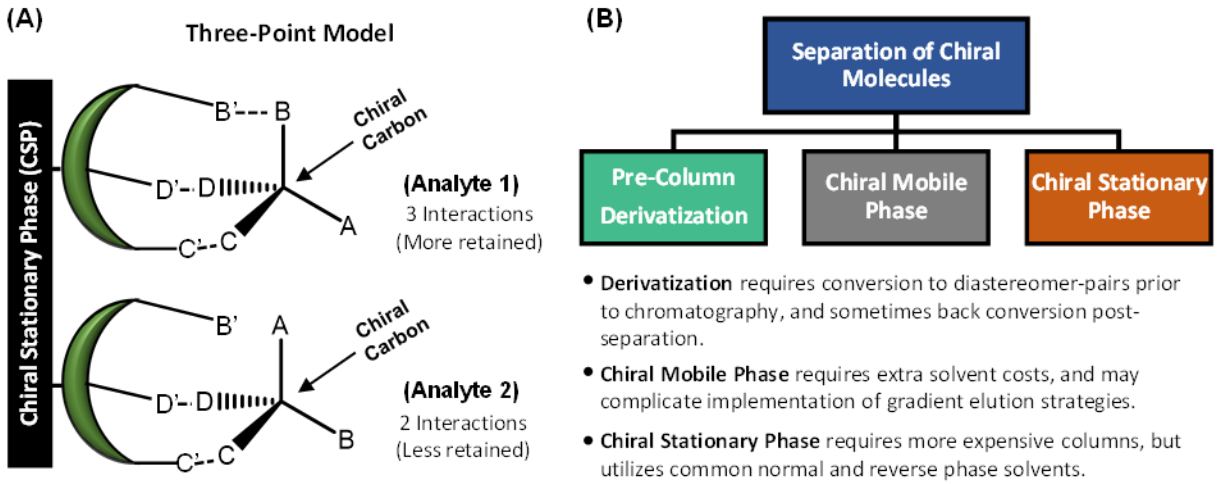

Figure 1.2. (A) Depiction of the classic three-point model used to describe stereoselection with the stationary phase in condensed phase chromatography. **(B)** Description of the three main approaches towards chiral separations in chromatography.

chromatographic separation functions to deconvolute the resulting mass spectra and enhance sensitivity by reducing ion suppression effects. As modern mass spectrometers are highly selective, an intrinsic molecular formula can often be determined based solely on high resolution mass analysis.[21] However, as a single molecular formula can be shared by many isomeric species, a key capability of chromatographic separations is to differentiate isomers through differences in physio-chemical affinities. Because constitutional isomers have distinct skeletal structures, and hence differing regions of localized polarity, many constitutional isomers may be differentiated by various chromatography approaches.[22] While efforts to combine chromatography and mass spectrometry have improved the separation efficiency for many isomeric systems, we primarily focus on the separation of chiral molecules, as they are currently the most difficult class of isomers to differentiate.

Historically, there are three general methodologies to distinguish chiral molecules via chromatographic techniques and these approaches are outlined in Figure 1.2 B. Pre-column derivatization of enantiomers prior to chromatographic analysis (utilizing both an achiral stationary and mobile phase) is popular in GC and LC. Briefly, prior to analysis both enantiomers are chemically modified to produce diastereomer pairs which are subsequently separated based on physical or chemical differences in an achiral environment. This technique has an advantage compared to other methods due to simplicity in stationary and mobile phase composition which can be readily adopted from previous achiral methods. However, as this particular method requires additional sample preparation steps before (and sometimes after) analysis, this technique is generally less favored than direct analysis methods. These strategies are described in numerous articles which provide an in-depth background on derivatization for chiral separations.[23-25]

An alternative approach to stereoisomer separations in chromatography utilizes chiral mobile phase additives to differentiate chiral molecules in a complex mixture. For example, in 1980 Gil-Av and Hare were able to separate L- and D- amino acids by LC on a conventional C18 column using a chiral mobile phase comprised of a low concentration solution of L-proline and copper acetate.[26] Because the mobile phase must be chiral to facilitate the separation of analytes in this method, traditional mobile phase compositions and gradient methods are difficult to implement. For these reasons, this method has decreased in popularity over time despite not requiring analyte derivatization and being successfully applied to chiral selectivity in several applications.[27,28]

For the remainder of our discussion on chromatography we will focus on the third approach to chiral separations, which utilizes chiral stationary phases (CSPs) combined with traditional mobile phase compositions (*e.g.* H2O, ACN, MeOH) to achieve chiral selectivity. An early example of this technique is the 1960's study by Gil-Av and coworkers exploring potential methods to separate enantiomer amino acid derivatives in GC.[29] As chiral stationary phases allow for direct analysis of enantiomer pairs in a complex mixture with no additional derivatization steps or complex mobile phase additives, this technique quickly gained favor due to experimental simplicity and is currently the preferred method in modern LC-MS applications with several reviews covering this topic in depth.[13,30]

1.2.1. Liquid Chromatography

With the advent of electrospray ionization (ESI)[31,32] liquid chromatography is now the preferred method of separation prior to mass analysis. While chiral mobile phases have illustrated

some propensity for LC separations, we will focus here on the current trend of utilizing chiral stationary phases to introduce stereochemical selectivity to a conventional LC setup. Briefly, several mechanisms of chiral selectivity are proposed for chiral LC separations, including dipole-dipole interactions, π-π staking, hydrogen bonding, inclusion complexation, and steric hindrance (see Figure 1.3 A).[33] Many modern CSPs utilize a combination of these strategies to enhance chiral recognition and selectivity. For example, many macrocyclic selectors such as cyclodextrin based CSPs possess pockets of hydrogen bonding in addition to larger areas of inclusion complexation which preferentially select one enantiomer over the other. While uncovering the intricacies of the partitioning interaction in chiral LC is important from a fundamental standpoint, for an in-depth explanation of the chemistry behind CSP selectivity the reader is directed to several comprehensive literature reviews which have been dedicated to this topic.[30,34]

Broadly speaking, while each specific column can incorporate various methods of enantiorecognition (Figure 1.3 A), there are three main classes of chiral columns (see Figure 1.3 B) utilized in research and industry.

Although many of these stationary phases provide selectivity, they often target a narrow scope of isomeric species for chiral recognition. For instance, the Pirkle-type CSP developed by William H. Pirkle's lab at Illinois (currently marketed as Whelk-O1 CSP by Regis Technologies) was initially developed to target the separation of *S*- and *R*- naproxen.[35] Naproxen is a commercially available non-steroidal anti-inflammatory drug (NSAID) that alleviates pain and soreness in the *S* chirality (the eutomer form), yet the distomer form (*R*-naproxen) exhibits no analgesic effect and has been implicated in liver toxicity. Although a controlled chiral synthesis of naproxen was patented in 1988,[36] given the acute toxicity of R-naproxen it is important to test for and quantify its presence. The Whelk-O1 CSP has been shown to provide baseline resolution of

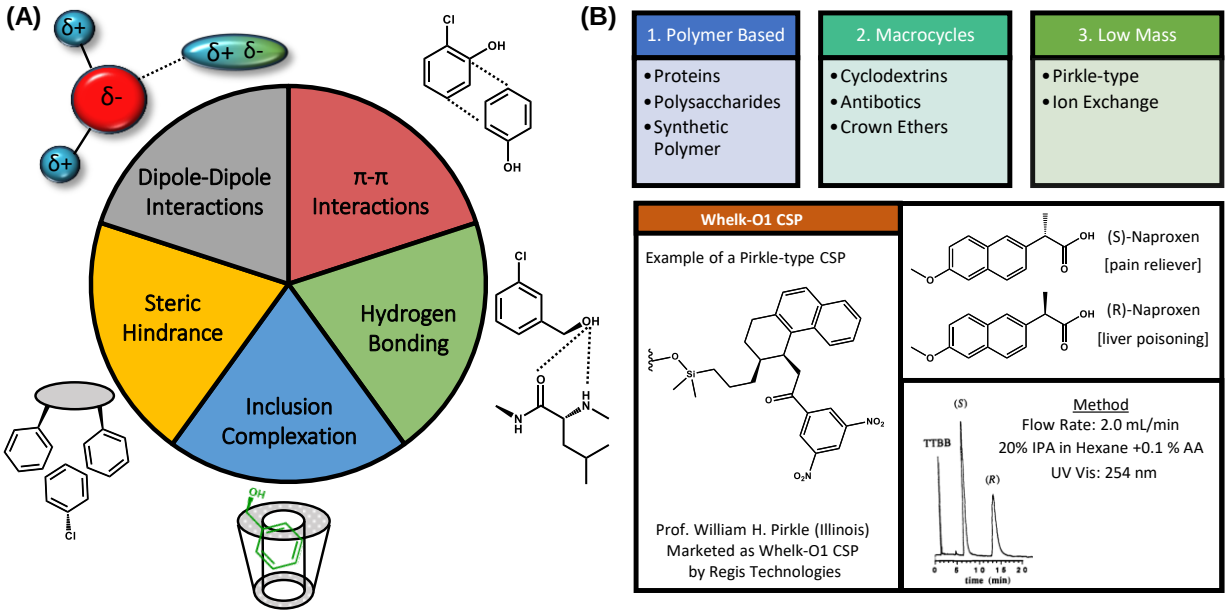

Figure 1.3. (A) Diagram illustrating several mechanisms for intermolecular interactions that facilitate chiral separation. **(B)** Description of the three main types of chiral stationary phases commercially available with corresponding description of the CSP. Included in the lower panel is a description of a commonly used Pirkle type CSP with reported separation obtained for enantiomers of Naproxen. Reprinted (adapted) with permission from Pirkle *et. al.* Copyright (1992) American Chemical Society.

the two enantiomers.[33] When enantioselectivity is achieved it can be described by determining the enantiomeric excess of the desired product (see Figure 1.3 B).

$$\% \text{ Enantiomeric Excess} = \frac{\text{Area}_A - \text{Area}_B}{\text{Area}_A + \text{Area}_B} \text{ x } 100 \quad (1)$$

While these types of separations are highly advantageous in pharmaceutical industries that focus on synthesizing a few target molecules in large quantities, their high degree of analytical selectivity may not be particularly beneficial when deployed in broadscale untargeted analysis. As mentioned previously, while many CSPs available in LC are highly selective, they typically require more diligent care and maintenance and are only compatible with a narrow range of mobile phase compositions. Also CSP columns are typically very expensive ($1,000 USD or more from 2017 estimates), which can be a barrier for adoption by modest research institutions or small companies developing interest towards chiral separations. Finally, many enantiomer separations require very specific mobile phase compositions, gradients and flow rates to obtain separation, which severely limits wide range applicability.

1.3. Electrophoresis-Mass Spectrometry

Ion mobility spectrometry (IMS) is an isomer selective gas-phase electrophoretic technique which is complementary to traditional chromatographic approaches. While GC and LC separate molecules based on differences in volatility or polarity, ion mobility is selective to differences in size, shape and charge in the gas-phase. Essentially, under an applied electric field (E_o) the gas-phase ion formed by the ionization process (*e.g.* APCI, MALDI, or ESI) migrates through an inert buffer gas (termed the drift gas) towards the detector, which is commonly a mass spectrometer in

modern research applications (see Figure 1.4). As an analogy, the drift gas is similar to the stationary phase in traditional chromatography, although strictly speaking IMS is not a chromatographic technique as the drift gas is not stationary and ions do not partition within it. The time required for an ion to traverse the drift region (termed drift time, t_d, equation 2) is proportional to the ion's mobility in the gas phase (K).

$$t_d = \frac{L}{KE_o} \tag{2}$$

Here, L is the length of the drift region. The drift time measured in IMS is similar to retention time in chromatography applications, and K is analogous to the normalized retention factor. It is common practice to convert raw ion mobility drift times to a collision cross section (CCS), which is both a fundamental ion property and a standardized value useful for cross-systems comparisons.[37,38] After accounting for relevant laboratory conditions and other experimental parameters (*e.g.* temperature, pressure and drift gas composition) the ion's collision cross section can be calculated using the fundamental low field ion mobility equation, which is commonly referred to as the Mason-Schamp relationship (equation 3), where *V* is the voltage applied in the drift tube (of length L), e_c is the elementary charge constant, N_o is the gas number density and mgas and mion are the masses of the drift gas and analyte, respectively.[39,40] An ion's CCS is a measure of its rotationally averaged surface area in the gas phase and is a descriptor of molecular size, typically reported in square angstroms ($Å^2$).

$$CCS = \frac{3 \cdot Ze_c}{16N_o} \cdot \left(\frac{2\pi}{k_b T}\right)^{\frac{1}{2}} \cdot \left(\frac{m_{ion}+m_{gas}}{m_{ion} \cdot m_{gas}}\right)^{\frac{1}{2}} \cdot \left(\frac{V \cdot t_d}{L^2} \cdot \frac{273.15}{T} \cdot \frac{P}{760}\right) \tag{3}$$

The classic instrument platform used to measure ion mobility (and hence collision cross section) is the drift tube ion mobility spectrometer (DTIMS), which utilizes a low magnitude and uniform electric field to conduct ion mobility separations (see Figure 1.4). Ions with sufficiently different gas phase electrophoretic mobilities (or CCS) are then separated in drift time space, and subsequent mass analysis determines the molecular formula and ion intensity. In this manner IM separations are complementary to mass analysis, and provide unique information in the form of size-mass relationships.[41] These two techniques are commonly interfaced to separate (IM) and detect (MS) isomer species in complex samples similar to LC-MS. Considering a hypothetical example in Figure 1.4 of folded forms of secondary peptide structure the more compact α-helix structure may have a reduced cross sectional area in the gas phase compared to the more open β-sheet form and hence these two theoretical conformers could be separated by ion mobility. If both molecules share the same molecular formula, the mass spectrometer alone could not differentiate between the two folded forms based solely on mass. Although there are many other instrumental designs for which IM separations have been investigated (*e.g.* Traveling Wave IM, High-Field Asymmetric Waveform IM, Differential Mobility Spectrometry) all IM techniques are selective to molecular size and shape. There are many literature reviews available which discuss the subtle differences in each technique.[42-44]

The inherent properties of IM offer several distinct advantages that have recently generated interest in the field both in lieu of and combined with chromatography. First, IM separations occur on the millisecond timescale, and hence readily interface with detection from mass spectrometry which operates on a micro to milli second timescale (see Figure 1.5). GC and LC separations occur on a timescale of minutes and in some cases can exceed one hour, which results in limited sample throughput in comparison to IM-MS analysis. Also, because the equivalent stationary phase in ion

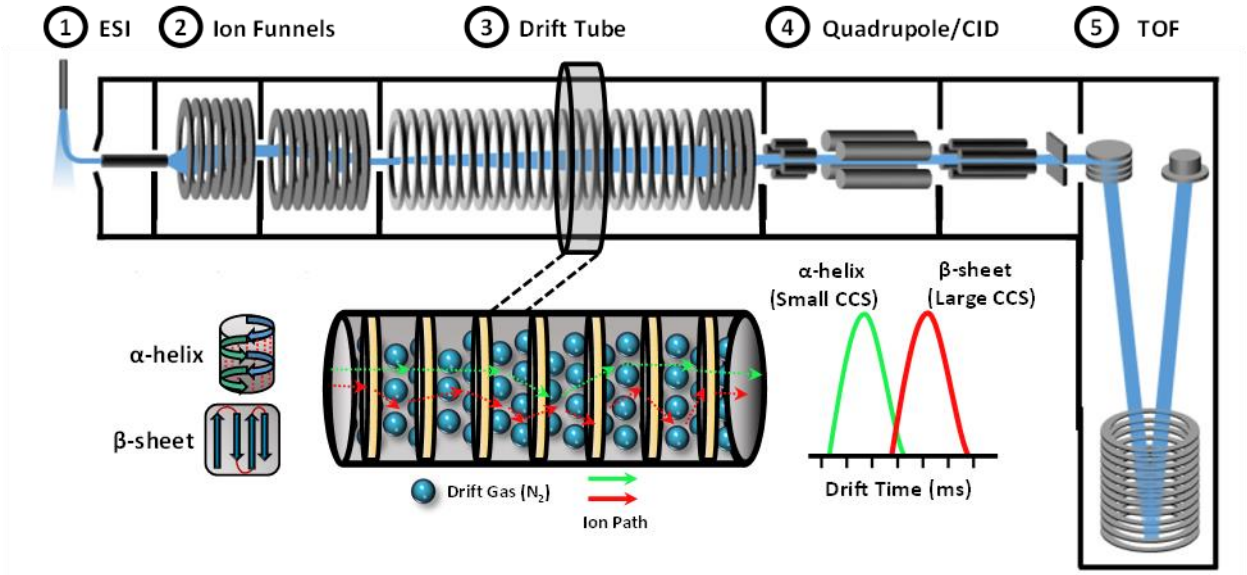

Figure 1.4. Instrument schematic of the Agilent 6560 uniform field ion mobility-mass spectrometer. Adapted from May *et. al.* 2015, Ref. 41 with permission from the Royal Society of Chemistry.

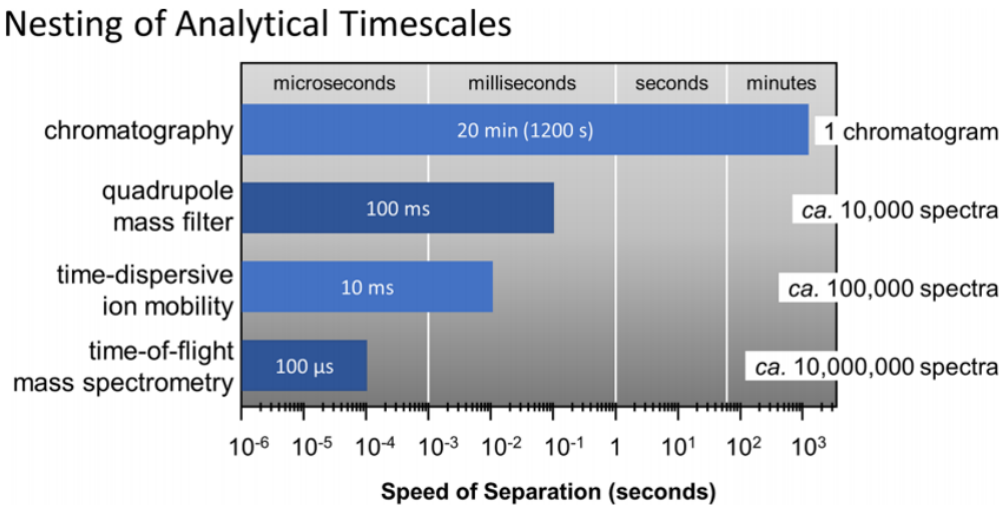

Figure 1.5. Timescale of analytical separations in an online LC-IM-QTOF experiment with corresponding number of spectra. Adapted with permission from May *et. al.*, Ref. 42. Copyright 2017 American Chemical Society.

mobility is the buffer gas (typically pure helium or nitrogen), there are no "column choices" or solvent elution profiles to optimize aside from drift gas composition. While this characteristic limits the amount of experimental variables which can be altered to enhance selectivity, analytical reproducibility is high and there exist no memory effects. In effect, once the experimental parameters of drift tube voltage and pressure are optimized, these variables are then held constant independent of sample composition, which simplifies experimental design and facilitates inter-laboratory comparisons. The remainder of this chapter will focus on exploring some recent isomer separations by this technique.

1.3.1. Isomer Separations by IM-MS

Traditional mass spectrometry analysis is isomerically blind, so a key application of IM separation prior to mass selection is focused on differentiating isomeric species, including some stereoisomers, although currently the application space for IM-MS separation of chiral isomers is limited. IM-MS separations have targeted isomers of many chemical systems including carbohydrates,[45] lipids,[46,47] peptides,[48] and organometallic complexes.[49] For example, recent work in our lab surveyed the intricacies of IM separation for amino acids related to the classically studied system of leucine and isoleucine (see Figure 1.6).[50] An analysis of 11 leucine/isoleucine isomers (molecular formula $C_6H_{13}NO_2$) illustrated that for small molecule systems (< 200 Da), constitutional isomers typically possessed larger differences in CCS in comparison to stereoisomers (diastereomer and enantiomers). Diastereomers did show distinct differences in CCS (although they were unresolvable in a multi-component mixture with the current instrumentation, see Figure 1.6 B-III). These findings are in agreement with other studies noting

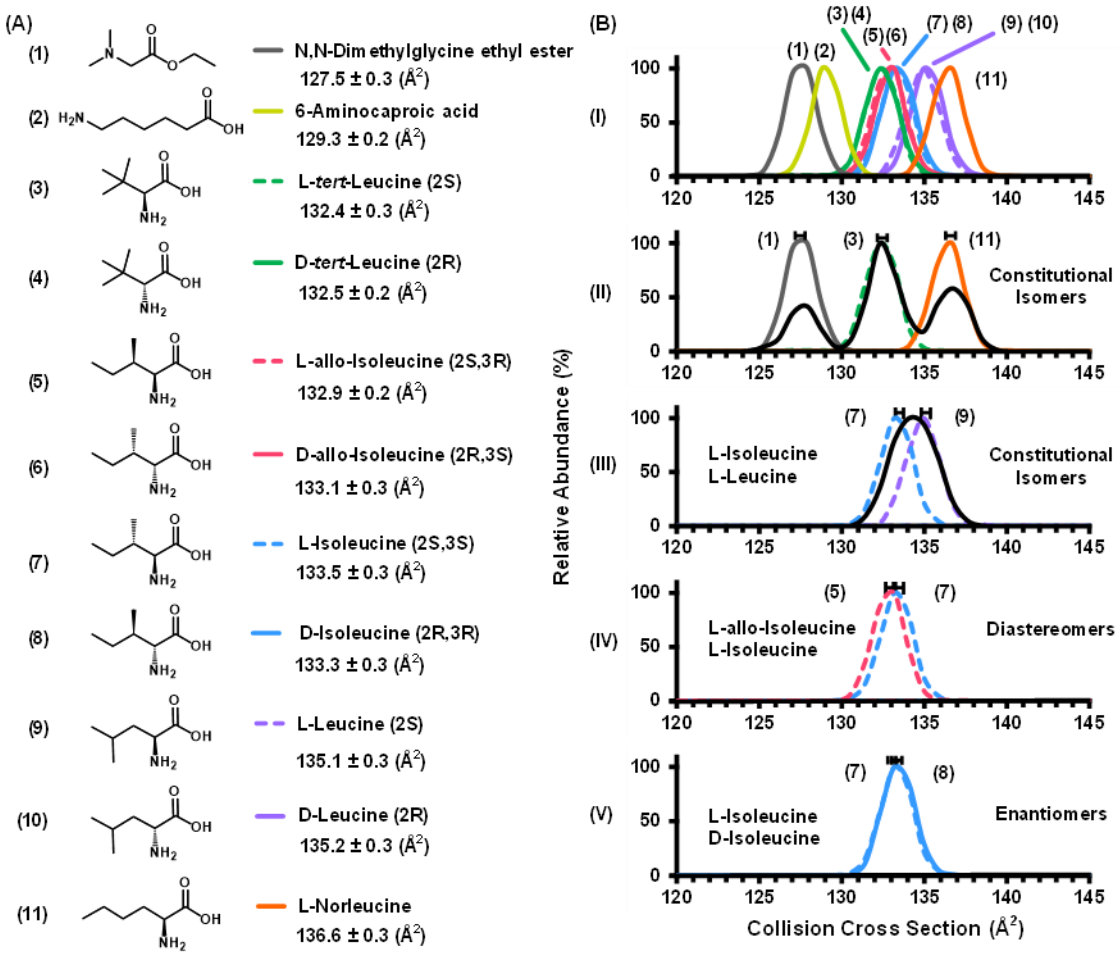

Figure 1.6. (A) Skeletal structures for 11 isomers related to leucine and isoleucine are shown with modifications of both bond coordination and stereochemistry. Also noted are the measured collision cross sections and corresponding standard deviations. **(B) (I)** Ion mobility arrival time distributions for all corresponding isomers are illustrated by analyzing individual standards. **(II** and **III)** Separations for constitutional isomers examined in this work, along with the corresponding mixtures (black traces). Stereoisomers **(IV** and **V)** have more structural similarities in cross section space, and hence are more challenging to separate. Adapted with permission from Dodds *et. al.*, Ref. 50, Copyright 2017 American Chemical Society.

that diastereomers have intrinsic differences in chemical and physical properties, which forms the basis of separation with other techniques (*e.g.* chiral chromatography). In comparison, the enantiomers investigated in this study possessed cross sectional differences within experimental error, suggesting they may not be resolvable by conventional uniform field IM. While these results were intuitive, they demonstrated that IM approaches exhibit similar tendencies towards separation of compounds comparable to the selectivity observed in traditional chromatography techniques, that is, constitutional isomers are more readily separated in contrast to stereoisomers.

Other studies by Hofmann and coworkers have examined IM separations of various isomeric carbohydrates utilizing traveling wave IM.[45] Their investigation of carbohydrate isomers demonstrated that constitutional rearrangements in monomer connectivity (1→3 vs. 1→4 linkages) and stereochemical variations in α/β bonds were more influential in IM separations in comparison to alterations in axial/equatorial functional groups. Likely the differences in α/β connectivity in covalent linkages alter the gas phase packing efficiency of the ion on a macromolecular level and hence induce larger structural changes in cross sectional area compared to axial/equatorial substitutions.

While these studies suggest that small chiral molecules are not separable by current IM instrumentation, larger peptides and proteins with L/D amino acid substitutions have been shown to produce cross sectional differences within the current level of detection). Also, preliminary results for larger chiral systems (nonapeptides, *ca.* 1100 Da) obtained in the author's laboratory yielded similar capacity for separating L/D amino acid substitutions by IM-MS. Desmopressin, a nine amino acid system (see Figure 1.7 A) yielded experimentally distinct cross sections for each

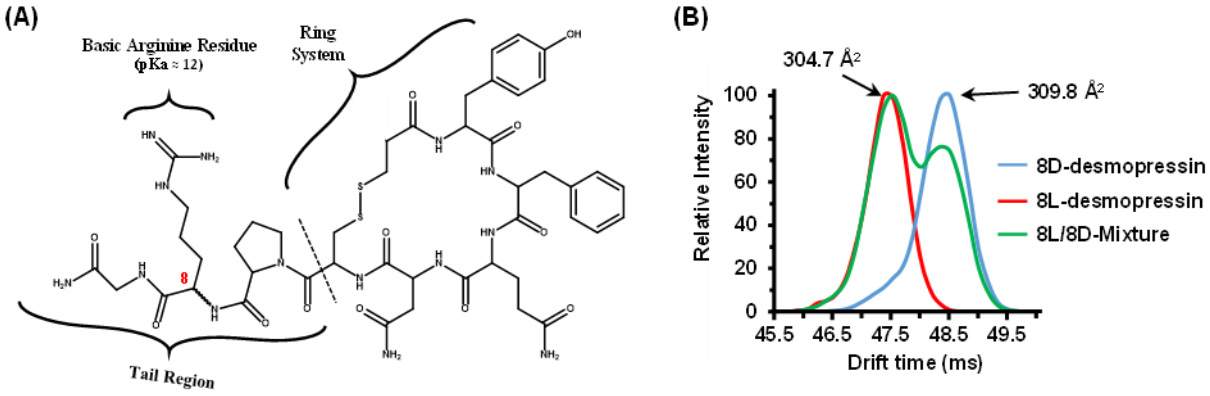

Figure 1.7. (A) The skeletal structure of desmopressin is illustrated along with specific regions for the ring and tail regions. **(B)** Experimental separation of desmopressin diastereomers with corresponding collision cross sections.

diastereomer studied, both of which are structurally identical except for differences in chirality at Arg 8. These desmopressin diastereomers possessed significantly different CCS values as to be nearly half-height resolved. The current hypothesis for this IM separation is that the change in chirality at Arg 8 produces a large structural shift in conformation between the tail and ring system of the molecule, and hence facilitates the separation of both isomers in a two-component mixture (see Figure 1.7 B). While these molecules are an exception to the challenge of separating stereoisomers by IM approaches, they do indicate a possible future of rapid separation of specific pharmaceuticals whereby changes in stereochemistry produce macromolecular rearrangements separable by IM. Such macromolecular stereoselectivity could be exploited through tailored chemical derivatization. Another approach to achieving chiral separations via ion mobility was demonstrated using chiral drift gas modifiers to provide selectivity towards enantiospecific separations. While a majority of ion mobility experiments are conducted in a single component high purity gas (*e.g.* helium or nitrogen), these drift gas modifier experiments introduce small quantities of a chiral dopant (*e.g.* (*S*)-2-butanol) to facilitate chiral selectivity.[52] Current research suggests that the chiral modifier interacts with the analyte in a similar fashion to the chromatographic approaches described above (via the three-point rule). The addition of a chiral modifier in the drift gas functions to retain one isomer form in preference. The two analyte isomers will subsequently have distinct drift times, facilitating separation in drift time space. However, as the addition of a chiral modifier inherently changes the composition of the drift gas (an integral component of the Mason-Schamp relationship), the collision cross sections measured from these experiments will be specific to the exact gas composition utilized, and thus the addition of these modifiers loses both structural context and makes cross-platforms comparisons challenging. Additionally, chiral separations by doped IM have only been demonstrated in this single study

using an ambient pressure IM, and thus this capability may be specific to this type of instrumentation.

1.4. Conclusions

In order for ion mobility to become a widely adopted separation technique, many instrument improvements are currently being developed to obtain increased selectivity of analytes based on differences in gas phase molecular structure. These new instruments utilize an increased number of interactions between the analyte and drift gas to improve separation efficiency, in similar manner to longer column length or increased packing efficiency in traditional chromatographic approaches. Examples of these new high-resolution ion mobility instruments include the high pressure drift tube IM-MS marketed by TOFWERK,[47] the trapped ion mobility spectrometer (timsTOF) produced by Bruker (Billerica, MA),[53] and new cyclic traveling wave devices currently undergoing simultaneous development by Waters Corporation (Milford, MA)[54] and Pacific Northwest National Lab (Richland, WA).[55] These new IM instruments are now demonstrating the capability to resolve some isomers with a level of selectivity approaching modern LC separations. For example, both LC and IM can provide baseline resolution of leucine and isoleucine isomers.[56]

While it is unlikely that IM will replace traditional methods of chromatography such as LC and GC, the relative speed of IM separations also enable this technique to be used in conjunction with traditional LC/GC-MS approaches.[1] For example, Lareau *et. al.* were able to analyze non-derivativized glycans by LC-IM-MS/MS utilizing traveling wave IM following LC separation on a traditional C18 column.[57] However, the lengthy gradients of LC may become a limiting factor

for high-throughput and large scale studies, and hence ion mobility approaches may be more amenable towards applications where rapid measurements are desirable. Therefore, the push for higher resolution IM instruments with separation capabilities rivaling those of traditional chromatographic approaches are a principle aim of future instrument design, and these emerging technologies may be more amendable to chiral separations by IM.

1.5. Acknowledgements

This chapter contains the invited book chapter from Chiral Analysis: Advances in Spectroscopy, Chromatography, and Emerging Methods: "Chiral Analysis in Mass Spectrometry: Applications of Chromatography and Ion Mobility," by James N. Dodds, Jody C. May, and John A. McLean. 2nd Ed. Prasad Polavarapu, Ed., Elsevier (to be published in 2018).

This work was supported in part using the resources of the Center for Innovative Technology at Vanderbilt University. Financial support for aspects of this research was provided by The National Institutes of Health (NIH Grant R01GM099218) and under Assistance Agreement No. 83573601 awarded by the U.S. Environmental Protection Agency. This work has not been formally reviewed by EPA. The views expressed in this document are solely those of the authors and do not necessarily reflect those of the Agency. EPA does not endorse any products or commercial services mentioned in this publication.

1.6. References

1. May, J. C.; McLean, J. A., Advanced Multidimensional Separations in Mass Spectrometry: Navigating the Big Data Deluge. *Annu. Rev. Anal. Chem.* **2016**, *9*, 387-409.

2. Herniman, J. M.; Langley, G. J.; Bristow, T. W.T.; O'Conner, G., The Validation of Exact Mass Measurements for Small Molecules using FT-ICRMS for Improved Confidence in the Selection of Elemental Formulas. *J. Mass Spectrom.* **2005**, *16*, 1100-1108.

3. Smith, C. A.; Grace, G. O.; Want, E. J.; Qin, C.; Trauger, S. A.; Brandon, T. R.; Custodio, D. E.; Abagyan, R.; Siuzdak, G., METLIN: A Metabolite Mass Spectral Database. *Proceedings of the 9th International Congress of Therapeutic Drug Monitoring & Clinical Toxicology, Louisville, Kentucky, April 23-28*, **2005**, *27*, 747-751.

4. May, J. C.; Morris, C. B.; McLean, J. A., Ion Mobility Collision Cross Section Compendium. *Anal. Chem.* **2017**, *89*, 1032-1044.

5. Cooks, R. G., Collision-induced dissociation: Readings and commentary. *J. Mass Spectrom.* **1995**, *30*, 1215-1221.

6. Lebedev, A. T.; Damoc, E.; Makarov, A. A.; Samgina, T. Y., Discrimination of Leucine and Isoleucine in Peptides Sequencing with Orbitrap Fusion Mass Spectrometer. *Anal. Chem.* **2014**, *86*, 7017-7022.

7. Simpson, D. C.; Smith, R. D., Combining capillary electrophoresis with mass spectrometry for applications in proteomics. *Electrophoresis* **2005**, *26*, 1291-1305.

8. Santos, F. J.; Galceran, M. T., Modern developments in gas chromatography-mass spectrometry-based environmental analysis. *J. Chromatogr. A.* **2003**, *1000*, 125-151.

9. Lee, M. S.; Kerns, E. H., LC/MS applications in drug development. *Mass Spectrom. Rev.* **1999**, *18*, 187-279.

10. Schmitz, H. H.; Artz, W. E., High-performance liquid chromatography and capillary supercritical-fluid chromatography separation of vegetable carotenoids and carotenoid isomers. *J. Chromatogr. A.* **1989**. *479*, 261-268.

11. Boussouar, I.; Chen, Q.; Chen, X.; Zhang, Y.; Zhang, F.; Tian, D.; White, H. S.; Li, H., Single Nanochannel Platform for Detecting Chiral Drugs. *Anal. Chem.* **2017**, *89*, 1110-1116.

12. Enders, J. R.; McLean, J. A., Chiral and Structural Analysis of Biomolecules Using Mass Spectrometry and Ion Mobility-Mass Spectrometry. *Chirality*. **2009**, *21*, 253-264.

13. Tang, M.; Zhang, J.; Zhuang, S.; Liu, W., Development of chiral stationary phases for high-performance liquid chromatographic separation. *Trac-Trend Anal. Chem*. **2012**, *39*, 180-194.

14. Berthod, A., *Chiral Recognition in Separation Methods*. Mechanisms and Applications. **2010**, 1-32.

15. Ettre, L. S.; Sakodynskii, K. I.; M. S., Tswett and the Discovery of chromatography I: Early work (1899-1903). *Chromatographia* **1993**, *35*, 223-231.

16. Abraham, M. H., 100 years of chromatography-or is it 171? *J. Chromatogr. A* **2004**, *1061*, 113-114.

17. Strain, H. H.; Sherma, J., Michael Tswett's contributions to sixty years of chromatography. *J. Chem. Educ.* **1967**, *44*, 235-237.

18. Tswett, M., Physical-chemical studies on the chlorophyll. Adsorption. *Ber. Dtsch. Bot. Ges.* **1906**, *24*, 316.

19. Martin, A. J. P.; Synge, R. L. M., A new form of chromatography employing two liquid phases. *Biochem. J.* **1941**, *35*, 91-121.

20. Gohlke, R. S., Time-of-Flight Mass Spectrometry and Gas-Liquid Partition Chromatography. *Anal. Chem.* **1959**, *31*, 535-541.

21. Marshall, A. G.; Hendrickson, C. L.; Shi, S. D., Scaling MS Plateaus with High-Resolution FT-ICRMS. *Anal. Chem.* **2002**, *74*, 252A-259A.

22. Bayer, E.; Grom, E.; Kaltenegger, B.; Uhmann, R., Separation of amino acids by high performance liquid chromatography. *Anal. Chem.* **1976**, *48*, 1106-1109.

23. Schurig, V., Separation of enantiomers by gas chromatography. *J. Chromatogr. A*, **2001**, *906*, 275-299.

24. Juvancz, Z.; Petersson, P., Enantioselectivity gas chromatography. *J. Microcolumn. Sep.* **1996**, *8*, 99-114.

25. Hashimoto, A.; Nishikawa, T.; Oka, T.; Takahashi, K.; Hayashi, T., Determination of free amino acid enantiomers in rat brain and serum by high-performance liquid chromatography after derivatization with N-tert.-butyloxycarbonyl-L-cysteine and o-phthaldialdehyde. *J. Chromatogr. B* **1992**, *582*, 41-48.

26. Gil-Av, E.; Tishbee, A.; Hare, P. E., Resolution of underivatized amino acids by reversed-phase chromatography. *J. Am. Chem. Soc.* **1980**, *102*, 5115-5117.

27. Stalcup, A. M.; Agyei, N. M., Heparin: A Chiral Mobile-Phase Additive for Capillary Zone Electrophoresis. *Anal. Chem.* **1994**, *66*, 3054-3059.

28. Guo, Z.; Wang, H.; Zhang, Y., Chiral separation of ketoprofen on an achiral C8 column by HPLC using norvancomycin as chiral mobile phase additives. *J. Pharm. Biomed. Anal.* **2006**, *41*, 310-314.

29. E. Gil-Av, B.; Feibush, R.; Charles-Sigler, R., Separation of enantiomers by gas liquid chromatography with an optically active stationary phase. *Tetrahedron Lett.* **1966**, 1009.

30. Cavazzini, A.; Pasti, L.; Massi, A.; Marchetti, N.; Dondi, F., Recent applications in chiral high performance liquid chromatography: A review. *Analytica Chimica Acta* **2011**, *706*, 205-222.

31. Yamashita, M.; Fenn, J. B., Electrospray ion source. Another variation on the free-jet theme. *J. Phys. Chem.*, **1984**, *88*, 4451-4459.

32. Dole, M.; Mack L. L.; Hines, R. L.; Mobley, R. C.; Ferguson L. D.; Alice, M. B., Molecular Beams of Macroions. *J. Chem. Phys*. **1968**. *49*, 2240-2249.

33. Pirkle, W. H.; Pochapsky, T. C., Considerations of chiral recognition relevant to the liquid chromatography separation of enantiomers. *Chem. Rev.* **1989**, *89*, 347-362.

34. Lämmerhofer, M., Chiral recognition by enantioselective liquid chromatography: Mechanisms and modern chiral stationary phases. *J Chromatogr. A*. **2010**, *1217*, 814-856.

35. Pirkle, W. H.; Welch, C. J.; Lamm, B., Design, Synthesis, and Evaluation of an Improved Enantioselective Naproxen Selector. *J. Org. Chem.* **1992**, *57*, 3854-3860.

36. Piccolo, O.; Valoti, E.; Giuseppina, V., Process for preparing naproxen. U. S. Patent 4,736,061 A, **1988**.

37. Paglia, G.; Williams, J. P.; Menikarachchi, L.; Thompson, J. W.; Tyldesley-Worster, R.; Halldórsson, S.; Rolfsson, O.; Moseley, A.; Grant, D.; Langridge, J.; Palsson, B. O.; Astarita, G., Ion Mobility Derived Collision Cross Sections to Support Metabolomics Applications. *Anal. Chem.* **2014**, *86*, 3985-3993.

38. Stow, S. M.; Causon, T. J.; Zheng, X.; Kurulugama, R. T.; Mairinger, T.; May, J. C.; Rennie, E. E.; Baker, E. S.; Smith, R. D.; McLean, J. A.; Hann, S.; Fjeldsted, J. C., An Interlaboratory Evaluation of Drift Tube Ion Mobility-Mass Spectrometry Collision Cross Section Measurements. *Anal. Chem.* **2017**, (submitted).

39. Mason, E. A.; McDaniel, E. W., Transport Properties of Ions in Gases; John Wiley & Sons: New York, **1988**; p. 560.

40. Siems, W. F.; Viehland, L. A.; Hill, H. H. Jr., Improved Momentum-Transfer Theory for Ion Mobility. 1. Derivation of the Fundamental Equation. *Anal. Chem.* **2012**, *84*, 9782-9791.

41. May, J. C.; Dodds, J. N.; Kurulugama, R. T.; Stafford, G. C.; Fjeldsted, J. C.; McLean, J. A., Broadscale resolving power performance of a high precision uniform field ion mobility-mass spectrometer. *Analyst* **2015**, *140*, 6824-6833.

42. May, J. C.; McLean, J. A., Ion Mobility-Mass Spectrometry: Time-Dispersive Instrumentation. *Anal. Chem.* **2015**, *87*, 1422-1436.

43. Fenn, L. S.; Kliman, M.; Mahsut, A.; Zhao, S. R.; McLean, J. A., Characterizing ion mobility-mass spectrometry conformation space for the analysis of complex biological samples. *Anal. Bioanal. Chem.* **2009**, *394*, 235-244.

44. May, J. C.; Goodwin, C. R.; Lareau, N. M.; Leaptrot, K. L.; Morris, C. B.; Kurulugama, R. T.; Mordehai, A.; Klein, C.; Barry, W.; Darland, E.; Overney, G.; Imatani, K.; Stafford, G. C.; Fjeldsted, J. C.; McLean, J. A., Conformational Ordering of Biomolecules in the Gas Phase: Nitrogen Collision Cross Sections Measured on a Prototype High Resolution Drift Tube Ion Mobility-Mass Spectrometer. *Anal. Chem.* **2014**, *86*, 2107-2116.

45. Hofmann, J.; Hahm, H. S.; Seeberger, P. H.; Pagel, K., Identification of carbohydrate anomers using ion mobility-mass spectrometry. *Nature* **2015**, *526*, 241-244.

46. Lalli, P. M.; Corilo, Y. E.; Fasciotti, M.; Riccio, M. F.; de Sa, G. F.; Daroda, R. J.; Souza, G. H.; McCullagh, M.; Bartberger, M. D.; Eberlin, M. N.; Campuzano, I. D., Baseline resolution of isomers by traveling wave ion mobility mass spectrometry: investigating the effects of polarizable drift gases and ionic charge distribution. *J. Mass Spectrom.* **2013**, *48*, 989-997.

47. Groessl, M.; Graf, S.; Knochenmuss, R., High resolution ion mobility-mass spectrometry for separation and identification of isomeric lipids. *Analyst* **2015**, *140*, 6904-6911.

48. Harper, B.; Neumann, E. K.; Stow, S. M.; May, J. C.; McLean, J. A.; Solouki, T., Determination of ion mobility collision cross sections for unresolved isomeric mixtures during tandem mass spectrometry and chemometric deconvolution. *Anal. Chim. Acta.* **2016**, *939*, 64-72.

49. Giles, K.; Williams, J. P.; Campuzano, I., Enhancements in travelling wave ion mobility resolution. *Rapid Commun. Mass Spectrom.* **2011**, *11*, 1559-1566.

50. Dodds, J. N.; May, J. C.; McLean, J. A., Investigation of the Complete Suite of the Leucine and Isoleucine Isomers: Toward Prediction of Ion Mobility Separation Capabilities. *Anal. Chem.* **2017**, *89*, 952-959.

51. Jia, C.; Lietz, C. B.; Yu, Q.; Li, L., Site-Specific Characterization of D-Amino Acid Containing Peptide Epimers by Ion Mobility Spectrometry. *Anal Chem.* **2014**, *86*, 2972-2981.

52. Dwivedi, P.; Wu, C.; Matz, L. M.; Clowers, B. H.; Siems, W. F.; Hill, H. H., Gas-Phase Chiral Separations by Ion Mobility Spectrometry. *Anal. Chem.* **2006**, *78*, 8200-8206.

53. Silveira, J. A.; Ridgeway, M. E.; Park, M. A., High Resolution Trapped Ion Mobility Spectrometry of Peptides. *Anal. Chem.* **2014**, *86*, 5624-5627.

54. Giles, K.; Wildgoose, J. L.; Pringle, S.; Langridge, D.; Nixon, P.; Garside, J.; Carney, P., *Characterising a T-Wave Enabled Multi-Pass Cyclic Ion Mobility Separator*. ASMS **2015**. Poster.

55. Deng, L.; Ibrahim, Y. M.; Baker, E. S.; Aly, N. A.; Hamid A. M.; Zhang, X.; Zheng, X.; Garimella, S. V. B.; Webb, I. K.; Prost, S. A.; Sandoval, J. A.; Norheim, R. V.; Anderson, G. A.; Tolmachev, A. V.; Smith, R. D., Ion Mobility Separations of Isomers based upon Long Path Length Structures for Lossless Ion Manipulations Combined with Mass Spectrometry. *ChemistrySelect*. **2016**, *1*, 2396-2399.

56. Groessl, M.; Graf, S., *Separation of isomers in lipidomics and metabolomics experiments by high resolution ion mobility spectrometry-mass spectrometry (IMS-MS).* ASMS **2016**. Poster.

57. Lareau, N. M.; May, J. C.; McLean, J. A., Non-derivatized glycan analysis by reverse phase liquid chromatography and ion mobility-mass spectrometry. *Analyst*, **2015**, *140*, 3335-3338.

58. Griffiths, J. A brief history of mass spectrometry. Anal. Chem. 2008, 80, 5678-5683.

CHAPTER 2

ISOMERIC AND CONFORMATIONAL ANALYSIS OF SMALL DRUG AND DRUG-LIKE MOLECULES BY ION MOBILITY-MASS SPECTROMETRY (IM-MS)

2.1. Introduction

The process of developing new drug candidates has changed significantly over time, as a result of the Human Genome Project and other technological advances in computational modeling and bioformatics.[1] For example, high-throughput screening methods provide unparalleled capacity to screen millions of chemical structures for potential drug efficacy,[2,3] as opposed to simply developing a target candidate and anticipating relevant biochemical action. Regardless of the desired approach towards production of novel drug candidate molecules by either reverse pharmacology, the classical approach, or natural product discovery,[4,5,6] most drugs take several years to develop and millions of dollars to become marketable as a requirement of validation through in-depth clinical trials, evaluation of safety risks and FDA approval.[7] As part of this development process, the analytical need to study the structural characteristics of these small molecules is imperative.

Structural characterization of potential drug candidates, either derived from natural sources or synthesized in the laboratory, is a complex and time consuming process, and for rapid analyses, pharmaceutical companies value the high degree of analytical selectivity and sensitivity afforded by modern mass spectrometry (MS) methods towards overall quality control of synthesized products and characterization of new drug targets.[8,9] Although mass spectrometers are highly selective, often able to assign a molecular formula for a target analyte based solely on molecular mass measurement, isomeric species are difficult to differentiate by traditional MS methods, even

with the addition of tandem MS/MS approaches.[10,11] Because the biological function of chemical compounds can change with their structural variation, isomeric species are a highly researched area of the pharmaceutical field.[12] Condensed phase separation techniques such as gas or liquid chromatography are often utilized to separate complex mixtures prior to mass analysis and provide the ability to separate isomers by differences in chemical properties, such as polarity or boiling point. These methods, while effective, are often highly selective to narrow classes of isomers and are not inherently high-throughput techniques. In this chapter, we describe the application of IM-MS, an emerging analytical technique for structurally characterizing small molecule isomer systems, with a particular focus on the role of IM-MS in characterizing biological systems and relevant pharmaceutical applications.

2.1.1. Isomers

Isomers are defined as compounds having the same molecular formula, but differing in their overall chemical structure.[13] Isomeric species are further sub-divided into categories that reflect their structural variations, which may include covalent bond rearrangements (constitutional isomers), stereochemical variations (stereoisomers), or rotational isomers, commonly referred to as rotamers. As constitutional isomers vary in skeletal structure between constituent atoms, these isomers possess a broad scope of biological activity based upon their particular structural arrangements. For example, the molecular formula $C_8H_9NO_2$ is reported to have 33 isomers by the PubChem database,[14] and many of these isomers have unique chemical behavior and physiological function (Figure 2.1). In one case, paracetamol (more commonly known as acetaminophen) is a well-known analgesic, yet its constitutional isomer, methyl anthranilate functions as a bird repellent and a flavor additive in drinks.[15] The structural makeup of constitutional isomers can also

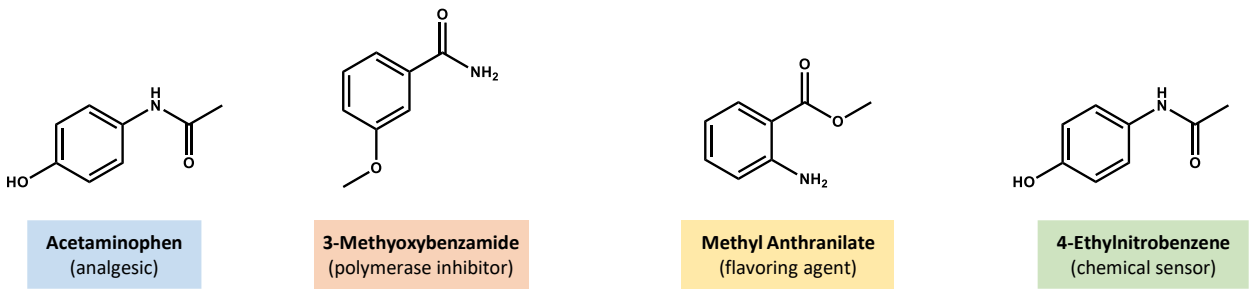

Figure 2.1. Structures related to four constitutional isomers of chemical formula $C_8H_9NO_2$ and corresponding function or typical use.

vary widely depending on their biological class. For example, lipid isomers typically vary in alkyl chain position and cis/trans double bond positioning,[16] while peptides tend to have sequence order variation or even amino acid substitutions comprised of the same chemical formula (*e.g.* leucine/isoleucine).[17]

In addition to constitutional isomers, compounds with the same molecular formula can differ in stereochemistry, (*i.e.* diastereomers and enantiomers) resulting in varying chemical and physical properties. For example, ethambutol is a 204 Da molecule ($C_{10}H_{24}N_2O_2$) possessing two stereocenters. In the (+) form (*S,S*) ethambutol is frequently used to treat tuberculosis.[18] However, with inversion of chirality at its two stereocenters to form (-) or (*R,R*) ethambutol, the molecule is known to cause blindness.[19] Isomers also exist for two compounds possessing the same chemical scaffold and chirality. For example, rotamers are small molecule conformers where multiple three-dimensional molecular structures can arise as a result of rotation around a single bond. In some cases this bond rotation gives rise to atropisomerism, which is the restriction of rotation around a single covalent bond which results in distinct optical isomers. A commonly cited rotamer example which exhibits freedom of rotation around a single bond are the Newman projections of butane.[20] In other cases where rotation is not restricted, different stable conformations are still possible, especially in protein analysis. Small molecules in particular are noted for producing a variety of conformations as a result of their flexibility.[21] Because of the diverse chemical activity that can exist within constitutional and conformational isomers, finding useful and efficient ways to explore the structure of these molecules can provide insight into their specific chemical properties.

For the past 15 years IM-MS has made large contributions in the analysis of constitutional and conformational isomers.[22,23,52] As result of the commercialization and rapid adoption of IM-MS instrumentation,[24,33,37] the Web of Science database cites over 3,500 articles in the last decade

related to IM-MS studies.[25] While ion mobility has been traditionally utilized to study large biological systems, more recently it has been applied to the study of smaller (< 400 Daltons) drug and drug-like molecules.[26,27] In this chapter, we describe the technique and theory of IM-MS, provide examples of the use of IM-MS to characterize various small drug and drug-like molecules, and provide some basic methodology towards collecting and analyzing IM-MS data using a commercially available IM-MS platform (Agilent 6560) as an example.[37]

2.2. Instrumentation and Theory

IM-MS is an emerging analytical technique that separates gas phase ions into two dimensions based upon molecular size and weight. In the mobility dimension, analyte ions are separated based upon their two-dimensional orientationally-averaged size in the gas phase (collision cross section, CCS), which provides information regarding their size and shape.[28,33] In the mass spectrometer dimension, separation is based upon the mass to charge ratio (m/z) of the analyte ion, which is directly correlated to its intrinsic molecular formula. Combined, IM-MS provides unique and important information regarding the gas-phase density preferences of different classes of molecules, which can identify unknown compounds which share similar structural scaffolds.[36,47]

There are four basic components of an IM-MS instrument: the ion source, the ion mobility separator, the mass analyzer, and the detector [Figure 2.2 (A)]. The type and arrangement of these components can vary depending on instrument vendor and experiment application.[29,30]

In the source region, analyte ions are commonly generated by electrospray ionization (ESI), which allows the option for directly coupling an LC separation. In ESI, ions enter the source as a

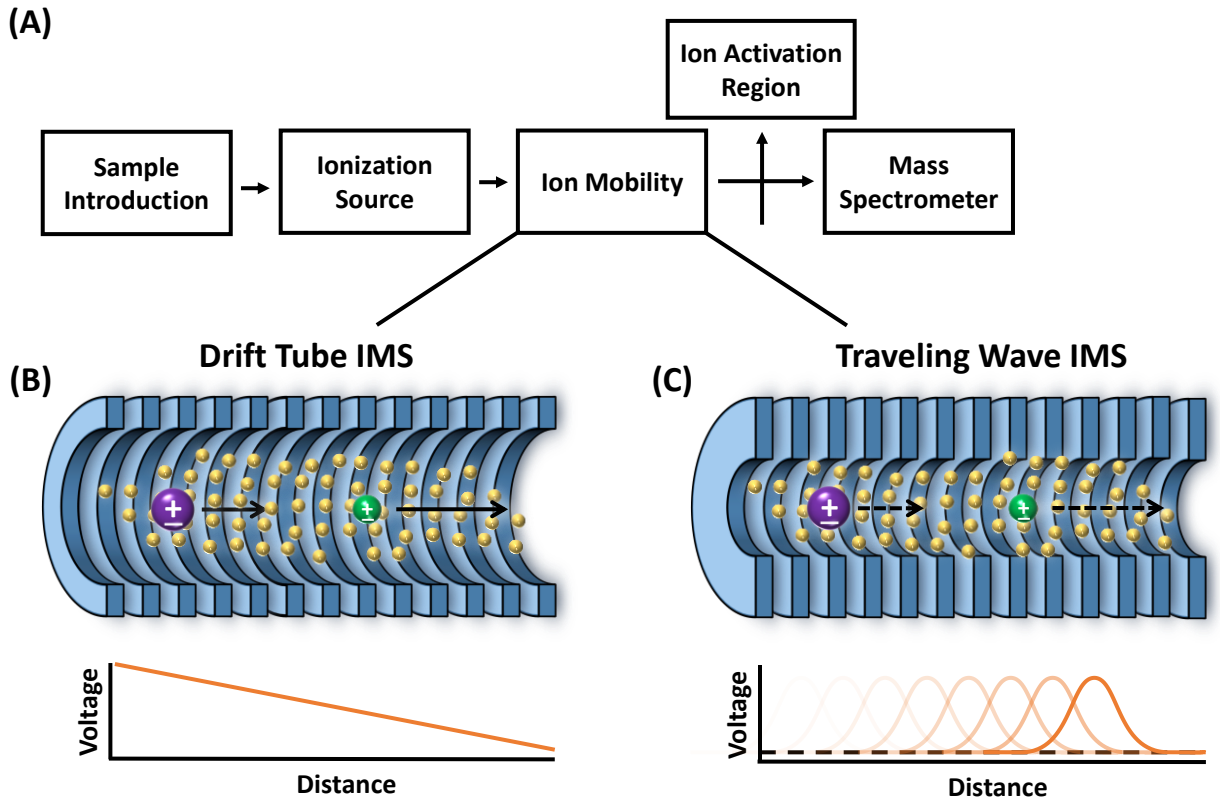

Figure 2.2. (A) Block diagram of a typical IM-MS instrument. Ions are separated in the presence of a neutral drift gas by **(B)** a declining electric field along a series of ring electrodes (DTIMS), or **(C)** by a pulse wave generated by applied sequential voltage along a series of ring electrodes (TWIMS).

liquid and are vaporized using a combination of gas flows and electric fields, which ultimately generate gas-phase ions. While ESI is the most commonly used ion source, other ion source types include laser and chemical ionization (*e.g.* MALDI and APCI).[31] ESI commonly produces protonated and deprotonated ions ($[M+H]^+$, $[M-H]^-$), as well as various alkali metal cation species, such as $[M+Na]^+$ and $[M+K]^+$, where M represents the neutral form of the molecule. Once ions are generated, they are released into the ion mobility spectrometer where they are separated based on their gas-phase size and shape (CCS). Following the mobility separation, ions enter the mass analyzer where they are separated by their mass-to-charge ratio (m/z). For more in-depth information regarding the experiment, we refer the reader to a recent literature review which covers the various IM techniques and instrumentation in detail.[32,33]

Ion mobility techniques can be broadly separated into two method types: time dispersive methods, which include drift tube and traveling wave ion mobility spectrometry (DTIMS and TWIMS, respectively), and space dispersive methods, which primarily include high field-asymmetric waveform IM and differential ion mobility spectrometry (FAIMS and DMS, respectively) which collectively operate as mobility filtering devices. The examples presented in this chapter will focus on recent applications of the time dispersive methods of DTIMS and TWIMS, which collectively represent the majority of IM instrumentation currently utilized.[33]

2.2.1. Drift Tube Ion Mobility

In drift tube ion mobility (DTIMS), the IM region consists of a series of ring electrodes contained within a neutral drift gas (typically helium or nitrogen) [Fig. 2.2 (B)].[34,35] DTIMS is operated at one of two pressure regimes: low (1-10 Torr) and elevated (*ca.* 760 Torr) pressures.

Typically, ion transmission is more efficient at reduced pressure, yet typically results in somewhat reduced IM resolving power from high diffusion. As ions are introduced into the drift tube, they are drawn through the drift region as a result of an applied electric field along the ring electrodes. During ion drift, the ions interact with the buffer gas at low energy and molecules with smaller rotationally averaged surface area (smaller CCS), transverse the region faster as a result of fewer collisions. Mathematically, the CCS of the analyte ion can be calculated using the Mason-Schamp equation[36,37] where K_0 is the measured mobility of the ion, *z* is the charge of the ion, *T* is the temperature of the drift gas, and N_0 is the number density of the drift gas at standard temperature and pressure. The terms *e* and k_B are the elementary charge and Boltzmann's constant, respectively.

$$\mathrm{CCS} = \frac{3ze}{16N_o}\left(\frac{2\pi}{\mu k_B T}\right)^{1/2}\frac{1}{K_0} \quad (1)$$

2.2.2. Traveling Wave Ion Mobility

Similar to DTIMS, a traveling wave ion mobility drift cell uses an inert buffer gas and a series of ring electrodes to move ions through the drift region, but typically the electrodes have smaller inner diameters than what is used in DTIMS to facilitate better axial ion focusing [Figure 2.2 (C)].[38,39] In TWIMS, ion pulses are mobility separated by sequentially applying a direct current voltage to the rings in a series along the drift cell to create a migrating potential along the length of the cell. These sequential low voltage pulses generate waves of electric potential that push ions through the drift region. As the wave propels the ions forward through the device, low energy elastic collisions occur between the analyte ions and the buffer gas. Smaller ions experience fewer collisions with the buffer gas, and as a result, traverse the drift region faster than larger ions,

resulting in shorter drift times. This mechanism is almost identical to what is experienced in DTIMS, but with the exception that larger ions are slower in TWIMS as a result of "falling over" the wave pulses during their transit through the cell. The drift times are converted to collision cross sections through a calibration procedure which takes into account the drift times and CCS of known internal standards.[40,41] The ion mobility spectra obtained from both TWIMS and DTIMS are qualitatively similar.

2.3. Current Work in Isomer Structural Separations

Historically, there have been several reported studies where DTIMS and TWIMS have been used to observe both constitutional and conformational structures of large molecules, where structural differences are significant and readily measured.[42,43,44] In this section, we will present some recent examples of the use of TWIMS and DTIMS to separate constitutional and conformational isomers in small molecule systems, which have been given less attention in the literature, but nonetheless are important avenues for developing IM-MS for the separation and characterization of drug and drug-like small molecule isomer systems.

2.3.1. Separation of Constitutional Isomers

Often chromatography resolution can be difficult to achieve for molecules with similar polarities, and hence constitutional isomers have been studied in detail by IM-MS. In an effort to differentiate molecules of interest from complex matrices (*e.g.* biological samples and natural product extracts), mobility techniques have investigated the separation of a wide variety of chemical classes including lipids, carbohydrates,[45,46] peptides[47,48] and fossil fuels.[49] As a specific

example, we will consider the highly studied isomer system of leucine and isoleucine, which represent a classically studied isomer pair from an analytical separation perspective, as both compounds have the same chemical formula ($C_6H_{13}NO_2$) and hence cannot be distinguished by MS measurements alone. From an ion mobility perspective, leucine and isoleucine have been shown to be differentiable using several ion mobility techniques, including FAIMS[50] and TWIMS.[51] In a recent study by Dodds *et al.*, 11 different leucine/isoleucine isomers were studied using DTIMS and focused on the positive ion forms of these molecules, $[M+H]^+$.[52] The sub-classes of isomers investigated in this study include enantiomers (two molecules whose stereochemistry is opposite at every chiral center), diastereomers (two molecules with multiple chiral centers of which some, but not all, have opposite stereocenters), and constitutional isomers related to leucine and isoleucine. A plot of the range of diversity in CCS for these compounds appears in Figure 2.3. As illustrated in the figure, the differences in the CCS vary depending on isomer type. For example, the enantiomers (*e.g.* L-leucine and D-leucine) show no statistical difference their measured collision cross sections, and similarly, diastereomers (*e.g.* L-isoleucine and L-*allo*-isoleucine) exhibit different CCS values, but are still very challenging to differentiate (typically 0.4% difference in CCS). However, as the molecules become more structurally diverse, the isomers possess more significant differences in cross section. Specifically, 3 constitutional isomers (N-N-dimethylglycine ethyl ester, L-tert-leucine, and L-norleucine) are structurally distinct enough to yield baseline or near-baseline separation and possess 3.6% and 3.1% difference in their respective empirical cross sections.

In addition to illustrating the separation of various constitutional isomers, the authors proposed a mathematical relationship correlating the percent difference in cross section of any two isomers of interest with respect to instrumental resolving power (R_p). Briefly, the efficiency of ion

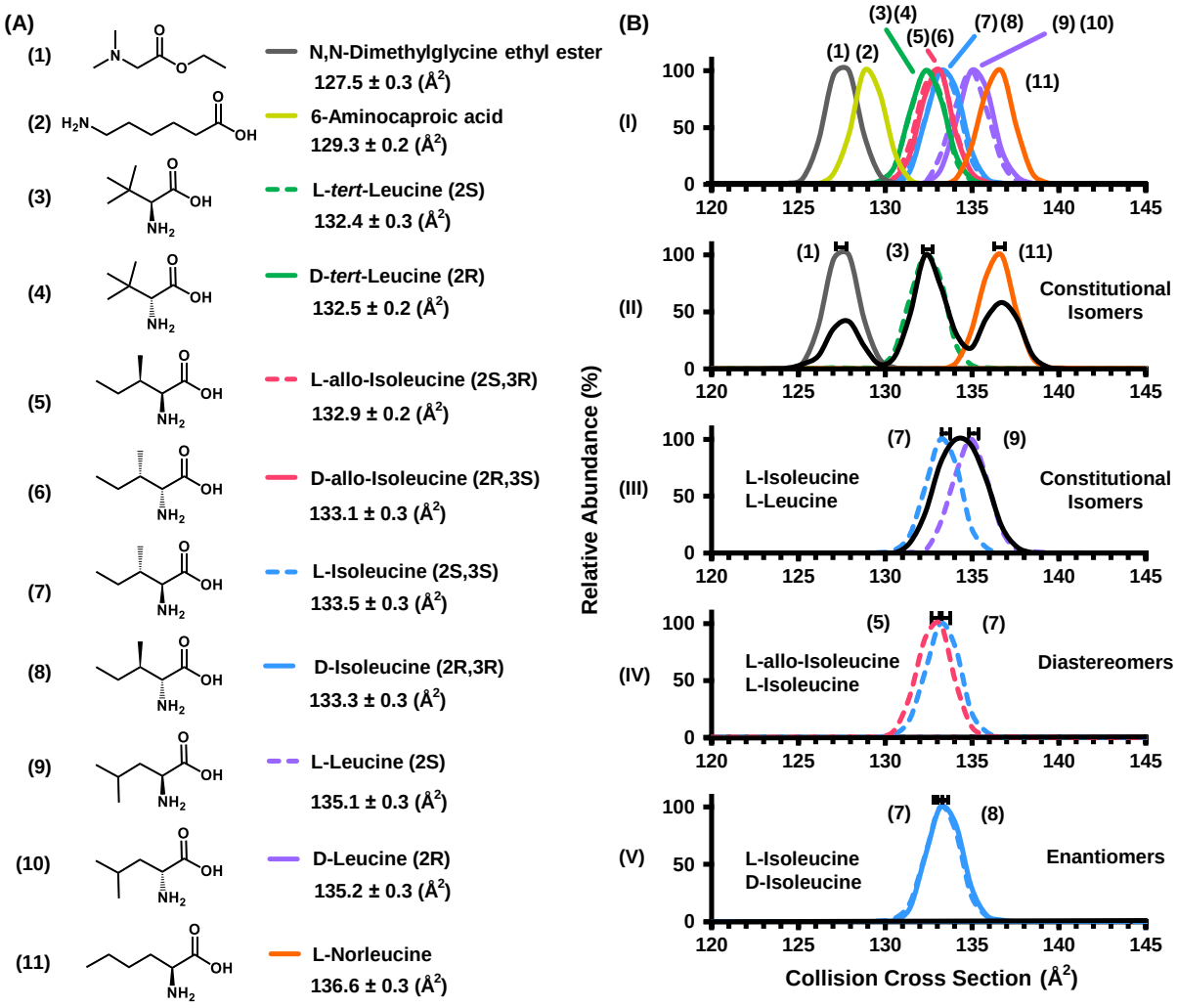

Figure 2.3. (A) Leucine/isoleucine isomers with chemical formula $C_6H_{13}NO_2$ examined in this study. Experimental cross sections with respective standard deviations are shown at the right with corresponding stereochemistry. **(B) (I)** Experimental IM spectra overlays for all isomer compounds (standard error bars omitted for clarity). **(II)** Overlay of the IM spectra corresponding to N,N-dimethylglycine ethyl ester, L-tert-leucine, and L-norleucine and the IM spectrum corresponding to the mixture (black). **(III)** Overlays of L-isoleucine and L-leucine in addition to the equal ratio mixture. **(IV** and **V)** Overlays of diastereomers and enantiomers, respectively. Adapted with permission from Ref. 52, Copyright 2017 American Chemical Society.

mobility instruments is described quantitatively in terms of resolving power, defined for DTIMS instruments as the ion drift time (t_d) divided by the width of the peak at half height (full width at half-maximum height, FWHM).

$$R_p = \frac{t_d}{FWHM} \quad (2)$$

As two isomers become more structurally similar (*i.e.* closer in terms of their cross sectional areas), higher levels of instrument efficiency (R_p) are required to resolve the isomeric species of interest. The final equation proposed in the above study relates separation efficiency, termed two-peak resolution ($R_{p\text{-}p}$) to instrumental resolving power and analyte cross sectional difference (Δ CCS%).

$$R_{p-p} = 0.00589x\, R_p x\, \Delta CCS\% \quad (3)$$

To illustrate the utility of the above equation, consider two isomers of interest who possess cross sectional differences of 1.0% (*e.g.* 200 $Å^2$ and 202 $Å^2$). The above equation predicts that separating these isomers to half height resolution (0.83 $R_{p\text{-}p}$) would require *ca*. 140 R_p. In this manner the study by Dodds and coworkers can predict how efficiently two isomers of interest will separate on a specific instrument platform, provided that the CCS of each analyte is previously known and the resolving power of the ion mobility instrument well characterized.

2.3.2. Separation of Conformational Isomers

Another biological class where IM-MS has been utilized to facilitate the separation of isomers is carbohydrates. Carbohydrates, or saccharides, are a class of compounds which includes sugars, starches, and cellulose. Carbohydrates are challenging systems to study with most

analytical techniques as they commonly exist as complex mixtures in nature with variations in skeletal structure, bond coordination, and stereochemistry (Figure 2.4). Studies are further complicated because many of the compounds in these mixtures have the same molecular formula (isomers) which again prevents them from being fully characterized using traditional mass spectrometry methods. This makes ion mobility a particularly intriguing tool to explore carbohydrate systems.

A recent example of the utility of IM to study carbohydrates was carried out by Li and coworkers.[53] In their study of sugars, TWIMS was used to measure drift time profiles for ions of monosaccharide-glycolaldehydes and disaccharides of various simple sugars. While this work is another example of the ability of ion mobility to separate constitutional isomers, there were occasions where the presence of multiple conformations appeared, even for what was believed to be a single analyte ion. For example, the monosaccharide glycolaldehyde β-D-glucopyranosyl-2-glycolaldehyde (β-D-glc-GA) was analyzed in negative mode ESI and produced a drift time profile that generates two distinct peaks for the deprotonated ion. The authors propose that the appearance of these multiple conformations may be attributed to several cyclic/acyclic forms produced by hemiacetal formation in the gas phase. While most conformers are typically noted for large bimolecular species (*i.e.* proteins), these small molecule analytes produced multiple distributions (peaks) for one ion form. Thus this work illustrated the possibility to observe conformers even in a relatively small molecule system.

The appearance of conformational isomers for small drug-like molecules has also become evident in studies related to thalidomide in the authors' laboratory. Thalidomide is a small molecule drug that is currently used primarily for the treatment of specific cancers and for alleviating various symptoms of leprosy. However, historically thalidomide is recognized as one

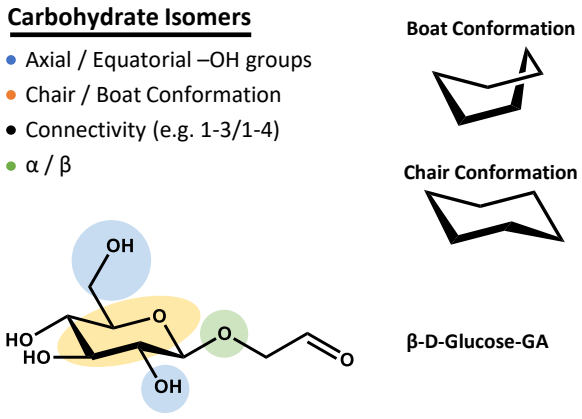

Figure 2.4. Complexity of carbohydrate isomers represented graphically pertaining to both constitutional isomers (connectivity isomers) and stereoisomers (axial/equatorial substitutions, chair/boat conformations, and α/β glycosidic linkage orientation).

of the first drugs whose different enantiomer forms produced drastically different biological effects. Figure 5 illustrates the structures and drift time profiles for the $[M+H]^+$ and $[M+H]^-$ ions of (*S*,-)-thalidomide and (*R*,+)-thalidomide along with corresponding CCS. The drift time profiles of both positive and negative mode ions for both enantiomers are identical. This result is expected as stereochemical differences in small molecules are not expected to result in different drift time distributions. However, multiple peaks were detected for both enantiomers of thalidomide in each ionization mode. Structurally, this observation is reasoned as being a consequence of the possibility for multiple molecular conformations arising from rotation around the single N-C bond that links the two ring moieties.

The development of methods for characterizing small drug and drug-like molecules has become an important focal point for the pharmaceutical industry. As a result there has been a concentrated effort towards discovering new technologies to aide in the development of new drugs. The examples presented in this work provide strong support for the use of IM-MS as an important analytical technology in exploring the structural diversity of constitutional and conformational isomers of small drug and drug-like molecules. In the following sections, we provide the materials and methods necessary to obtain an IM-MS spectra for small molecules (here *S*-thalidomide, 258 Da) using a commercially available IM-MS platform (Agilent IM-MS 6550).

2.4. Materials

a) The sample preparation described here is for use with direct infusion via a syringe pump operated at low flow rates (*i.e.* 5-100 µL/min). As with any analytical study, it is beneficial to have analyte samples and solvents with optimal purity for analysis. In this study, S-thalidomide was

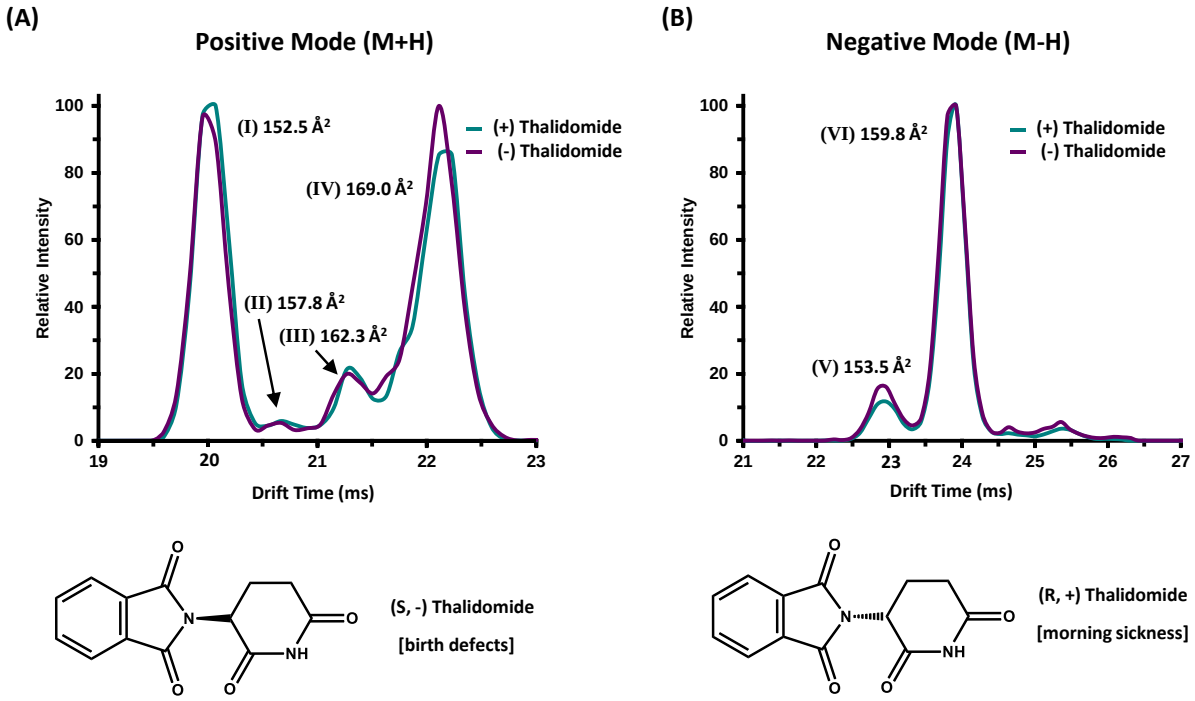

Figure 2.5. Drift time profiles of (*R*) and (*S*) thalidomide enantiomers with corresponding CCS observed in both positive and negative mode (**A** and **B**, respectively) for nitrogen drift gas. Structures are illustrated at the bottom for chiral reference.

purchased from Sigma-Aldrich and the solvent (Optima LC-MS grade Water) was obtained from Fisher Scientific. A range of analyte concentration can be used and should be selected based upon instrument sensitivity and limits of detection. Standard protocol for this instrument using direct infusion recommends an analyte concentration of 1-10 μg/mL. For the experiment described here, a 10 μg/mL sample of S-thalidomide was prepared using 10 mM ammonium acetate in water.

b) The instrument must be tuned prior to data collection in order to perform at optimal sensitivity, resolution, and accuracy. Towards this end a commercially-available tune mix solution containing several standards over a range of masses and mobilities was used (Agilent Tune Mix, part number G1969-85000). Specifics of the tuning method are described in the methods section.

c) Direct infusion was carried out using a 500 μL glass syringe and a kD Scientific syringe pump. Flow rates were as described in the methods section to follow.

d) Collection of IM-MS data was obtained using Agilent Mass Hunter Acquisition Software (v.7.00). Data workup of IM-MS distributions was performed using Agilent IM-MS Browser Software (v. 7.02)

2.5. Methods

The method described below is for new users to the Agilent 6560 IM-MS instrument who have general knowledge of traditional mass spectrometry operation. It is intended to provide the novice user with the basic steps necessary to obtain a routine IM-MS spectra. It is not intended to provide an exhaustive description of all instrument settings and their uses. The reader should consult their service manual for extended instructions and a comprehensive description of settings.

2.5.1. Preparing the Instrument

a) To ensure drift time and collision cross section reproducibility, check instrument pressures in each of the following instrument compartments: the high pressure funnel region should be set to 4.80 Torr (+/- 0.02), trap funnel region pressure at 3.80 Torr (+/- 0.01), and drift tube pressure should be maintained at 3.95 Torr (+/- 0.01). A pressure regulation manifold (alternate gas kit, Agilent) is recommended here in order to automatically maintain these pressure settings. Alternatively, the user may choose to monitor and make manual adjustments to the drift tube pressure in order to maintain the precision of the IM measurements.

b) Open the Agilent Mass Hunter Workstation Data Acquisition Program. Under the "Context" menu (Figure 6A), choose the "Tune" setting to perform an autotune. The source temperatures and voltages will be preset for the Agilent Tune Mixture (Figure B.1), and the ion polarity and scan mode will be selected as a function of the molecules of interest per individual experiment (low mass mode (50-250 m/z), normal mode (50-1700 m/z), or high mass range (100-3200 m/z). In this case we are investigating thalidomide (258 Da), and have selected the normal instrument tuning mode (50-1700 m/z).

c) Select the "Tune and Calibration" tab [Figure B.1 (C)]. Select desired ionization mode (positive mode is used here), TOF (time of flight), mass calibration/check, and the corresponding mass range depending on the analyte to be studied. Once settings have been chosen, click "Apply" to apply these settings prior to tuning [(Figure B.1 (D)].

d) Ensure that the calibrant line contains adequate calibrant solution and is plumbed into the primary nebulizer before starting the autotune. It is recommended that at minimum, a quarter of the calibration bottle volume (*ca.* 30 mL) be filled with calibration solution prior to tuning. Turn

on the tune mix by right clicking in the Q-TOF selection box [Figure B.1 (E)] and selecting calibrant.

e) When the tune mix ions appear in the spectra window (*e.g.*, m/z 322, 622, and 922 in positive ion mode), click on the "Start TOF Mass calibration" button [Figure B.1 (F)].

f) Upon tune completion, a calibration report will be generated as a portable document file (.pdf) file. From this report, ensure that signal intensity is greater than 1 x 10^5 ion counts and that the ion mobility resolution is between 40-60. If not, the user may wish to repeat the autotune procedure. After tuning, click the "Instrument State" tab [Figure B.1 (G)], and then click "Save" and "Apply".

g) Once the instrument is tuned in the desired ion mode, switch to the acquisition mode under the context menu [Figure B.1 (A)] to start collecting data.

2.5.2. Data Acquisition (consult Figure 7)

a) Load the pre-existing low mass method in the drag-down box in method editor and click "Apply" [(Figure B.2 (A)]. If the user is interested in collecting collision cross sections, the method should include a voltage gradient in the drift tube region in order subtract out the non-mobility flight time. This voltage gradient can be accessed under the "Advanced Parameters" tab of the method editor screen, [Figure B.2 (B)]. For a detailed explanation of the voltage gradient method we refer the reader to Ref. 36 and its Supporting Information to describe the non-mobility component of the drift time, and subsequent conversion to CCS.

b) Load the sample in the syringe and syringe pump for direct infusion. Ensure that the syringe pump is set with the correct syringe diameter in order to output the correct flow rates. Although flow rate will vary based on specific instrument source settings and sensitivity, the flow rate used here is 1-10 µL/min. Turn on the syringe pump. Once sample reaches the instrument, analyte ion peaks begin to appear in the mass window.

c) NOTE: If minimizing sample consumption is important, the user may wish to conduct step 4 prior to turning on the syringe pump.

d) To setup the data acquisition, select the "Sample Run" tab at the bottom of the method editor screen [Figure B.2 (C)]. In the sample run mode, name the file [Figure B.2 (D)] and select the path directory [Figure B.2 (E)] for your file.

e) To acquire data, click the forward arrow [Figure B.2 (F)] in the sample run screen.

2.5.3. Data Workup

a) After data acquisition is complete, load the "Agilent Mass Hunter IM-MS Browser" software and open the desired file. OPTIONAL: Once the file has opened, select "Condense File" under the "Actions" tab [Figure B.3 (A)]. Condensing files will compress the data from each experimental sequence into a single frame, which is convenient for viewing multiple segment runs (*e.g.*, CCS experiments) or long infusion experiments.

b) In IM-MS Browser, you can view the resulting mass spectrum [Figure B.3 (B)], drift spectra data [Figrue B.3 (C)] and the 2-D plot of mass-to-charge vs drift time [Figure B.3 (D)] for

all ions in the sample. In the example spectrum of thalidomide [Figure B.3 (E)], we will focus on the mass-to-charge ion at 259.0708, $[M+H]^+$.

c) Expand the Counts vs. Mass-To-Charge window by right clicking and holding on the mass axis and dragging over the desired mass range. (To expand or contract any axis right click hold any axis and move the mouse right or left.) To move the peak right or left, left click and hold the axis and drag accordingly [Figure B.3 (B)].

d) To obtain a drift time spectrum for a specific mass-to-charge region, right click and drag over the desired ion in the drift time vs m/z region. This produces a box around the desired ion [Figure B.3 (F)]. Command "Ctrl X" copies the selected region and "Ctrl D" pastes the spectra in the user drift spectra window [Figure B.3 (G)].

e) This work flow was repeated for each thalidomide enantiomer in both positive and negative ion mode and a processed version is illustrated in the main text as Figure 2.5.

2.6. Acknowledgements

This chapter contains the invited book chapter in Bioinformatics and Drug Delivery: Methods and Protocols, 3rd Ed. in the Methods in Molecular Biology Series: "Isomeric and Conformational Analysis of Small Drug and Drug-Like Molecules by Ion Mobility-Mass Spectrometry (IM-MS)," by Shawn T. Phillips, James N. Dodds, Jody C. May, and John A. McLean. Richard S. Larson and Tudor Oprea, Eds. Springer (to be published in 2018).

Financial support for aspects of this research was provided by The National Institutes of Health (NIH Grant R01GM099218) and under Assistance Agreement No. 83573601 awarded by

the U. S. Environmental Protection Agency. This work has not been formally reviewed by EPA. The views expressed in this document are solely those of the authors and do not necessarily reflect those of the Agency. EPA does not endorse any products or commercial services mentioned in this publication. Furthermore, the content is solely the responsibility of the authors and does not necessarily represent the official views of the funding agencies and organizations. The authors also thank the VU Center for Innovative Technology for support and assistance.

2.7. References

1. Chail, H., DNA sequencing technologies key to the Human Genome Project. *Nature Education* **2008,** *1*, 219.

2. Shekhar, P. C.; Smoczynski, R.; Tretyn, A., Sequencing technologies and genome sequencing. *J. Appl. Genet.* **2011,** *52*, 413-435.

3. Zhang, J. H.; Chung, T. D.; Oldenburg K. R., A simple statistical parameter for use in evaluation and validation of high throughput screening assays. *J. Biomol. Screen* **1999,** *4*, 67-73.

4. Takenaka, T., Classical vs reverse pharmacology in drug discovery. *BJU Int.* **2001,** *88*, 7-10.

5. Harvey, A. L.; Edrada-Ebel, R.; Quinn, R. J., The re-emergence of natural products for drug discovery in the genomics era. *Nat. Rev. Drug Discov.* **2015,** *14*, 111-129.

6. Vaidya, A. D. B., Reverse pharmacology-A paradigm shift for drug discovery and development. *Current Research in Drug Discovery* **2014,** *1*, 39-44.

7. Roses, A. D., Pharmacogenetics in drug discovery and development: a translational perspective. *Nat. Rev. Drug Discov.* **2008,** *7*, 807-817.

8. Nageswara Rao, R.; Talluri, M. V., An overview of recent applications of inductively coupled plasma-mass spectrometry (ICP-MS) in determination of inorganic impurities in drugs and pharmaceuticals. *J. Pharm. Biomed. Anal.* **2007,** *43*, 1-13.

9. Kauppila, T. J.; Wiseman, J. M.; Ketola, R. A.; Kotiaho, T.; Cooks, R. G.; Kostiainen, R., Desorption electrospray ionization mass spectrometry for the analysis of pharmaceuticals and metabolites. *Rapid Commun. Mass Spectrom.* **2006,** *20*, 387-392.

10. Cooks, R. G., Special feature: Historical. Collision-induced dissociation: readings and commentary. *J. Mass Spectrom.* **1995,** *30*, 1215-1221.

11. Wells, J. M.; McLuckey, S. A., Collision-induced dissociation (CID) of peptides and proteins. *Methods Enzymol.* **2005,** *402*, 148-185.

12. Nguyen, L. A.; He, H.; Pham-Huy, C. Chiral drugs: An overview. *Int. J. Biomed Sci.* **2006,** *2*, 85-100.

13. McMurry, J. Organic Chemistry. **2008** *7th ed.* Belmont, CA.

14. NCBI.NLM.NIH.Gov. Search terms "C8H9NO2." Accessed 18 Apr 2017

15. Ferreres, F.; Giner, J. M.; Tomás-Barberán, F. A., A comparative study of hesperetin and methyl anthranilate as markers of the floral origin of citrus honey. *J. Sci. Food Agric.* **1994,** *65*, 371-372.

16. Groessl, M.; Graf, S.; Knochenmuss, R., High resolution ion mobility-mass spectrometry for separation and identification of isomeric lipids. *Analyst* **2015,** *140*, 6904-6911.

17. Xiao, Y.; Vecchi, M. M.; Wen, D., Distinguishing between leucine and isoleucine by integrated LC-MS analysis using Orbitrap Fusion mass spectrometer. *Anal. Chem.* **2016,** *88*, 10757-10766.

18. Takayama, K.; Kilburn, J. O., Inhibition of synthesis of arabinogalactan by ethambutol in mycobacterium smegmatis. *Antimicrob. Agents Chemother.* **1989,** *33*, 1493-1499.

19. Chatterjee, V. K.; Buchanan, D. R.; Friedmann, A. I.; Green, M., Ocular toxicity following ethambutol in standard dosage. *Br. J. Dis. Chest.* **1986,** *80*, 288-291.

20. Carey, R., Organic Chemistry. **1996,** *3rd ed.* McGraw Hill, New York, 89-92.

21. Kothiwale, S.; Mendenhall, J. L.; Meiler, J., BCL::CONF: small molecule conformational sampling using a knowledge based rotamer library. *J. Cheminform.* **2015,** 7:47.

22. Paglia, G., Williams, J. P.; Menikarachchi, L.; Thompson, J. W.; Tyldesley-Worster, R.; Halldórsson, S.; Rolfsson, O.; Moseley, A.; Grant, D.; Langridge, J.; Palsson, B. O., Astarita, G., Ion mobility derived collision cross sections to support metabolomics applications. *Anal. Chem.* **2014,** *86*, 3985-3993.

23. Enders, J. R.; McLean, J. A., Chiral and Structural Analysis of Biomolecules Using Mass Spectrometry and Ion Mobility –Mass Spectrometry. *Chirality* **2009,** *21*, 253-264.

24. Pringle, S. D.; Giles, K.; Wildgoose, J. L.; Williams, J. P.; Slade, S. E.; Thalassinos, K.; Bateman, R. H.; Bowers, M. T.; Scrivens, J. H., An investigation of the mobility separation

of some peptide and protein ions using a new hybrid quadrupole/travelling wave IMS/oa-TOF instrument. *Int. J. Mass Spectrom.* **2007,** *261*, 1-12.

25. Web of Science. Thomson Reuters. Search terms "Ion Mobility" AND "Mass Spectrometry." Articles from 2002-2017. Accessed 15 May, **2017**

26. Paglia, G.; Astarita, G., Metabolomics and lipidomics using traveling-wave ion mobility mass spectrometry. *Nat. Protoc.* **2017,** *12*, 797-813.

27. Stow, S. M.; Lareau, N. M.; Hines, K. M.; McNees, C. R.; Goodwin, C. R.; Bachmann, B. O.; McLean, J. A., *in* "Natural Products Analysis: instrumentation, methods, and applications" (Havlíček, V. and Spížek, J., Eds.) **2014,** 397-432, John Wiley & Sons, Inc., Hoboken, NJ.

28. Sundarapandian, S.; May, J. C.; McLean, J. A., Dual source ion mobility mass-spectrometer for direct comparison of ESI and MALDI collision cross section measurements. *Anal. Chem.* **2010,** *82*, 3247-3254.

29. Cumeras, R.; Figueras, E.; Davis, C. E.; Baumbach, J. I.; Grácia, I., Review on ion mobility spectrometry. Part 1: Current instrumentation. *Analyst* **2015,** *140*, 1376-1390.

30. Cumeras, R.; Figueras, E.; Davis, C. E.; Baumbach, J. I.; Grácia, I. Review on ion mobility . Part 2: Hyphenated methods and effects of experimental parameters. *Analyst* **2015,** *140*, 1391-1410.

31. Adamov, A.; Mauriala, T.; Teplov, V.; Laakia, J.; Pedersen, C. S.;Kotiaho, T., Sysoev, A. A. Characterization of a high resolution drift tube ion mobility spectrometer with a multi-ion source platform. *Int. J. Mass Spectrom.* **2010,** *298*, 24-29.

32. Kanu, A. B.; Dwivedi P.; Tam, M.; Matz, L.; and Hill, H. H. Jr. Ion mobility–mass spectrometry. *J. Mass Spectrom.* **2008**, *43*, 1–22

33. May, J. C.; McLean, J. A., Ion mobility-mass spectrometry: Time-dispersive instrumentation. *Anal. Chem.* **2015,** *87*, 1422-1436.

34. Jurneczko, E.; Kalapothakis, J.; Campuzano, I. D.; Morris, M., Barran, P. E., Effects of drift gas on collision cross sections of a protein standard in linear drift tube and traveling wave ion mobility mass spectrometry. *Anal. Chem.* **2012,** *84*, 8524-8531.

35. Ujma, J.; Giles, K.; Morris, M.; Barran, P. E. New high resolution ion mobility mass spectrometer capable of measurements of collision cross sections from 150 to 520 K. *Anal. Chem.* **2016,** *88*, 9469-9478.

36. Mason, E. A.; McDaniel, E. W. Transport Properties of Ions in Gases, **1988,** John Wiley and Sons, Indianapolis, IN.

37. May, J. C.; Goodwin, C. R.; Lareau, N. M.; Leaptrot, K. L.; Morris, C. B.; Kurulugama, R. T.; Mordehai, A.; Klein C., Barry, W.; Darland, E.; Overney, G.; Imatani, K.; Stafford, G. C.; Fjeldsted, J. C., McLean, J. A. Conformational ordering of biomolecules in the gas phase: Nitrogen collision cross sections measured on a prototype high resolution drift tube ion mobility-mass spectrometer. *Anal. Chem.* **2014,** *86*, 2107-2116.

38. Giles, K.; Williams, J. P.; Campuzano, I. Enhancements in travelling wave ion mobility resolution. *Rapid Commun. Mass Spectrom.* **2011,** *25*, 1559-1566.

39. Shvartsburg, A. A.; Smith, R. D. Fundamentals of traveling wave ion mobility spectrometry. *Anal. Chem.* **2008,** *80*, 9689-9699.

40. Bush, M. F.; Campuzano, I. D.; Robinson, C. V. Ion mobility mass spectrometry of peptide ions: effects of drift gas and calibration strategies. *Anal. Chem.* **2012,** *84*, 7124-7130.

41. Hines, K. M.; May, J. C.; McLean, J. A.; Xu, L. Evaluation of collision cross section calibrants for structural analysis of lipids by traveling wave ion mobility-mass spectrometry. *Anal. Chem.* **2016,** *88*, 7329-7336.

42. Lanucara, F.; Holman S. W.; Gray, C. J.; Eyers, C. E. The power of ion mobility-mass spectrometry for structural characterization and the study of conformational dynamics. *Nat. Chem.* **2014,** *6*, 281-294.

43. May, J. C.; McLean, J. A. A uniform field ion mobility of melittin and implications of low-field mobility for resolving fine cross-sectional detail in peptide and protein experiments. *Proteomics* **2015,** *15*, 2862-2871.

44. Shvartsburg, A. A.; Tang, K.; Smith, R. D. Two-dimensional ion mobility analyses of proteins and peptides. *Methods Mol. Biol.* **2009,** *492*, 417-445.

45. Kurulugama, R. T.; Darland, E.; Kuhlmann, F.; Stafford, G.; Fjeldsted, J. Evaluation of drift gas selection in complex sample analyses using a high performance drift tube ion mobility-QTOF mass spectrometer. *Analyst* **2015,** *140*, 6834-6844.

46. Gaye, M. M.; Nagy, G.; Clemmer, D. E.; Pohl, N. L. Multidimensional analysis of 16 glucose isomers by ion mobility spectrometry. *Anal. Chem.* **2016,** *88*, 2335-2344.

47. Glaskin, R. S.; Valentine, S. J.; Clemmer, D. E. A scanning frequency mode for ion cyclotron mobility Spectrometry. *Anal. Chem.* **2010,** *82*, 8266-8271.

48. Fenn, L. S.; McLean, J. A. Structural separations by ion mobility-MS for glycomics and glycoproteomics. *Methods Mol. Biol.* **2013,** *951*, 171-194.

49. Lalli, P. M.; Corilo, Y. E.; Rowland, S. M.; Marshall, A. G.; Rodgers, R. P. Isomeric separation and structural characterization of acids in petroleum by ion mobility mass spectrometry. *Energy Fuels* **2015,** *29*, 3626-3633.

50. Barnett, D. A.; Ells, B.; Guevremont, R.; Purves, R. W. Separation of leucine and isoleucine by electrospray ionization-high field asymmetric waveform ion mobility spectrometry-mass spectrometry. *J. Am. Chem. Soc.* **1999,** *10*, 1279-1284.

51. Knapman, T. W.; Berryman, J. T.; Campuzano, I.; Harris, S. A.; Ashcroft, A. E. Considerations in experimental and theoretical collision cross-section measurements of small molecules using travelling wave ion mobility spectrometry-mass spectrometry. *Int. J. Mass Spectrom.* **2010,** *298*, 17-23.

52. Dodds, J. N.; May, J. C.; McLean, J. A. Investigation of the complete suite of the leucine and isoleucine isomers: Toward prediction of ion mobility separation capabilities. *Anal. Chem.* **2017,** *89*, 952-959.

53. Li, H.; Bendiak, B.; Siems, W. F.; Gang, D. R.; Hill, H. H. Jr. Ion mobility mass spectrometry analysis of isomeric disaccharide precursor, product and cluster ions. *Rapid Commun. Mass Spectrom.* **2013,** *27*, 2699-2709.

CHAPTER 3

ASSESSING ION MOBILITY RESOLVING POWER THEORY FOR BROADSCALE MOBILITY ANALYSIS WITH A HIGH PRECISION UNIFORM FIELD ION MOBILITY-MASS SPECTROMETER

3.1. Introduction

In the early ion mobility literature, the term "resolving power" was used to characterize the precision and accuracy of an ion mobility spectrometer and was based on the sharpness of a single peak.[1,2] In its initial use, resolving power was a qualitative metric used to compare the relative capabilities of one ion mobility technique or instrument to another. Following the commercialization and development of ambient pressure, uniform field ion mobility spectrometry (IMS) in the 1970s,[3–5] there were several attempts at quantifying the IMS separation efficiency including the use of theoretical plate numbers,[6] two-peak resolution,[8,9] and single-peak resolving power.[7,10,11] Of these, the single peak resolving power was widely adopted and is currently the conventional means by which the separation efficiency of IMS is quantified.[12,13] The experimentally measured ion mobility resolving power (R_m) is a dimensionless ratio defined as the mobility drift time (t_d) divided by the width of the peak (Δt_d):

$$R_m = \frac{t_d}{\Delta t_m} \tag{1}$$

Here, the drift time is measured from the centroid of the ion mobility peak and the peak width is determined using the full width at half maximum (FWHM) definition. The single peak resolving power can be used to directly compare the achievable resolution of different IMS instruments utilizing the same ion mobility technique. Thus, a temporal resolving power definition can directly assess the separation performance between uniform field instruments, but an

alternative definition such as a cross-section based resolving power may be more applicable to compare, for example, a uniform field drift tube to a traveling-wave instrument.[14]

The theoretical drift time of an ion in a uniform electric field is described by a rearrangement of the ion mobility proportionality equation:[15]

$$t_d = \frac{L}{K \cdot E_0} \tag{2}$$

where L is the drift length (cm), K is the ion mobility constant ($cm^2\ V^{-1}\ s^{-1}$) measured under the experimental conditions (*i.e.*, not using a standardized temperature and pressure), and E_0 is the electric field ($V\ cm^{-1}$) in which the IMS separation is being conducted. Equation 2 can be linked through the commonly reported "reduced mobility" value (K_0) by multiplying the right hand side by the standardized temperature and pressure conditions:

$$t_d = \frac{L}{K_0 \cdot E_0} \cdot \left(\frac{273.15}{T} \cdot \frac{P}{760}\right) \tag{3}$$

Here, T and P are the temperature (in K) and pressure (in Torr), respectively, of the drift tube. Equation 3 provides a direct theoretical prediction of the drift time of an ion with a known reduced mobility value under conditions in which the electric field and drift length are well-characterized, such as the case in uniform field IMS. A theoretical expression for peak width, necessary to predict the denominator in equation (1), is somewhat more complicated. Revercomb and Mason derived a peak width expression which includes considerations for ion diffusion and the width of the initial ion packet (gate width, t_g):[7]

$$\Delta t = \left({t_g}^2 + \frac{16ln2 \cdot k_B \cdot T}{V \cdot z \cdot e} \cdot {t_d}^2 \right)^{\frac{1}{2}} \quad (4)$$

Here, three correction terms (α, β, and γ) are introduced and the value of these terms are found through linear regression analysis of empirical data. The α term replaces the diffusion term coefficient in equation (4) ($16\ln 2k_b/ze$) and is related to the ion drift time (residence time in the instrument). Deviations from the value of the diffusion term are attributed to broadening during ion drift, such as effects caused by field inhomogeneity, space-charge, and inelastic ion-neutral interactions. The β term accounts for dependencies on the initial ion gate pulse width, which include space-charge effects and distortions associated with the initial gating event. The γ term is a catch-all for additional sources of variance, such as peak broadening occurring outside of the ion mobility region, detector effects, and post-acquisition distortion of the arrival time distribution. For ideal correspondence to eqn (4), $\alpha = 0.957 \times 103$ V K^{-1}, $\beta = 1$, and $\gamma = 0s^2$.

Combining eqn (3) and (6) with eqn (1) yields the following theoretical expression, termed the semi-empirical resolving power (RSE):

$$R_c = \frac{\frac{L}{K_0 \cdot E_0} \cdot \left(\frac{273.15}{T} \cdot \frac{P}{760} \right)}{\left({t_g}^2 + \frac{16ln2 \cdot k_B \cdot T}{V \cdot e \cdot z} \cdot {t_d}^2 \right)^{\frac{1}{2}}} \quad (5)$$

Once a semi-empirical linear regression analysis is conducted for a particular instrument platform, the correction terms can be included in equation (7) to provide a theoretical means of predicting the resolving power for any analyte with a known gas-phase reduced mobility. The obvious caveat to this semi-empirical approach is that the solution to the correction terms in equation (6) and (7) are instrument-specific and will not have predictive capabilities beyond that of the instrument configuration in which the initial evaluation data was obtained.

In this report, we investigate the extent of agreement between ion mobility resolving power theories and experimental results obtained on a commercially-available ion mobility-mass spectrometer (IM-MS). The IM-MS used in this work is a recently developed uniform field IMS coupled to a quadrupole time-of-flight MS.[22] This instrument is based on the IM-MS designs by Smith and coworkers[23–26] and incorporates a low-pressure (*ca.* 4 Torr) drift tube bracketed by electrodynamic ion funnels for efficient ion trap gating and transmission between spectrometer components. Because this instrument operates at uniform electric field and under conditions of constant temperature and pressure, it is expected that a semi-empirical treatment of resolving power theory should garner further insight into the separation performance of such instruments under constant conditions of controlled IMS parameters.

3.2. Experimental

A commercially-available MS tuning solution consisting of a range of symmetrically-branched phosphazines (Agilent tuning mixture, ATM; Agilent Technologies, Santa Clara, CA) was used to generate the ion mobility data necessary for determining the semi-empirical terms. This ATM solution is predissolved in an acetonitrile/water solution (95:5, % v : v) at a weight-to-volume (w/v) concentration of less than 0.01% for each constituent. The ATM solution was diluted by a factor of ten using a 59:1 (v:v) acetonitrile : water solution prior to use. For generalized comparisons, SDGRG peptide (Sigma-Aldrich), ten-carbon quaternary ammonium salt (TAA10, Sigma-Aldrich) and melittin peptide (Sigma-Aldrich) were obtained as dry powders and used at working concentrations of *ca.* 1 μg mL^{-1}. SDGRG and melittin were reconstituted in a 1:1 methanol:water solution with *ca.* 1% trifluoroacetic acid to promote protonation. TAA10 was dissolved in a 1:1 methanol:chloroform solution.

3.2.1. Uniform Field IM-MS Instrument

The instrumentation used in this study is a commercial IM-MS (6560 Ion Mobility-QTOF, Agilent) and has been described in detail previously.[22] A conceptual schematic detailing the major components of the instrument is contained in Figure 3.1. Briefly, ions are transferred to the ion mobility region through a heated capillary and a two-stage ion funnel. The first ion funnel stage operates at elevated pressures and serves to collect and focus ions exiting the capillary.[24] The second ion funnel stage is configured as a dual-gate ion funnel trap,[25] which operates in a trap-and-release scheme to introduce discretely-gated ion pulses into the IMS. An ion storage time of 2000 μs is used for these experiments. The ion release time (gate width) can be defined anywhere from 0 to upwards of several hundred ms, although for this study the gate widths were surveyed in the range of 100 to 500 μs. Following their release from the ion trap, ions are introduced directly into a uniform field drift tube operated at ambient temperature, which was slightly elevated for all days in which the data was obtained (305.4 ± 0.6 K). The drift tube is constructed from 0.6 mm thick guard rings of 5 cm inner diameter, has a length of 78.1 cm, and is capable of operating in a drift field range from 0.7 to 25 V cm^{-1} (E/N of 0.5 to 19.3 T_d at 4 Torr). Nitrogen (UHP), helium (UHP), and carbon dioxide (Coleman Grade) maintained at *ca.* 4 Torr are used for ion mobility separations described in this work. All gases are passed through a gas purifier trap (nitrogen and helium; RMSN and RMSH, Agilent; for carbon dioxide, and regulated into the IMS through a precision flow controller (640B 10 Torr range, MKS Instruments) monitoring the read-out from an absolute pressure capacitance gauge (CDG 500, Agilent) mounted directly on the drift tube chamber. In a single experiment, this flow controller setup is capable of maintaining a constant drift tube pressure to ±0.01 Torr, which enables high measurement reproducibility. To ensure

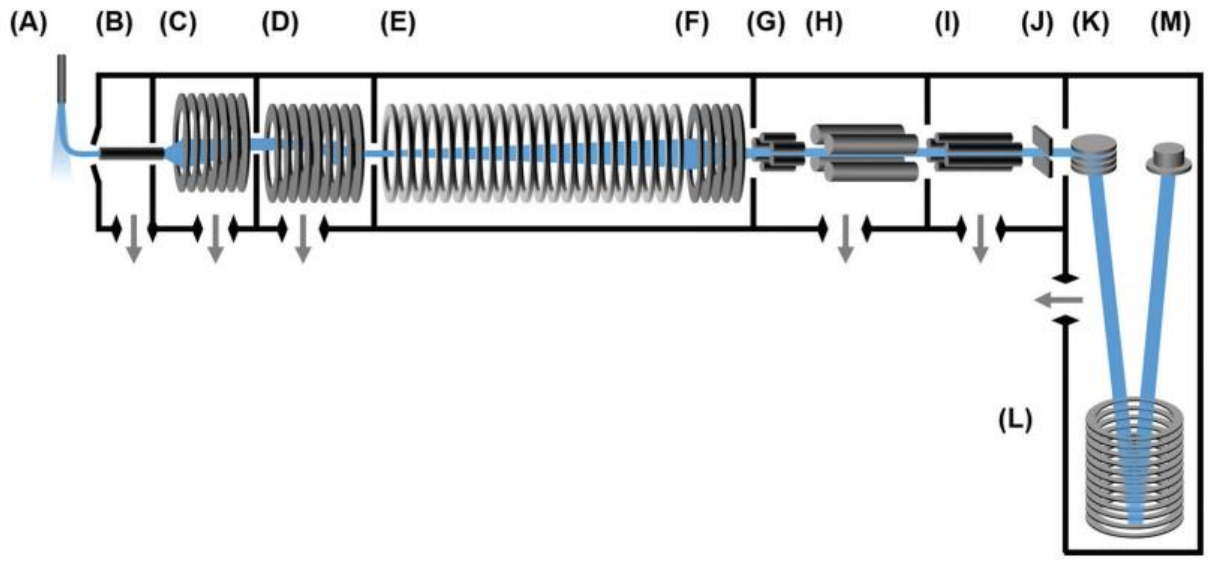

Figure 3.1. A generalized schematic of the uniform field IM-MS used in this work. Instrument components are as follows: **(A)** orthogonal "Jet Stream" electrospray ion source, **(B)** ion transfer capillary, **(C)** high pressure ion funnel, **(D)** trapping ion funnel, **(E)** uniform field drift tube, **(F)** rear ion funnel, **(G)** transfer hexapole, **(H)** quadrupole mass filter, **(I)** hexapole collision cell, **(J)** beam compressor, and **(K)** time-of-flight mass spectrometer, with **(L)** 2-stage reflectron and **(M)** microchannel plate detector. The ion beam path is highlighted in blue.

purity, the IMS is operated at an elevated pressure with respect to the trapping ion funnel region. For nitrogen and carbon dioxide, this pressure difference is *ca.* 150 mTorr. For helium, it was found that a difference of *ca.* 230 mTorr or greater is necessary to ensure drift gas purity. Following IMS separation, radially diffuse ions are recollected by a third ion funnel located at the exit end of the drift tube. This rear ion funnel is operated at the same pressure (4 Torr) as the drift tube with a DC field of *ca.* 18 V cm^{-1}. Following the IMS, ions are transferred through a hexapole into the high vacuum Q-TOF stage of the instrument, where they are analyzed by their mass-to-charge. Optional mass selection and ion activation (collision-induced dissociation) can be conducted in this interfacing region between the IM and MS stages, though these schemes are not utilized in this present work. Although the time-of-flight mass spectrometer is capable of a resolving power greater than 40,000 ($m/\Delta m$), for purposes of these experiments the instrument was operated with settings designed to improve sensitivity and mass transmission range ("extended dynamic range" mode), and this resulted in a mass resolving power of *ca.* 20,000.

The ATM solution used to evaluate the semi-empirical fits was infused into one of two ion sources: a dual electrospray ionization source (dual "Jet Stream", Agilent), or an orthogonally-configured nano-electrospray ionization source (G1992A Nanospray, Agilent). For the Jet Stream source, the ATM solution was infused from the "reference B" sample solution reservoir with the default injection backpressure. For nanoelectrospray, the ATM solution was directly infused using a syringe pump (Cole-Parmer) at a flow rate of *ca.* 1 μL min^{-1}.

3.2.2. Analytical Precision

The instrumentation used in this work is considered a "high precision" ion mobility instrument in that it is capable of obtaining reproducible measurements of the mobility drift time to better than 0.1 ms. For conversion of drift time measurements to ion transport coefficients (K_0 and collision cross section), this represents a relative error of better than 0.5%.[22] Analytical precision affects the reproducibility of the ion mobility drift time, but does not directly affect the FWHM.

3.3. Data Acquisition and Analysis

All ion mobility data was obtained using the MassHunter Data Acquisition software (Agilent). A software feature which allows individual experimental sequences to be defined was utilized to obtain consecutive ion mobility spectra at various drift potentials between 350 and 1750 V (4.5 to 22.4 V cm^{-1}) in increments of 100 V. This corresponds to instrument settings from 600 V to 2000 V for the "drift tube entrance" potential and 250 V for the "drift tube exit" potential. For each sequence, data was signal averaged for 2 minutes. These drift voltage sequence experiments were acquired for initial ion gate widths ranging from 100 to 500 μs in 100 μs increments, which corresponds to the ion release time setting in the instrument control software. Following acquisition, each segmented data file was analyzed using the MassHunter IMS Browser software (Agilent). Peaks of interest were isolated and their centroid drift time values and FWHM were extracted as tabulated data using capabilities within the software. In some cases, the FWHM was determined manually. K_0 values necessary to conduct the resolving power analysis were obtained directly from the software, using procedures previously described.[22] Briefly, this involves conducting drift time measurements for a sequence of fields in order to determine the time

component associated with ion transit outside of the mobility region. K_0 can then be solved *via* equation (3).

3.3.1. Semi-empirical Fitting Procedure

The semi-empirical coefficients (α, β, and γ) for equation (6) and (7) were determined for each ion system using procedures outlined by Siems *et al.*[12] Details of the procedure as utilized in this study are included in the ESI. Briefly, this involves a linear regression analysis of equation (6). The α coefficient is the slope of the best-fit line to data projected as Tt_d^2/V (the diffusion parameter) versus Δt^2 for a series of ions. The β coefficient is determined from a slope of the best-fit line to data plotted as t_g^2 versus Δt^2. The γ coefficient is obtained through orthogonal correlation of results from the linear regression analysis of α and β. Plots corresponding to this analysis are contained in Figure C.5 and C.7. A strong correlation was observed between the ion species and the β and γ coefficients, so these terms were replaced with an equation which includes K_0 (Figure C.8). These coefficients and coefficient equations are summarized at the bottom of Table 1.

3.4. Results and Discussion

3.4.1. Factors affecting semi-empirical coefficients

Because each of the semi-empirical coefficients are associated with a specific component of variance from equation 6, their deviation from the "ideal" values (equation 4) can provide some insight into the physical source of band broadening within the instrument. For the α coefficient, previous work has demonstrated this value is consistently larger in stand-alone drift tube

Ion	K_0 ($cm^2\ V^{-1}\ s^{-1}$)	$\alpha \times 10^3$ ($V\ K^{-1}$)	β	γ (ms^2)
m/z 322	1.39	0.87	0.536	0.07
m/z 622	1.01	0.84	0.298	0.06
m/z 922	0.83	0.93	0.181	0.07
m/z 1222	0.72	0.96	—	0.07
m/z 1522	0.64	0.96	—	0.15
m/z 1822	0.58	0.89	—	0.24
m/z 2122	0.53	0.87	—	0.30
m/z 2422	0.49	0.97	—	0.25
m/z 2722	0.46	0.87	—	0.48

$\alpha = 0.91 \times 10^3$
$\beta = 0.3145\ (K_0)^2 - 0.035\ (K_0)$
$\gamma = 0.0434\ (K_0)^{(-2.811)}$

[a] K_0 is calculated in nitrogen from 4 replicate measurements; variable gate width data for the β coefficient experiments was limited to *m/z* 322, 622, and 922.

Table 3.1. Summary of results from the semi-empirical linear regression analysis. K_0 values are for nitrogen drift gas[a]

instruments than the ideal value of 0.957 × 10−3 V K^{-1}, with experimental α values of *ca.* 1.2 × 10−3 V K^{-1} or greater.[12] This observation has been previously attributed to inhomogeneity in the electric field. In this work, we obtain an average α value of 0.910 × 10−3 V K^{-1} (Table 3.1), which does not depend strongly on the ion species (Figure C3). The α value found in this study is close to the ideal value. A cursory explanation would be that the drift tube in this work operates with a high degree of homogeneity, yet ions also pass through an electrodynamic ion funnel prior to being measured (Figure 1F). Because α is essentially the magnitude of the response of the peak width to the drift time, we can only say that for the current instrumentation, peaks broaden as expected from diffusion. This may be a general characteristic of drift tubes coupled to MS via a conductance-limiting aperture, as the previous work had been carried out on ambient pressure instrumentation using relatively large diameter Faraday plate detectors which would sample the entire radially-diffuse ion cloud. The explanation of β and γ is not so straightforward. Previous work had characterized these coefficients using measurements obtained from a single ion (Cl^-, H_3O^+, or O_2^-), and thus the β and γ values were previously reported as a single value for each instrument geometry evaluated. In this present study, we evaluated these semi-empirical terms using a series of analytes possessing a wide range of mobility values. Thus, our results for β and γ are different for each ion investigated (Table 3.1). For β, we obtain a range of values from 0.181 to 0.536, which is significantly smaller than the ideal situation of β = 1. In the previous study by Siems *et. al.*, β was consistently greater than 1 (*ca.* 1.1 to 1.6). Since β is a multiplier for the gate width, this coefficient represents a correction for peak width variations which are caused during the ion gating event. Values greater than 1 were explained as originating from additional band broadening due to space-charge effects (Coulombic repulsion), which would become greater as the pulse width was increased, *i.e.*, as more ions were introduced per pulse. In contrast, all of the β values measured in

this work were well below 1, suggesting that the resulting ion pulse widths are narrower than would be expected from the time duration that the ions are admitted into the drift tube via the control software (*i.e.*, the applied temporal gate width). We infer that this is a consequence of conducting the ion gating using an ion trap, rather than a more traditional electrostatic ion depletion gate (Tyndall or Bradbury-Nielsen gate). A similar ion compression effect has been observed when operating the ion gate region using multiple grid stages,[27,28] and we suggest a field-focusing behavior may also be occurring in the present instrumentation which utilizes a similar 2-grid structure in the region of ion confinement.[25] We note that unlike what is observed for most ambient pressure IMS instruments, this instrument operates closer to the diffusion limit in terms of resolving power. For γ, the ideal value is 0 s^2, that is, no additional sources of variance other than the initial gate width and normal diffusion.[16] For previous drift tubes, the value for γ was found to vary anywhere from 0.47×10^{-8} s^2 to as high as 2.1×10^{-8} s^2 , 12 which corresponds to an added variance of between *ca.* 0.07 to 0.14 ms. In this work, the value of γ determined for the present instrumentation was found to be ion dependent, with upper values of 4.8×10^{-7} s^2 (Table 3.1), which corresponds to a variance of *ca.* 0.69 ms. This value of γ is about 5-fold greater than what was determined in the previous study, where the source of band broadening was attributed to image current induction and detector response effects for the Faraday detector used. For the present IM-MS instrument, the IMS spectra are obtained through temporal correlation of ion signal from the electron multiplier in the MS stage. Microchannel plate electron multipliers exhibit peak broadening effects on the order of picoseconds,[29] and so detector effects would not be an issue in this current work. We suggest that the primary source for γ is due to ion transit through the rear ion funnel, which is not accounted for in the length term used to determine the theoretical drift time from equation 3. This claim is supported by the observation that γ is mobility-dependent

(Table 3.1). The relatively large values for γ suggest that there is a significant contribution to band-broadening occurring in the rear funnel, yet the measured resolving power values and the analysis of the α coefficient both suggest that the instrument is operating near the diffusion limit. One explanation for this is that the band broadening which occurs in the rear funnel is counteracted by the additional mobility separation which occurs due the rear funnel operating as an extension of the drift tube. The additional contribution of the rear ion funnel as a mobility separator which operates with no significant loss in resolving power has been noted in a previous study.[23] While the data in this current work also suggests that the funnel operates as an extension of the drift tube, no attempt was made to match the field between the drift tube and the rear funnel, which would be expected to further improve the quantitative agreement between experiment and theory. Finally, it is worth noting that drift time correction is not utilized in this study due to the difficulty in determining the peak width contribution of the non-mobility transit time of the ions. While not investigated further here, the temporal contribution of the rear ion funnel is well characterized and could be incorporated into the ion mobility peak width theory in the form of an added source of variance, as the ion funnel length (11.6 cm), pressure (4 Torr), and electric field (17.8 V cm^{-1}) used in this present study are known.

3.4.2. Empirical Correlation of Theoretical Resolving Power

Once the semi-empirical coefficients are determined for a wide range of gate widths and ion systems, equation 7 can be expanded in order to generate a generalized resolving power expression which describes the performance of the current instrumentation. These results are provided as equation (S10) in the ESI. An evaluation of both the conditional and semi-empirical theories

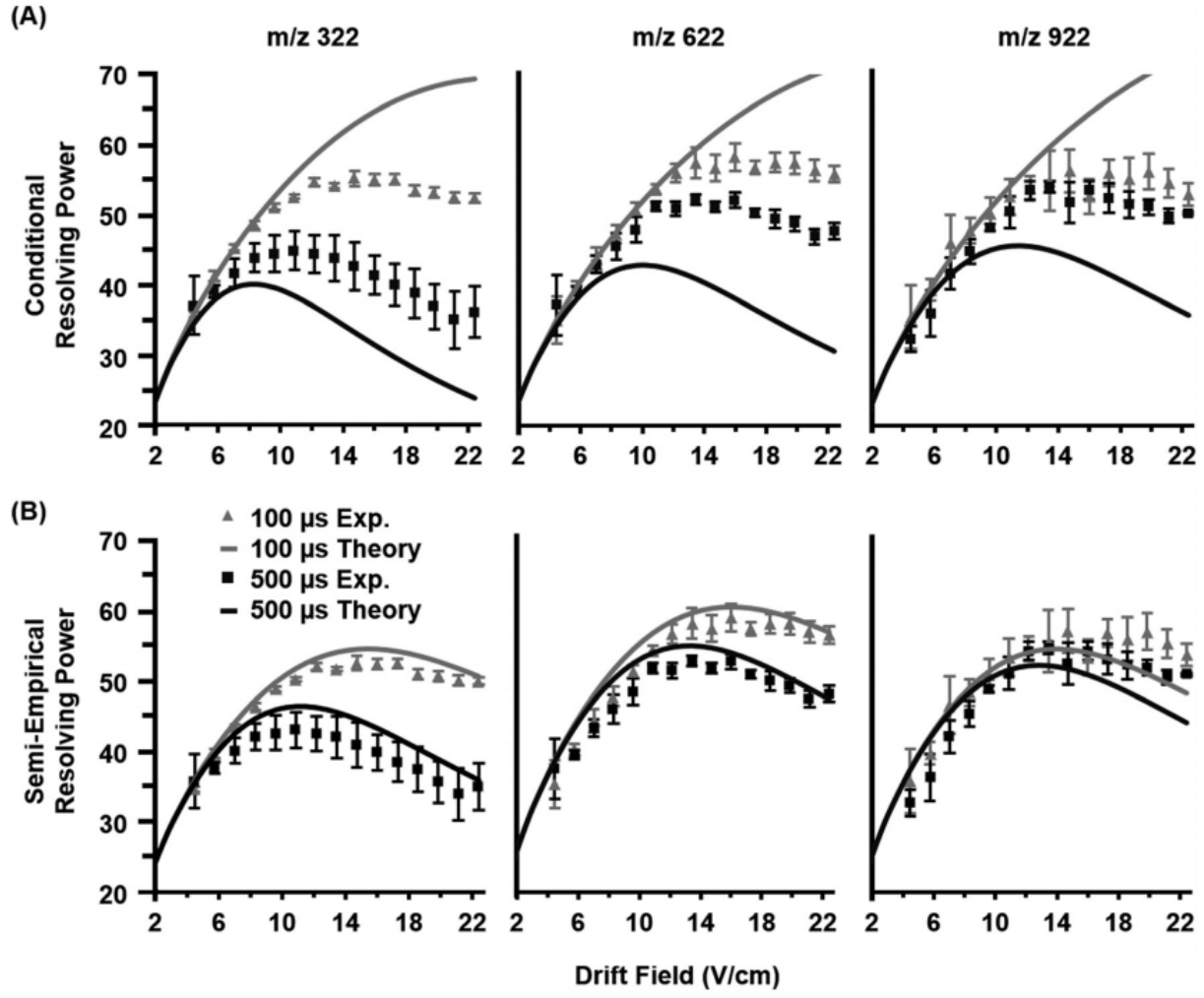

Figure 3.2. Empirical resolving power curves (data points) compared to theory (solid lines) as a function of the ion mobility separation field (drift field) for three molecular ions (nominal m/z 322, 622, and 922). Error bars for each point are obtained from four replicate measurements. **(A)** The conditional resolving power (R_c) from equation (5) predicts the qualitative trends of the experimental observations, but quantitative correlation varies based on the ion system and gate width used. **(B)** The semi-empirical resolving power (RSE) from equation (7) exhibits a more quantitative correlation than the conditional resolving power for all gate widths investigated in this study (100, 200, 300, 400, and 500 µs). For clarity, only the data for 100 and 500 µs gate widths are shown.

is contained in Figure 3.2 for the m/z 322, 622, and 922 ions. Experimental data is projected as points with error bars obtained from 4 replicate measurements. Of general note is that in many cases, the error associated with the measured resolving power for a single data point is in excess of 5%. This reflects the challenges associated with obtaining quantitatively-reproducible measurements of the peak width, as opposed to the drift time which exhibits close correlation to equation 3 (Figure B.1). In Fig. 2.1 A, the conditional resolving power theory via equation 5 exhibits only qualitative agreement with experimental results, with significant deviation being observed at low and high gate widths. Conditional resolving power consistently predicts significantly better resolving power when using lower gate widths, but the data suggests that this is only significant when studying low-mass ions (*i.e.*, ions possessing high K_0 values above *ca.* 1 $cm^2\ V^{-1}s^{-1}$). Experimental results indicate that higher mass ions do not benefit significantly in resolving power from smaller gate widths, and so for such studies, increasing the gate width would be advantageous to improve instrument sensitivity. This gate width dependence on the accuracy of equation 5 is consistent with previous observations,[13] and deviation has also been noted in experimental measurements at extreme pressures (up to 2280 Torr).[30] Note that a gate width of 200 μs is commonly utilized in IMS studies, and under this condition, there is a coincidentally good correlation between conditional resolving power theory and experimental results (Figure C.2), which suggests that deviations between theory and experiment are not obvious under routine investigations. To our knowledge this work represents the first study where the conditional resolving power was explicitly tested for ions spanning a wide range of reduced mobilities (Table 3.1), and in particular, for larger ions with K_0 values below *ca.* 1 $cm^2\ V^{-1}s^{-1}$ as what would be encountered for biomolecules. This work also represents the first comprehensive study of resolving power theory for reduced pressure IMS. Because the present instrumentation is configured in a

manner that is far from the conditions assumed by conditional resolving power (*i.e.*, ion trap gating, sub-ambient IMS pressures, and post-mobility focusing via the ion funnel), the observed deviations between conditional resolving power theory and empirical results is not surprising, particularly for larger ions which spend more time in the IMS stage of the instrument. Figure B.2 B contains the results from the semi-empirical resolving power theory via eqn (7) utilizing the methods described in the ESI. A significant improvement in the correlation between experiment and theory is observed in this case across all initial ion gate widths investigated (100 to 500 μs, cf. Figure C.3). Some deviation does occur for the lower mobility ion, m/z 922, where the semi-empirical treatment underpredicts the resolving power by about 15% on the high end, which is a fairly consistent deviation across all gate widths at this mobility (Figure C.3). Similar results are also observed for the m/z 2722 ion (Figure C.4). The m/z 922 ion was explicitly used in the initial evaluation of the semi-empirical theory, and so better correlation was anticipated, but this would appear to be a more realistic expectation of accuracy when working with a theory generalized against a wide range of parameters. Because both the conditional and semi-empirical resolving power expressions account for the ion's reduced mobility, a 3-dimensional resolving power curve can be obtained which is ion species dependent. Figure 3.3 contains the resulting 3D analysis for both the conditional resolving power of eqn (5) (Figure C.3 A), and the semi-empirical resolving power of equation 7 (Figure C.3 B). Both curves were generated using a drift gas pressure of 4.00 Torr and a temperature of 304.2 K and describe the performance of singly-charged ions only. A gate width of 200 μs was also chosen for comparison between the two theories, as the best correlation between conditional resolving power and experimental data was observed at this setting, meaning any differences observed between the two theories at this gate width is expected

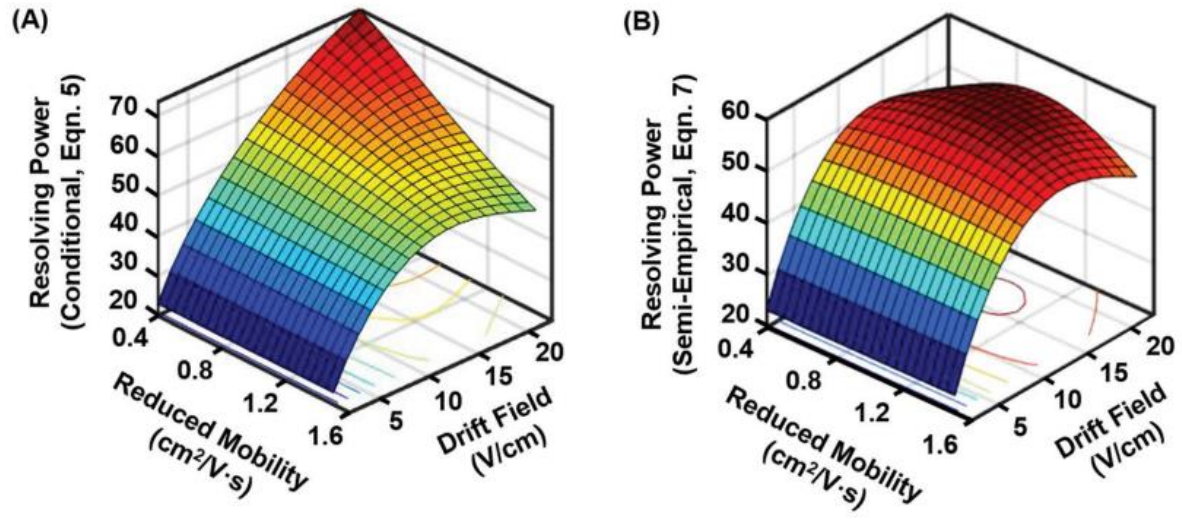

Figure 3.3. 3D resolving power curves projecting the predicted resolving power for singly-charged ions across a range of drift fields and ion mobilities. **(A)** Conditional resolving power (equation 5), and **(B)** semi-empirical resolving power via equation (7) using coefficient expressions obtained in this current work. Both expressions assume 4 Torr drift gas pressure with an initial gate width of 200 μs. As compared with the conditional resolving power, the semi-empirical resolving power predicts a relatively narrow drift field range for accessing the optimal resolving power, as well as a more uniform resolving power response for a wide range of ion species.

to be significant. Conditional resolving power predicts that higher resolving powers are accessible as the mobility of the ion decreases (*i.e.*, large ions), and that accessing these higher resolving powers requires different drift fields.[18] This observation suggests that conditional resolving power theory underestimates diffusional effects that increase with lower mobilities, which is accounted for in the semiempirical treatment. Additionally, the semi-empirical treatment pertaining to observations from the current instrument indicates that the resolving power performance is relatively linear across a range of ion mobilities. This observation is better illustrated by extracting the resolving power maxima (highest values) for both 3D surfaces and plotting these as a function of K_0 (Figure C.4 A). This analysis indicates there is good correlation between conditional and semi-empirical resolving power theory at high mobilities (fast ions) where ions spend a limited amount of time in the mobility region, but deviation becomes significant in the low mobility (slow ions) regime. This deviation between the two theories occurs at a K_0 of *ca.* 1 $cm^2\ V^{-1}s^{-1}$, which for a peptide drifting in nitrogen represents an analyte mass of *ca.* 500 Da.[22] Additional molecular class specific mobility ranges for nitrogen drift gas are projected at the bottom of the plot to help frame these observations in the context of practical results. The implication of this observation is that for the current instrumentation, the accuracy of predictions made by the conditional resolving power theory are limited to small analyte systems (*i.e.*, ions with high K_0 values). A second observation which can be made from Figure C.3 is that the highest resolving power values predicted by the semi-empirical theory are fairly constant and experimentally-accessible across a relatively narrow range of drift fields (between 14 and 17 V cm^{-1}). This can be better illustrated by plotting the drift field corresponding to the highest resolving power values as a function of the ion's reduced mobility (Figure C.4 B). Thus, in practice, accessing high resolving power values should require only minor adjustments to the drift field. Taken collectively, these observations

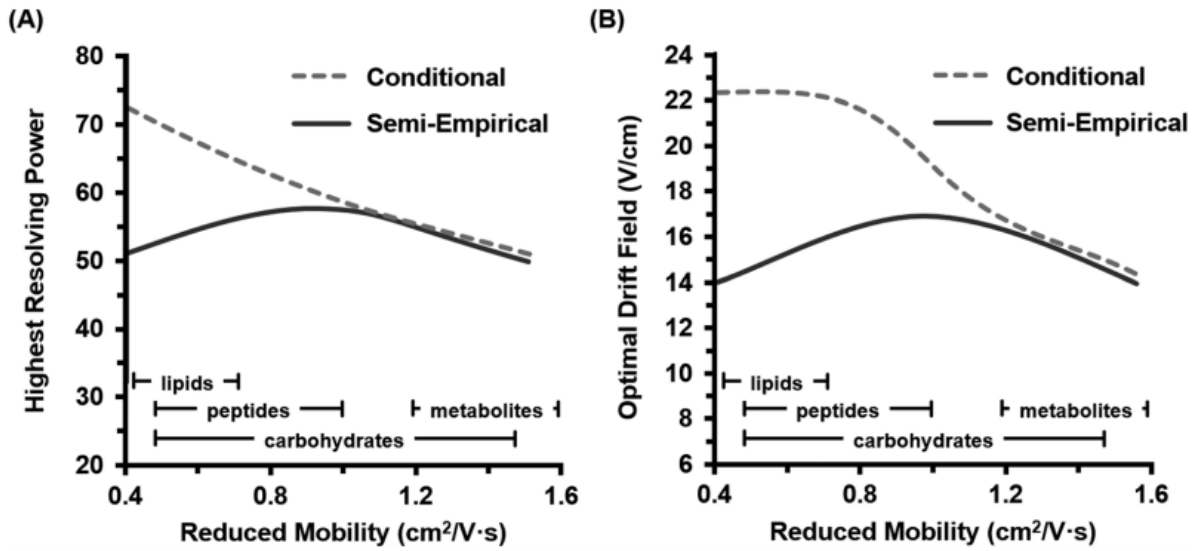

Figure 3.4. Plots of the highest achievable resolving power values predicted by both theories for singly-charged ions. Trends are extracted from the maxima in Figure 3.3 (*i.e.*, the "crest" of each surface plot). **(A)** The highest (optimal) resolving power accessible as a function of the reduced mobility. Corresponding molecular class-specific mobility ranges are also provided for ion mobility in nitrogen drift gas (lower bars). **(B)** The required drift field necessary to access the optimal resolving power as a function of the reduced mobility. Both projections indicate that the semi-empirical resolving power theory predicts a narrow range of both optimal resolving powers (50 to 60) and drift fields (14 to 17 Vcm^{-1}) across a fairly wide range of mobilities.

suggest that the present instrumentation performs at optimal resolving power for a wide dynamic range of ion species under similar operational conditions. This may be a general observation for all ion mobility instrumentation, as quantitative investigations of the conditional resolving power to date have focused only on small analytes with reduced mobility values greater than 1.2 $cm^2 V^{-1}s^{-1}$,[13,18,31,32] although this study also represents the first test of conditional resolving power theory for reduced pressure IMS, so these results may also be specific to subambient pressure operation around 4 Torr.

3.4.3. Broadscale Validity of Semi-Empirical Results

In order to further investigate the extent of correlation between experiment and theory, three ions systems exhibiting vastly different gas-phase transport properties were compared against the current theories. The ion systems used in this comparison are: (1) a small peptide in nitrogen with a K_0 close to 1 (SDGRG, K_0 = 1.02 $cm^2V^{-1}s^{-1}$),[22] (2) a quaternary ammonium cation in carbon dioxide, which exhibits very low mobility (TAA10, K_0 = 0.50 $cm^2V^{-1}s^{-1}$), and (3) a triply-charged peptide (melittin bee venom) in helium,[33] which has a very high gas phase mobility (K_0 = 3.03 $cm^2V^{-1}s^{-1}$). Typical operational conditions (200 μs gate width and 4 Torr drift gas) are used in these comparisons. Note that both theories are drift gas independent, since both theoretical expressions describe ion transport in terms of the gas-phase reduced mobility, which inherently accounts for differences in ion motion in various drift gases. Thus, the theories developed in this work are applicable to a variety of drift gases. Experimental results for the three ion systems are contained in Figure 3.5. For ions with reduced mobility values around *ca.* 1 $cm^2V^{-1}s^{-1}$, both theories correlate well with experimental results (Figure 3.5 A). This is consistent with the previous observation for m/z 622 (K_0 = 1.01 $cm^2V^{-1}s^{-1}$) at this gate width (Figure C.2 and C.3).

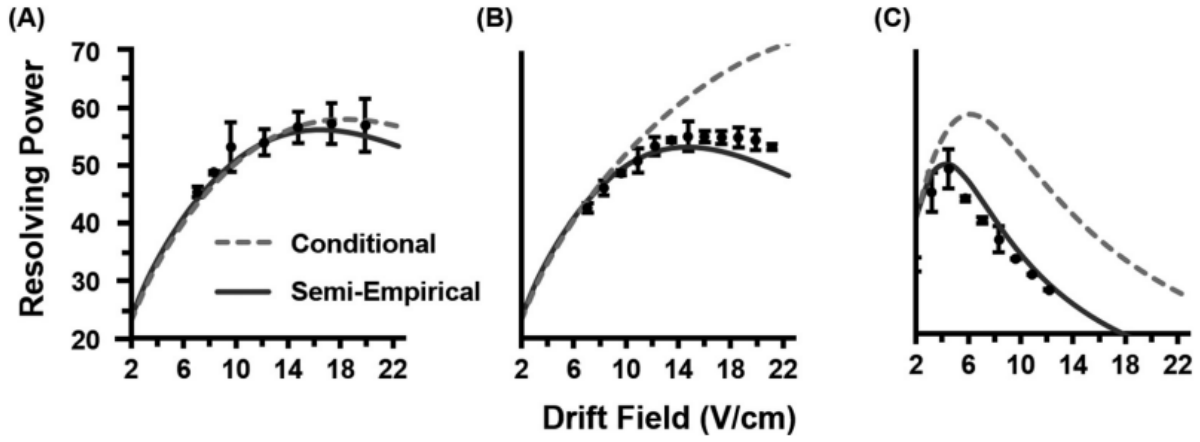

Figure 3.5. Comparison of experiment and theories generalized to a wide range of reduced mobility values. **(A)** Singly-charged SDGRG peptide measured in nitrogen drift gas (K_0 = 1.02 $cm^2V^{-1}s^{-1}$) exhibits good correlation to both theories. **(B)** Singly-charged quaternary ammonium cation with ten-carbon branches (TAA10) measured in carbon dioxide drift gas possesses a very low mobility value (K_0 = 0.50 $cm^2V^{-1}s^{-1}$), and here the semi-empirical resolving power better predicts the experimental resolving power of this system. **(C)** The triply-charged melittin peptide in helium drift gas exhibits a high mobility (K_0 = 3.03 $cm^2V^{-1}s^{-1}$) as well as being multiply-charged, which despite the unconventionally high mobility still shows good correlation to the semi-empirical resolving power developed in this work.

At low mobilities, which represents large ions or ions drifting in more massive drift gases (such as carbon dioxide in this case), conditional resolving power theory significantly overestimates the magnitude of the resolving power, whereas the semiempirical theory correlates closely to experimental results, albeit with slightly underestimated predictions (Figure 3.5B). This is similar to the trends observed for the m/z 922 system (Figures 3.2C, S2 and S3). In the third case for very high mobility ions, both theories show qualitative agreement, with semiempirical theory correlating better than conditional resolving power (Figure 3.5 B). Note that in this latter system, a multiplycharged ion is evaluated (z = 3), and thus requires that the integer charge state be introduced into the denominator of the diffusion term in the semi-empirical theory. Extension of the semi-empirical theory to higher charge-state systems was not an original intention of this work, but results are indeed favorable. We caution here, however, that preliminary work with a protein exhibiting even higher charge states (myoglobin, z = 9 to 24) has not resulted in the good correlation to semi-empirical theory as seen for the melittin system, so further refinement to the theory is necessary. While the systems in Figure 3.5 represent extreme cases in terms of the reduced mobility, the good correlation observed indicates that the semi-empirical theory can be qualitatively extended beyond the range in which it was initially evaluated (*cf.*, Table 3.1).

3.5. Conclusions

A wide-scale evaluation of two current theories for ion mobility resolving power (conditional and semi-empirical) was applied to high precision results obtained on a recently developed IM-MS instrument. The predictive capabilities of conditional resolving power theory were found to be qualitatively good for high mobility ions (*e.g.*, small molecules), but deviated significantly for low mobility ion systems and gate widths beyond 200 μs. Better correlation to

experimental observations was found for a semi-empirical treatment of resolving power which was developed using empirical data on the current instrumentation, and initial evaluation of the semi-empirical theory demonstrated good correlation across a relatively wide range of ion mobilities (K_0 between 0.50 and 3.03 $cm^2V^{-1}s^{-1}$). The semi-empirical theory was used to generalize the performance of the current instrument and results suggest that the instrumentation is capable of accessing the optimal resolving power for a wide range of analytes within a relatively narrow range of drift fields, independent of the drift gas utilized. When taken collectively, these observations indicate that the linear response of the instrument in terms of ion mobility separation efficiency is high. The decreased dependency of the gate width on the accessible resolving power for lower mobility ions (K_0 below *ca.* 1 $cm^2V^{-1}s^{-1}$) indicates that for higher mass studies (greater than m/z of *ca.* 500), the gate width may be increased to improve sensitivity without a significant loss in resolving power. As with any semi-empirical treatment, the results are specific to the instrumentation and experimental conditions used in this study, namely operating the drift tube at *ca.* 4 Torr and ambient temperature, and investigating low charge-state ions. Conditional resolving power is thus recommended over the current semi-empirical theory for estimating the accessible resolving power for ion mobility instrumentation that differs significantly from the present study, such as ambient pressure drift tubes and stand-alone IMS instruments. Finally, it should be noted that obtaining quantitatively reproducible resolving power values on any drift tube platform is challenging without careful attention to maintaining drift gas purity and stability of all important ion mobility conditions, specifically drift fields, gas pressures, temperatures, and robust methods to extract the quantitative data (drift time centroids and temporal peak widths) from the raw measurements. The high precision capabilities of the present instrumentation greatly facilitates these types of quantitative studies.

3.6. Acknowledgements

This chapter contains the published research article: James N. Dodds, Jody C. May, and John A. McLean, "Broadscale Resolving Power Performance of a High Precision Uniform Field Ion Mobility-Mass Spectrometer," *Analyst*, **2015,** *140*, 6824-6833.

J.C.M, J.N.D, and J.A.M. thank M. Ray Keller for assistance in data analysis and Katrina L. Leaptrot for reviewing various drafts of the manuscript. Vanderbilt authors gratefully acknowledge a Thought Leader award from Agilent Technologies. Financial support for this research was provided by Agilent Technologies, the National Institutes of Health National Center for Advancing Translational Sciences (NIH-NCATS Grant 4UH3TR000491-3), the National Science Foundation (MRI CHE-1229341), the Vanderbilt Institute of Chemical Biology, the Vanderbilt Institute for Integrative Biosystems Research and Education, and Vanderbilt University.

3.7. References

1. Israel, H.; Schulz, L., The Mobility-Spectrum of Atmospheric Ions-Principles of Measurements and Results. *Terr. Magn. Atmos. Electr.* **1933** *38*, 285-300.

2. Bradbury, N. E.,The Absolute Values of the Mobility of Gaseous Ions in Pure Gases. *Phys. Rev.* **1932**, *40*, 508-523.

3. Cohen, M. J.; Karasek, F. W., Plasma Chromatography-A New Dimension for Gas Chromatography and Mass Spectrometry. *J. Chromatogr. Sci.* **1970**, *8*, 330-337.

4. Cram, S. P.; Chesler, S. N., Coupling of High Speed Plasma Chromatography with Gas Chromatography. *J. Chromatogr. Sci.*, **1973,** *11*, 391–401.

5. Karasek, F. W. Plasma Chromatography. *Anal. Chem.*, **1974,** *46*, 710A-720A.

6. Spangler, G. E.; Collins, C. I., Peak Shape Analysis and Plate Theory for Plasma Chromatography. *Anal. Chem.* **1975**, *47*, 403-407.

7. Revercomb, H. E.; Mason, E. A., Theory of Plasma Chromatography/Gaseous Electrophoresis. Review, *Anal. Chem.* **1975**, *47*, 970-983.

8. F. W. Karasek, Study of Technology Relating to Plasma Chromatography Sensing Tubes, Final Report, Contract #8SU77-00227, University of Waterloo Research Institute, Waterloo, Ontario, Canada, **1980**.

9. Carrico, J. P.; Sickenberger, D. W.; Spangler, G. E.; Vora, K. N.,Simple Electrode Design for Ion Mobility Spectrometry. *J. Phys. E: Sci. Instrum.*, **1983,** 16, 1058-1062.

10. Rokushika, S.; Hatano, H.; Baim, M. A.; Hill, H. H., Resolution Measurement for Ion Mobility Spectrometry. *Anal. Chem.* **1985**, *57*, 1902-1907.

11. Watts, P.; Wilders, A., On the Resolution Obtainable in Practical Ion Mobility Systems. *Int. J. Mass Spectrom. Ion Processes,* **1992,** *112*, 179-190.

12. Siems, W. F.; Wu, C.; Tarver, E. E.; Hill, H. H.; Larsen, P. R.; McMinn, D. G., Measuring the Resolving Power of Ion Mobility Spectrometers. *Anal. Chem.*, **1994,** *66*, 4195-4201.

13. Kanu, A. B.; Gribb, M. M.; Hill, H. H., Predicting Optimal Resolving Power for Ambient Ion Mobility Spectrometry. *Anal. Chem.* **2008**, *80*, 6610-6619.

14. May, J. C.; McLean, J. A., Ion Mobility-Mass Spectrometry: Time-Dispersive Instrumentation. *Anal. Chem.* **2015,** *87*, 1422-1436.

15. Mason, E. A.; McDaniel, E. W., *Transport Properties of Ions in Gasses,* **1998.**

16. Spangler, G. E., Expanded Theory for the Resolving Power of a Linear Ion Mobility Spectrometer. *Int. J. Mass Spectrom.* **2002**, *220*, 399-418.

17. Glasser, M. L., Peak Shape Analysis for Ion Mobility Spectroscopy. *J. Appl. Phys.* **1988,** *63*, 4823-4831.

18. Davis, E. J.; Williams, M. D.; Siems, W. F.; Hill, H. H., Voltage Sweep Ion Mobility Spectrometry. *Anal. Chem.* **2011,** *83*, 1260-1267.

19. Verbeck, G. F.; Ruotolo, B. T.; Gillig, K. J.; Russel, D. H., Resolution Equations for High-Field Ion Mobility. *J. Am. Soc. Mass Spectrom.*. **2004**, *15*, 1320-1324.

20. Mariano, A. V.; Su, W.; Guharay, S. K., Effect of Space Charge on Resolving Power and Ion Loss in Ion Mobility Spectrometry. *Anal. Chem.* **2009,** *81*, 3385-3391.

21. Tolmachev, A. V.; Clowers, B. H.; Belov, M. E.; Smith, R. D., Coulombic Effects in Ion Mobility Spectrometry. *Anal. Chem.* **2009,** *81*, 4778-4787.

22. May, J. C.; Goodwin, C. R.; Lareau, N. M.; Leaptrot, K. L.; Morris, C. B.; Kurulugama, R. T.; Mordehai, A.; Klein, C.; Barry, W.; Darland, E.; Overney, K.; Imatani, K.; Stafford, G. C.; Fjeldsted, J. C.; McLean, J. A., Conformational Ordering of Biomolecules in the

Gas Phase: Nitrogen Collision Cross Sections Measured on a Prototype High Resolution Drift Tube Ion Mobility-Mass Spectrometer. *Anal. Chem.* **2014**, *86*, 2107-2116.

23. Tang, K.; Shvartsburg, A. A.; Lee, H.-N.; Prior, D. C.; Buschbach, M. A.; Li, F.; Tolmachev, A. V.; Anderson, G. A.; Smith, R. D., *Anal. Chem.* **2005,** *77*, 3330-3339.

24. Baker, E. S.; Clowers, B. H.; Li, F.; Tang, K.; Tolmachev, A. V.; Prior, D. C.; Belov, M. E.; Smith, R. D., Ion Mobility Spectrometry-Mass Spectrometry Peformance Using Electrodynamic Ion Funnels and Elevated Drift Gas Pressures. *J. Am. Soc. Mass Spectrom.* **2007,** *18*, 1176-1187.

25. Clowers, B. H.; Ibrahim, Y.; Prior, D. C.; Danielson, W. F.; Belov, M.; Smith, R. D., Enhanced Ion Utilization Efficiency Using an Electrodynamic Ion Funnel Trap as an Injection Mechanism for Ion Mobility Spectrometry. *Anal. Chem.* **2008**, *80*, 612-623.

26. Ibrahim, Y. M.; Baker, E. S.; Danielson, W. F.; Norheim, R. V.; Prior, D. C.; Anderson, G. A.; Belov, M. E.; Smith, R. D., Development of a New Ion Mobility (Quadrupole) Time-of-Flight Mass Spectrometer. *Int. J. Mass Spectrom.* **2015,** *377*, 655-662.

27. Du, Y.; Wang, W.; Li, H., Bradbury-Nielsen-Gate-Grid Structure for Further Enhancing the Resolution of Ion Mobility Spectrometry. *Anal. Chem.* **2012,** *84*, 5700-5707.

28. Du, Y.; Wang, W.; Li, H., Resolution Enhancement of Ion Mobility Spectrometry by Improving the Three-Zone Properties of the Bradbury-Nielsen Gate. *Anal. Chem.* **2012**, *84*, 1725-1731.

29. Wiza, J. L., Microchannel Plate Detectors. *Nucl. Instrum.Methods* **1979,** *162*, 587-601.

30. Davis, E. J.; Dwivedi, P.; Maggie, T.; Siems, W. F.; Hill, H. H., High-Pressure Ion Mobility Spectrometry. *Anal. Chem.* **2009,** *81*, 3270-3275.

31. Kaplan, K.; Graf, S.; Tanner, C.; Gonin, M.; Fuhrer, K.; Knochenmuss, R.; Dwivedi, P.; Hill, H. H., Resistive Glass IM-TOFMS. *Anal. Chem.* **2010**, *82*, 9336-9343.

32. Roscioli, K. M.; Davis, E.; Siems, W. F.; Mariano, A.; Su, W. S.; Guharay, S. K.; Hill, H. H., Modular Ion Mobility Spectrometer for Explosives Detection Using Corona Ionization. *Anal. Chem.* **2011,** *162*, 587-601.

33. May, J. C.; McLean, J. A., A Uniform Field Ion Mobility Study of Melittin and Implications of Low-Field Mobility for Resolving Fine Cross-Sectional Detail in Peptide and Protein Experiments. *Proteomics* **2015,** *15*, 2862-2871.

CHAPTER 4

INVESTIGATION OF THE COMPLETE SUITE OF THE LEUCINE AND ISOLEUCINE ISOMERS: TOWARDS PREDICTION OF ION MOBILITY SEPARATION CAPABILITIES

4.1. Introduction

The separation of isomers, or compounds that contain the same atomic composition yet possess different chemical structures, has been an active area of analytical chemistry since the first isomer separation was documented by Pasteur in 1849.[1] The biological activity of compounds exhibit isomeric specificity which manifests in a broad range of physiological processes including metabolic pathways,[2] reactive oxygen species,[3] and cancer research.[4] Isomers represent a broad range of structural heterogeneity which are classified based on differences either in bond coordination or stereochemistry. Compounds that differ as a result of physical rearrangement of chemical bonds, (*i.e.* constitutional isomers) represent the most structurally diverse isomer class. Stereoisomers are compounds which have identical branching between atoms but differ in chirality at one or more stereocenters. A specific sub-class of chiral molecules are enantiomers which exhibit mirrored stereochemistry. Biological compounds tend to exist in only one particular stereochemistry,[5] such as the amino acids, which predominately exist in the L- form. While the precise origin of stereochemistry preference is still unknown, observations of chirality in meteorite samples and in deep space suggests L- stereochemistry preferences are primordial.[6,7] Due to identical chemical compositions, chemical isomers are of the same mass and thus are challenging to separate by traditional mass spectrometry techniques alone. Tandem MS/MS methods such as collision induced dissociation[8,9] and electron transfer dissociation[10-12] can alleviate these challenges in cases where two isomers either differ in bond dissociation energies or possess

constitutional arrangements that produce unique fragmentation spectra. However, for structurally similar isomers, fragment ions are often shared by both precursors and hence tandem MS is not sufficient to confidently identify these components in a biological mixture (see Figure D.1, Supporting Information).[13,14]

Ion mobility-mass spectrometry (IM-MS) has gained recent interest as a rapid separation technique which can be applied to the separation and characterization of isomers.[15-20] Although condensed phase separation techniques such as gas and liquid chromatography can be tailored for the separation of specific isomeric classes, IM-MS operates on a timescale that is several orders of magnitude faster and can be used in conjunction with condensed phase separations and tandem MS/MS techniques.[21,22] IM-MS is a particularly useful analytical combination in that the mass spectrometry separates molecules based on their intrinsic mass, whereas ion mobility provides a complimentary separation based on molecular size and shape based on the gas-phase collision cross section (CCS). While there has been significant progress in correlating the CCS to the primary molecular structure and composition,[23-25] it is challenging to predict CCS particularly for isomeric systems. Consequently, the ability of IM-MS to separate any given isomeric system is difficult to predict without referring to empirical studies.

For our study of isomeric separations we chose to investigate the classic amino acid isomer system leucine and isoleucine, which has been previously studied by both chromatography approaches[26-28] and various ion mobility techniques including field asymmetric waveform ion mobility spectrometry (FAIMS),[29-31] traveling wave ion mobility spectrometry (TWIMS),[32] and uniform field ion mobility operated at ambient pressure.[33] This small molecule system (131 Da) was chosen as it is large enough to possess a diverse family of isomers yet small enough not to exhibit significant higher-order structural effects (*i.e.* conformers) that would otherwise

complicate the interpretation of results. A total of eleven leucine/isoleucine isomers ($C_6H_{13}NO_2$) were chosen for this study, including four biologically-relevant forms (L-leucine, L-isoleucine, L-norleucine, and L-*tert*-leucine) which collectively include examples of different bond coordination and stereochemistry (Figure 4.1). Although nonlinear field IM-MS techniques (*e.g.*, FAIMS) have been shown to enhance the separation of these types of isomers, drift tube ion mobility spectrometry (DTIMS) was specifically chosen for this work, as this uniform field-based technique facilitates the quantitative comparison of separations through the empirical measurement of the CCS.

4.2. Experimental Methods

4.2.1. Preparation of Standards

Optima LC-MS grade water and ammonium acetate were purchased from Fisher Scientific (Fair Lawn, NJ, USA). 6-aminocaproic acid, L-norleucine, D-leucine, L-isoleucine, L-allo-isoleucine, N,N-dimethylglycine ethyl ester, and L-leucine were purchased from Sigma-Aldrich (St. Louis, MO, USA). D-*tert*-leucine, D-allo-isoleucine, L-*tert*-leucine and D-isoleucine were purchased from Alfa Aesar (Ward Hill, MA, USA). Samples were prepared at an initial concentration of 1 mg/mL and were subsequently diluted in water buffered with 10 mM ammonium acetate (pH 6.5) to a final concentration of 10 μg/mL for analysis. No additional acid was needed to promote protonation. All isomers investigated in this work are summarized in Figure 4.2.

4.2.2. Experimental Parameters

A commercial uniform field ion mobility-mass spectrometer (6560, Agilent Technologies, Santa Clara, CA, USA) was used to obtain high resolution mass spectrometry and ion mobility data (nominally 15,000 and 60, respectively). Details of the instrument have been previously described.[34,35] Briefly, the instrument consists of a uniform field 78.1 cm drift tube coupled to a tandem quadrupole time-of-flight (QTOF) mass spectrometer. The drift tube is bracketed by electrodynamic ion funnels and ion mobility separations were conducted in nitrogen drift gas (4.00 Torr, *ca.* 30°C) for these studies. All samples were directly infused using a syringe pump (Cole-Palmer, Vernon Hills, IL) operated at 10 µL/min into a thermally-assisted electrospray ionization source (Agilent Jet Stream). The instrument was operated in positive ion mode with 3.8 kV applied to the ion transfer capillary and 1.8 kV applied to the ion focusing nozzle. Source temperatures were kept low (200 °C) to aid in ionization of fragile molecules.

Ion mobility parameters were adjusted to obtain maximum resolving power as described previously.[36,37] These prior studies indicate that the resolving power for drift tubes is optimized when the initial ion pulse width is small, and hence the gate width (referred to as "Trap Release Time" in this instrument) was set to a short duration (100 μs) relative to the ion drift time which is on the order of tens of milliseconds. The drift field also strongly affects the instrument resolving power, and separations were conducted at drift voltages which maximize the resolving power within the mobility and mass range of the analytes, corresponding to 14.7 V/cm (see Figure D.2, Supporting Information). The nominal resolving power (58 ± 2) was consistent for all analytes investigated and represents the optimal values for singly-charged analytes for this particular instrument (see Table D.1, Supporting Information).[37] All mobility spectra correspond to the protonated species of the $C_6H_{13}NO_2$ molecule. Other adducts observed (M+Na and M+K) were not evaluated further in this study.

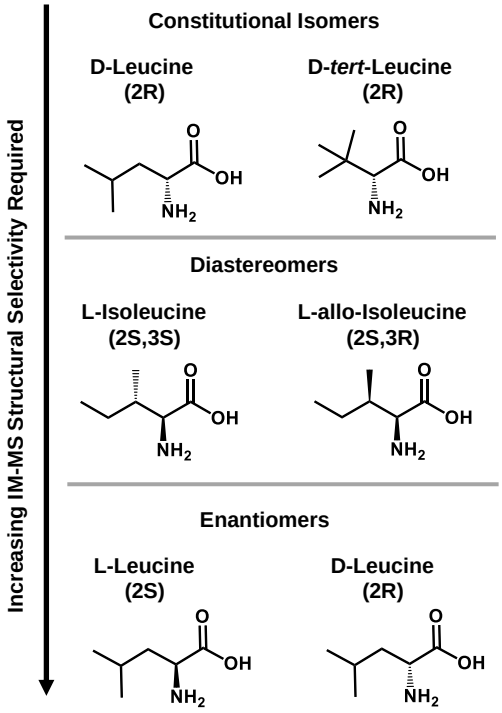

Constitutional Isomers
Structural rearrangement of constituent atoms.

Diastereomers
Two molecules that posses one or more (but not all) opposite stereochemistry for a given number of stereocenters.

Enantiomers
Two molecules that have opposite stereochemistry at every point of chirality.

Figure 4.1. Isomer classifications for various pairs of leucine or isoleucine compounds with corresponding definitions.

4.2.3. Collision Cross Section Measurements

Cross sections were determined from a stepped field technique in which the applied voltage across the drift tube was varied in 7 increments from 550 to 1550V (7.0 to 19.8 V/cm, or 6 to 16 Td at 4 Torr) in order to determine the time ions reside outside the drift cell. The corrected drift times are then used with relevant laboratory conditions (pressure, temperature) to obtain a collision cross section value based on the fundamental low field equation, commonly referred to as the Mason-Schamp relationship (Figure D.3, Supporting Information).[38,39]

4.3. Results and Discussion

4.3.1. Isomer Classifications and Separations

Figure 4.2 A illustrates the chemical structures of the 11 leucine/isoleucine isomers ($C_6H_{13}NO_2$) with corresponding collision cross sections and standard deviations obtained in this study. All of the isomers exhibit a nitrogen cross section that spans approximately 10 square angstroms (from *ca.* 127 to 137 $Å^2$) with an average CCS of 133 $Å^2$. The percent relative standard deviation of all CCS values is *ca.* 0.2% for 7 sequential replicate measurements of each analyte. Mobility spectra and corresponding ion mobility data are provided in Supporting Information (Figure D.4 and Table D.1, respectively). Figure 4.2 B-I contains the overlaid IM spectra of all 11 isomers which were individually measured. No secondary peak features are observed for any of the individual analytes, and mobility peaks are narrow with a resolving power at the limit of the instrumentation for singly-charged ions (*ca.* 60).[37] Figure 4.2 B-II illustrates the overlaid mobility profiles for the constitutional isomers N,N-dimethylglycine ethyl ester (1), L-*tert*-leucine (3), and L-norleucine (11). These three constitutional isomers possess a percent difference in cross section

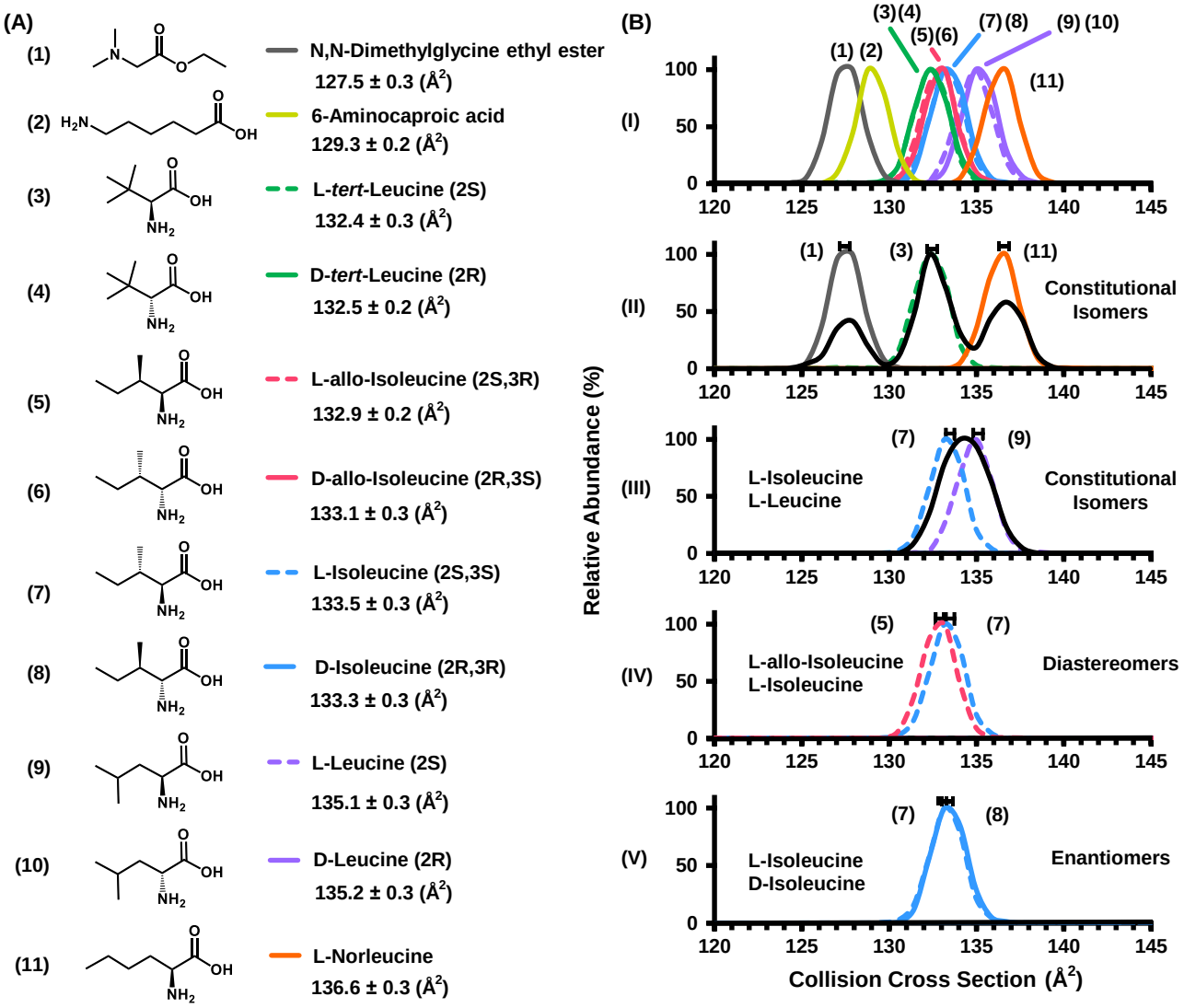

Figure 4.2. (A) The leucine/isoleucine isomers with chemical formula $C_6H_{13}NO_2$ examined in this study. Experimental cross sections with respective standard deviations are shown at the right with corresponding stereochemistry. **(B) (I)** Experimental IM spectra overlays for all isomer compounds (standard error bars omitted for clarity). **(II)** Overlay of the IM spectra corresponding to N,N-dimethylglycine ethyl ester, L-tert-leucine, and L-norleucine and the IM spectrum corresponding to the mixture (black). **(III)** Overlays of L-isoleucine and L-leucine in addition to the equal ratio mixture. **(IV** and **V)** Overlays of diastereomers and enantiomers, respectively. IM spectra corresponding to the mixture of standards in **(IV)** and **(V)** can be found in the supporting information (see Figure D.4).

of 3.6%and 3.1%, respectively. This CCS difference is sufficient to allow for near baseline separation of the corresponding three component mixture (black trace). Figure 4.2 B-III depicts an overlay of L-isoleucine and L-leucine, which have a 1.2% difference in cross section. These two isomers are also classified as constitutional isomers, but are more structurally similar compared to the three analytes in panel B-II. While the mobility overlays of these two compounds are distinctly different, the analysis of the corresponding mixture indicates that they are unresolvable at the current level of resolving power (*ca.* 60).

Figure 4.2 B-IV and V contain the overlaid IM spectra of diastereomers and enantiomers respectively. Although the cross sections for L-allo-isoleucine and L-isoleucine are statistically different (*ca.* 0.4%), the mixture of both diastereomers yields a single broad distribution (see Figure D.5, Supporting Information). For the enantiomers, the centroids of each peak are not statistically different. Specifically, the difference in their cross sections (0.2 $Å^2$) is within the standard error of the measurement (± 0.3 $Å^2$, or 0.2%). Collectively, these observations demonstrate that for relatively simple small molecules, constitutional isomers show the most disparate cross sectional differences, followed by diastereomers and enantiomers, respectively. While the correlation between structural and CCS differences is an intuitive result, these observations underscore that small molecules of this size and class predominately undergo structurally-selective IM separations under conditions of low *E* fields in nitrogen drift gas.

4.3.2. Peak Shape Modeling in Ion Mobility

Drift profiles collected from uniform field ion mobility represent a composite of individual ion arrival times and can be described by a normal distribution. Rigorously, peak shape fitting in DTIMS is accomplished using the ion transport or flux equation,[39,40] but it was found that this higher level of peak fitting did not contribute to the accuracy of the fit and added an unnecessary level of complexity. Therefore, a simple Gaussian fit was used to describe the ion mobility arrival time distributions. The mean of the normal distribution represents either the measured drift time (*i.e.* the peak centroid) or cross section, and the standard deviation of the peak itself (σ) can be derived from the measured full width at half the maximum height (FWHM = 2.355 σ). Note that this standard deviation is not the same as the standard deviation reported for the CCS uncertainty, the latter of which is associated only with the peak centroid and is determined from replicate experimental measurements.

Figure 4.3 A illustrates the modeled mobility distributions and experimental data (dashed and solid lines, respectively) for L-isoleucine and L-norleucine (dashed lines) which are overlaid with experimental measurements (solid lines). Both peaks are separated in the individual overlays by *ca.* 70%, yet when a mixture of the two compounds is analyzed with equal peak abundance (Figure 4.3 B), the actual valley between the two peaks is about 50% *i.e.*, half-height separation. The importance of this distinction between the separation of a true mixture versus individual overlays can also be noted for the mixture of leucine and isoleucine in Figure 2 as well as the stereoisomer mixtures spectral overlays provided in the Supporting Information (Figure D.5). For a given separation of two components the optimal resolution will occur when both species are in equal abundance as defined by equal ion mobility peak areas. This would occur in an equimolar mixture only if both species exhibit the same ionization efficiency. The normal

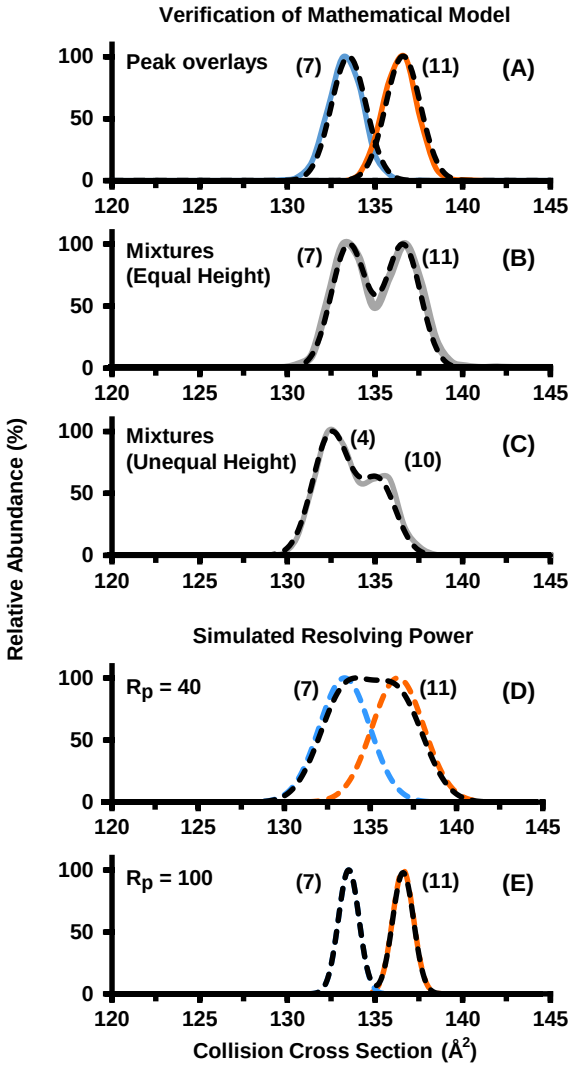

Figure 4.3. Experimental (solid lines) and modeled distributions (dashed) for isomer standards and mixtures. (A) Individual overlays for L-isoleucine (light blue) and L-norleucine (orange). (B) Mixtures of L-isoleucine and L-norleucine in equal relative abundance. (C) Experimental and modeled distributions of an unequal height mixture for D-leucine (60%) and D-*tert*-leucine (100%). Modeled separations for L-isoleucine and L-norleucine at simulated lower (D) and higher (E) resolving power.

distribution model allows for simulation of both equal abundance mixtures (Figure 4.3 B) as well as practical mixtures that do not have equal abundance for each isomer. Panel C of Figure 4.3 portrays a mixture of D-leucine and D-*tert*-leucine and illustrates that an unequal ratio of two isomers can be modeled by scaling the relative abundance of the isomer in lower abundance (60% for D-leucine) as compared to the base peak. Typically, if two compounds exhibit half-height separation (50% valley, FWHM) as in panel B, the two peaks are still distinguishable even if the relative abundance of the two isomers is fairly disparate (secondary peak exhibiting around 25% of the peak area of the base peak). As the percent difference in cross section between the two peaks increases, the relative abundance of the two analytes has significantly less of an impact on the overall separation (see Figure D.6, Supporting Information).

4.3.3. Resolving Power and Separations

Resolving power for drift tube instruments has been extensively studied previously.[41-43] Resolving power (R_p) is a single peak measurement defined in DTIMS as in the ion drift time (t_d) divided by the peak full width at half maximum height (FWHM).

$$R_p = \frac{t_d}{FWHM} \quad (1)$$

Because the relative CCS of analytes is not altered in low-field DTIMS, the peak width has a significant effect on the resulting separations. In other words, at low field, the relative spacing of analytes in either the drift time or CCS scale (the dispersion dimension) does not change and so narrowing the peak width will directly benefit the resulting resolution of two closely-spaced analyte peaks. Resolving power is thus an important metric for characterizing the resolution in

low-field DTIMS instruments. Other ion mobility techniques such as TWIMS or FAIMS do not exhibit a simple relationship between resolution and their respective dispersion dimensions, and so the relationship between single-peak resolving power and two-peak resolution are more complicated and this will be the subject of future work.

A relevant and important question is how much resolving power is actually needed for a routine separation of chemical isomers. This idea has been approached in mass spectrometry by Marshall[44] who noted that mass resolution precedes in "plateaus" of separating analyte systems exhibiting similar mass differences (*e.g.*, adducts and isotopes). In order to expand this concept to uniform field studies, the mathematical modeling developed in this study was used to map the separation of two hypothetical IM peaks for varying degrees of cross sectional similarity. For a given percent difference in cross section, there exists a minimum peak width (resolving power) needed to obtain separation in a drift tube instrument. The results for 10, 50, and 90% separation are shown in Figure 4.4. Note that for simplicity, the plot in Figure 4.4 was constructed considering two peaks of equal abundance. The correlation of values depicted in Figure 4.4 was verified experimentally using data from the current study (circle 3) as well as higher resolving power data from other uniform field studies (circles 1 and 2). For example, a recent high pressure DTIMS demonstrated the half-height separation of phosphatidylcholine lipid isomers exhibiting a *ca.* 0.4% cross sectional difference by operating at greater than 300 resolving power (circle 1).[45] In another study, ambient pressure DTIMS was able to demonstrate the separation of leucine and isoleucine to half-height (circle 2).[46] To connect these observations to physically meaningful systems, various isomer classes are portrayed with ranges of percent difference in cross section based on the isomers in this study (colored regions, Figure 4.4).

Classically, the quality of a separation is quantified in terms of two-peak resolution ($R_{p\text{-}p}$), which is defined as the distance between peak centers divided by their average peak widths (Equation 2). A coefficient of 1.18 (2.355 σ / 2) is included in order to define the peak widths in half-height terms.

$$R_{p-p} = 1.18 \cdot \frac{t_{d(B)} - t_{d(A)}}{FWHM_{(B)} - FWHM_{(A)}} \quad (2)$$

The insets in Figure 4.4 contain theoretical distributions corresponding to two overlapping peaks of equal height, and indicate that the scale for two-peak resolution is between *ca.* 0.5 and 1.5 for unresolved and completely resolved peaks, respectively. Through substitution of equations 1 and 2, resolving power and resolution have been shown to be directly correlated in ion mobility by Tabrizchi[47] through the selectivity factor (α).

$$R_{p-p} = 0.589 \cdot R_p \cdot \frac{\alpha - 1}{\alpha} \quad (3)$$

For ion mobility, the selectivity factor is the ratio of the separation parameter for the two peaks which for DTIMS can be described in terms of drift time,[47] reduced mobility,[46] or CCS. As collision cross section represents an important physical descriptor of molecular size which is now routinely obtainable, we have made substitutions for CCS instead of α. By examining the normal distribution corresponding to the separations obtained for the leucine and isoleucine isomers, we were able to confirm Tabrizchi's findings, and the result is Equation 4, which relates resolving power and the percent difference in CCS ($\Delta_{CCS,\%}$) to overall separation efficiency in terms of the two-peak resolution.

$$R_{p-p} = 0.00589 \cdot R_p \cdot \Delta_{CCS,\%} \quad (4)$$

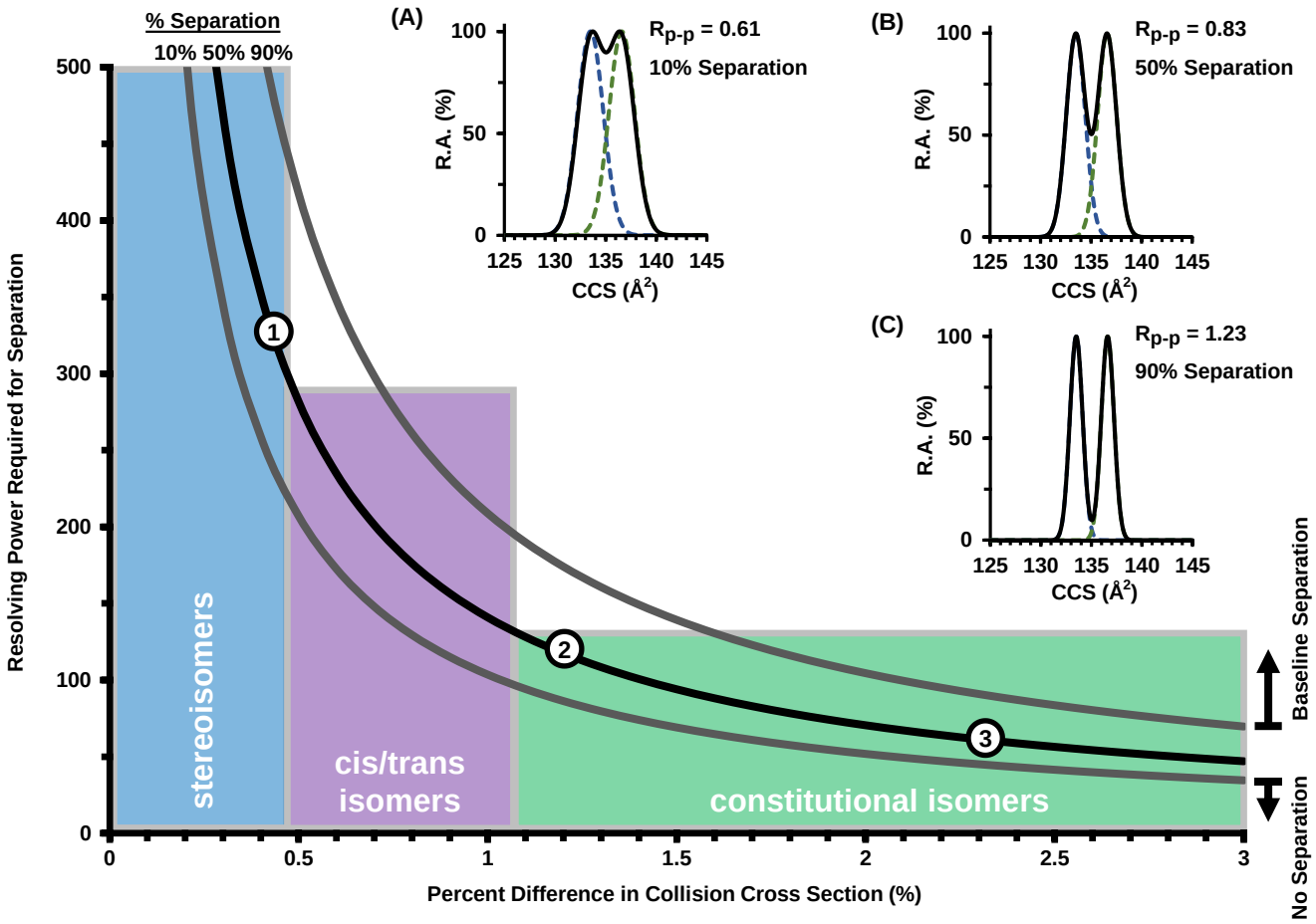

Figure 4.4. A plot of the resolving power required to separate two compounds for a given percent difference in CCS for uniform field ion mobility. The middle trace (solid black) represents a half-height separation (50%). Theoretical traces for 90, 50, and 10% separation are illustrated in the top right insets **(A, B,** and **C)** with their corresponding values for two-peak resolution. Quantiles are based on observations from this study. Experimental observations are also noted for previous uniform field studies (circles 1 and 2) and the current study (3).

To verify Equation 4 experimentally, we examined a baseline separation of the isomers D-leucine and 6-aminocaproic acid. The predicted resolving power of 57 for each of the two isomers with a cross section difference of 4.5% should provide a peak-to-peak resolution of 1.50 using equation 4. Comparison of these predictions to experimental data showed *ca.* 5 % error in the prediction with an actual two-peak resolution of 1.43, which has 94% separation, or only 6% peak overlap. The corresponding experimental and theoretical ion mobility distributions for this system are contained in Figure 5.5 A. To examine the accuracy for equation 4 on a broad scale, the experimental drift times and peak widths for each of the 11 isomers were matched in a pairwise comparison and the two-peak resolution ($R_{p\text{-}p}$) was calculated for all iterations (55 pairs). Collectively, over 67% of the resolution values determined from overlaying each experimental distribution deviate by less than 0.1 from values predicted through equation 4. For reference, the insets in Figure 5 illustrate a two-peak resolution difference of 0.1 for two closely spaced peaks. Overall, the predicted resolutions for the isomer matches are in agreement to experimental measurements across a wide range of percent difference in cross section. This agreement illustrates the general applicability of equation 4 to predict separations for both structurally similar molecules (small % difference in CCS) as well as two isomers that are readily separated (large % difference in CCS). For reference, Figure 5 also includes vertical dotted lines (blue) which delineate the number of corresponding isomer pairs which are resolvable *via* different degrees of resolving power. For example, at 50 resolving power, the analysis predicts that 30% of the 55 isomer pairs can be resolved. A resolving power of 100 is predicted to separate 60% of the pairs, whereas at 200 resolving power, 74% of the isomer pairs are predicted to be resolved. Finally, to resolve all isomer pairs, theory predicts a required ion mobility resolving power of *ca.* 2000 (Table 4.1), which is approximately an order of magnitude higher than current state-of-the-art

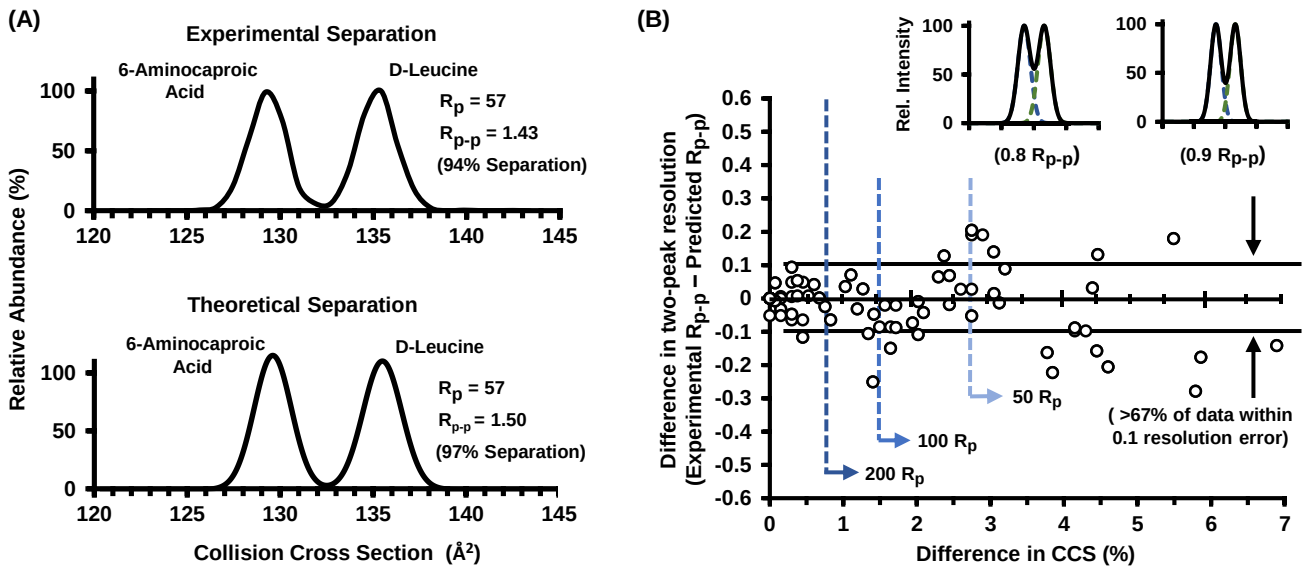

Figure 4.5. (A) Experimental (top) and theoretical (bottom) separation of 6-aminocaproic acid and D-leucine. Predicted two peak resolution is within a *ca*. 5% error from the experimental resolution of the two component mixture. **(B)** Comparison of the predicted separation via equation 4 with experimental data corresponding to the overlay of 55 pairwise matched isomers examined in this study. More than 67% of the separations result in less than 0.1 error in two-peak resolution. A difference in R_{p-p} of 0.1 is illustrated in the top two theoretical traces. For half height separations, a resolving power of 200 is sufficient to separate 74% of the isomer pairwise matches. Resolving powers of 100 and 50 would be able to separate 60% and 30% of the isomer matches, respectively.

instrumentation.[48-50] It should be noted, however, that this determination of separation potential for closely related isomers in Table 4.1 (within 0.4%) is based solely on percent difference in CCS and should be taken as such noting the precision of the CCS measurement (± 0.2-0.3%). These isomers may not be separable despite increases in resolving power due the level of precision in CCS with the current instrumentation. Another practical approach for isomer separation in ion mobility utilizes the introduction of chiral drift gas modifiers, such as (*S*)-2-butanol,[51] to facilitate separation of isomers based on differences in stereochemistry.

4.4. Conclusions

In this current study of small molecule isomers (131 Da), typically enantiomers were on average 0.1% different in cross section. For diastereomers, the percent difference in cross section was found to be around 0.4%. Constitutional isomers represented the most resolvable isomer class, but CCS differences varied significantly, with percent differences in cross section ranging from 0.3 to 6.9%. The predictable performance of uniform field DTIMS and the capability of deriving molecular information in the form of the CCS allows for the development of a mathematical model which relates percent differences in CCS to both single peak resolving power (R_p) and two-peak resolution ($R_{p\text{-}p}$). It was found that the instrument utilized could resolve at half-height approximately one-third of the isomers chosen for this study, which represent a significant number of stereoisomers and enantiomers which are mostly unresolvable. The current state-of-the-art resolving power is approximately 250 for ambient pressure DTIMS[50] and trapped ion mobility (TIMS),[48] which can theoretically resolve about three-quarters (*ca.* 78%) of the isomer pairs. Finally, the model developed predicts that a resolving power in excess of 2000 would be necessary to resolve all combinations of the leucine/isoleucine isomers investigated in this study. Other

compounds		% difference in CCS	predicted R_p [a]
	Enantiomers		
D-leucine	L-leucine	0.07	1904
D-isoleucine	L-isoleucine	0.15	939
D-allo-isoleucine	L-allo-isoleucine	0.15	937
	Diastereomers		
D-isoleucine	D-allo-isoleucine	0.15	939
D-isoleucine	L-allo-isoleucine	0.30	469
L-isoleucine	L-allo-isoleucine	0.45	313
	Constitutional Isomers		
L-allo-isoleucine	D-*tert*-leucine	0.30	467
L-leucine	L-isoleucine	1.19	118
D-leucine	D-*tert*-leucine	2.02	70
D-leucine	6-aminocaproic acid	4.46	32

[a]The predicted resolving power is calculated based on the percent difference in CCS for the isomer pairs and eq 4.

Table 4.1. Predicted resolving power required to separate each of the isomer pairs at half height.

studies from the author's laboratory show that larger systems (nonapeptides, *ca.* 1100 Da) exhibit large differences in cross section (2.0%) for diastereomers due to macromolecular rearrangements based on stereochemistry. Larger molecular systems, however, will also possess significantly more possible isomeric forms than the relatively small system investigated in this current work[22] and can exist as conformers which are expected to impose greater demands on the required ion mobility resolving power. The correlation between CCS and resolution developed in this and ongoing work are expected to benefit the development of computational approaches which can predict the separation of any two compounds with known CCS given that the resolving power of the ion mobility instrument utilized is well-characterized. This in turn will provide the capability for prediction of ion mobility separation behavior so as long as a high precision experimental measurement of the CCS (or other transport property) exists. The broadscale applicability of equation 4 and Figure 4.4 to other ion mobility techniques (*e.g.*, FAIMS/DMS, TWIMS, and TIMS) is currently under investigation.

4.5. Acknowledgements

This chapter contains the published research article: James N. Dodds, Jody C. May, and John A. McLean, "Investigation of the Complete Suite of the Leucine and Isoleucine Isomers: Towards Prediction of Ion Mobility Separation Capabilities," *Analytical Chemistry* **2017,** *89*, 952-959.

Financial support for aspects of this research was provided by The National Institutes of Health (NIH R01GM099218) and under Assistance Agreement No. 83573601 awarded by the U.S. Environmental Protection Agency. It has not been formally reviewed by EPA. The views

expressed in this document are solely those of the authors and do not necessarily reflect those of the Agency. EPA does not endorse any products or commercial services mentioned in this publication. Furthermore, the content is solely the responsibility of the authors and does not necessarily represent the official views of the funding agencies and organizations.

4.6. References

1. Flack, H. D. Louis Pasteur's Discovery of Molecular Chirality and Spontaneous Resolution in 1848, Together with a Complete Review of His Crystallographic and Chemical Work. *Acta Cryst.* **2009**. *A65*, 371-389.

2. Cruz-Hernandez, C.; Deng, Z.; Zhou, J.; Hill, A. R.; Yurawecz, M. P.; Delmonte, P.; Mossoba, M. M.; Dugan M. E. R.; Kramer, J. K. G. Methods for Analysis of Conjugated Linoleic Acids and Trans-18:1 Isomers in Dairy Fats by Using a Combination of Gas Chromatography, Silver-Ion Thin-Layer Chromatography/Gas Chromatography, and Silver-Ion Liquid Chromatography. *Journal of AOAC International* **2004**, *87*, 545-562.

3. Lecoq, S.; Perin, F.; Plessis, M. J.; Strapelias, H.; Duquesne, M. Comparison of the in vitro Metabolisms and Mutagenicitiesof dibenzo[a,c]anthracene, dibenzo[a,j]anthracene and dibenzo[a,j]anthracene: Influcene of Norharman. *Carcinogenisis* **1989**, *10*, 461-469.

4. Kelly, N. S.; Hubbard, N. E.; Erickson K. L. Conjugated Linoleic Acid Isomers and Cancer. *Journal of Nutrition* **2007**, *137*, 2599-2607.

5. Brewer, A.; Davis, A. P. Chiral Encoding May Provide a Simple Solution to the Origin of Life. *Nature Chemistry* **2014**, *6*, 569-574.

6. Cronin, J. R. and Sandra Pizzarello. Enantiomeric Excesses in Meteoritic Amino Acids. *Science* **1997**, *275*, 951-955.

7. McGuire, B. A.; Carroll, P. B.; Loomis, R. A.; Finneran, I. A.; Jewell, P. R.; Remijan, A. J.; Blake, G. A. Discovery of the Interstellar Chiral Molecule Propylene Oxide. *Science* **2016**, *352*, 1449-1452.

8. Cooks, R. G. Collision-Induced Dissociation: Readings and Commentary. *J. Mass Spectrom.* **1995**, *30*, 1215-1221.

9. Wells, J. M.; McLuckey, S. A. Collision-Induced Dissociation (CID) of Peptides and Proteins. *Methods Enzymol.* **2005**, *402*, 148-185.

10. Syka, J. E.; Coon, J. J.; Schroeder, M. J.; Shabanowitz, J.; Hunt, D. F. Peptide and Protein Sequence Analysis by Electron Transfer Dissociation Mass Spectrometry. *Proc. Nat. Acad. Sci. U.S.A.* **2004**, *101*, 9528-9533.

11. Lebedev, A. T.; Damoc, E.; Makarov, A. A.; Samgina, T. Y., Discrimination of Leucine and Isoleucine in Peptides Sequencing with Orbitrap Fusion Mass Spectrometer. *Anal. Chem.* **2014,** *86*, 7017-7022.

12. Xiao, Y. Vecchi, M. M.; Wen, D. Distinguishing between Leucine and Isoleucine by Integrated LC-MS Analysis Using an Orbitrap Fusion Mass Spectrometer. *Anal. Chem.* **2016,** *88*, 10757-10766.

13. Zaia, J. Mass Spectrometry of Oligosaccharides. *Mass Spectrom. Rev.* **2004**, *23*, 161-227.

14. Blanksby, S. J.; Mitchell, T. W. Advances in Mass Spectrometry for Lipidomics. *Ann. Rev. Anal. Chem.* **2010**, *3*, 433-465.

15. Hagen, D. F. Characterization of Isomeric Compounds by Gas and Plasma Chromatography. *Anal. Chem.* **1979**, *51*, 870-874.

16. Wu, C.; Siems, W. F.; Hill, H. H., Jr. Secondary Electrospray Ionization Ion Mobility Spectrometry/Mass Spectrometry of Illicit Drugs. *Anal. Chem.* **2000**, *72*, 396-403.

17. Srebalus Barnes, C. A.; Hilderbrand, A. E.; Valentine, S. J.; Clemmer, D. E. Resolving Isomeric Peptide Mixtures: A Combined HPLC/Ion Mobility-TOFMS Analysis of a 4000-Component Combinatorial Library. *Anal. Chem.* **2002**, *74*, 26-36.

18. Fenn, L. S.; McLean, J. A. Structural Resolution of Carbohydrate Positional and Structural Isomers Based on Gas-Phase Ion Mobility-Mass Spectrometry. *Phys. Chem. Chem. Phys.* **2011**, *13*, 2196-2205.

19. Forsythe, J. G.; Stow, S. M.; Nefzger, H.; Kwiecien, N. W.; May, J. C.; McLean, J. A.; Hercules, D. M. Structural Characterization of Methylenedianiline Regiosomers by Ion Mobility-Mass Spectrometry, Tandem Mass Spectrometry, and Computational Strategies: I. Electrospray Spectra of 2-Ring Isomers. *Anal. Chem.* **2014**, *86*, 4362-4370.

20. Lalli, P. M.; Corilo, Y. E.; Fasciotti, M.; Riccio, M. F.; de Sa, G. F.; Daroda R. J.; Souza, G. H.; McCullagh M.; Bartberger, M. D.; Eberlin M. N.; Campuzano I. D. Baseline Resolution of Isomers by Traveling Wave Ion Mobility Mass Spectrometry: Investigating the Effects of Polarizable Drift Gasses and Ionic Charge Distribution. *J. Mass Spectrom.* **2013**, *48*, 989-997.

21. May, J. C.; McLean, J. A. Ion Mobility-Mass Spectrometry: Time-Dispersive Instrumentation. *Anal. Chem.* **2015**, *87*, 1422-1436.

22. May, J. C.; McLean, J. A. Advanced Multidimensional Separations in Mass Spectrometry: Navigating the Big Data Deluge. *Annu. Rev. Anal. Chem.* **2016**, *9*, 387-409.

23. Shah, A. R.; Agarwal, K.; Baker, E. S.; Singhal, M.; Mayampurath, A. M.; Ibrahim, Y. M.; Kangas, L. J.; Monroe, M. E.; Zhao, R.; Belov, M. E.; Anderson, G. A.; Smith, R. D. Machine Learning Based Prediction for Peptide Drift Times in Ion Mobility Spectrometry. *Bioinformatics* **2010**, *26*, 1601-1607.

24. Oliferenko, A. A.; Tian, F.; Karelson, M.; Katritzky, A. R. Prediction of Peptide IMS Cross Sections from Extended Molecular Connectivity. *Int. J. Mass Spectrom.* **2012**, *314*, 1-5.

25. Gonzales, G. B.; Smagghe, G.; Coelus, S.; Adriaenssens, D.; De Winter, K.; Desmet, T.; Raes, K.; Van Camp, J. Collision Cross Section Prediction of Deprotonated Phenolics in a Travelling-Wave Ion Mobility Spectrometer Using Molecular Descriptors and Chemometrics. *Anal. Chim. Acta.* **2016**, *924*, 68-76.

26. Junge, M.; Huegel H.; Marriott, P. J. Enantiomeric Analysis of Amino Acids by Using Comprehensive Two-Dimesional Gas Chromatography. *Chirality*. **2007**, *19*, 228-234.

27. Lim, G.; Nam H.; Park, C.; Mun, S. Effect of Liquid-Phase Composition on the Henry's Constants of Valine, Isoleucine, and Leucine in a Capcell-Pack C18 Chromatography. *J. Liq. Chromatogr. Relat. Technol.* **2013**, 36, 180-196.

28. Moreno-González, D.; Toraño, J. S.; Gámiz-Gracia, L.; García-Campaña A.M.; de Jong, G. J.; Somsen, G. W., Micellar Electrokinetic Chromatography-Electrospray Ionization Mass Spectrometry Employing a Volatile Surfactant for the Analysis of Amino Acids in Human Urine. *Electrophoresis*. **2013**, *34*, 2615-2622.

29. Barnett, D. A.; Ells, B.; Guevremont R. Purves, R.W. Separation of Leucine and Isoleucine by Electrospray Ionization-High Field Asymmetric Waveform Ion Mobility Spectrometry-Mass Spectrometry. *J. Am. Soc. Mass Spectrom.* **1999**, *10*, 1279-1284.

30. McCooeye, M.; Mester, Z. Comparison of Flow Injection Analysis Electrospray Mass Spectrometry and Tandem Mass Spectrometry and Electrospray High-Field Asymmetric Waveform Ion Mobility Mass Spectrometry and Tandem Mass Spectrometry for the Determination of Underivatized Amino Acids. *Rapid Commun. Mass Spectrom.* **2006**, *20*, 1801-1808.

31. Shvartsburg, A. A.; Creese, A. J.; Smith, R. D.; Cooper, H. J. High-Resolution Differential Ion Mobility Separations Using Helium-Rich Gases. *Anal. Chem.* **2010**, *82*, 8327-8334.

32. Knapman, T. W.; Berryman, J. T.; Campuzano, I.; Harris, S. A.; Ashcroft, A. E. Considerations in Experimental and Theoretical Collision Cross-Section Measurements of Small Molecules using Travelling Wave Ion Mobility Spectrometry-Mass Spectrometry *Int. J. Mass Spectrom.* **2010**, *298*, 17-23.

33. Asbury, G. R.; Hill, H. H., Evaluation of Ultrahigh Resolution Ion Mobility Spectrometry as an Analytical Separation Device in Chromatographic Terms. *J. Microcolumn Separations*. **2000**, *12*, 172-178.

34. May, J. C.; Goodwin, C. R.; Lareau, N. M.; Leaptrot, K. L.; Morris, C. B.; Kurulugama, R. T.; Mordehai, A.; Klein, C.; Barry, W.; Darland, E.; Overney, G.; Imatani, K.; Stafford, G. C.; Fjeldsted, J. C.; McLean, J. A. Conformational Ordering of Biomolecules in the Gase Phase: Nitrogen Collision Cross Sections Measured on a Prototype High Resolution Drift Tube Ion Mobility Mass-Spectrometer. *Anal. Chem.* **2014**, *86*, 2107-2116.

35. May, J. C.; McLean, J. A. A Uniform Field Ion Mobility Study of Melittin and Implications of Low-Field Mobility for Resolving Fine Cross-Sectional Detail in Peptide and Protein Experiments. *Proteomics* **2015**, *15*, 2862-2871.

36. Kanu, A. B.; Gribb, M. M.; Hill, H. H. Predicting Optimal Resolving Power for Ambient Pressure Ion Mobility Spectrometry. *Anal. Chem.* **2008**, *80*, 6610-6619.

37. May, J. C.; Dodds, J. N.; Kurulugama, R. T.; Stafford, G. C.; Fjeldsted J. C.; McLean, J. A. Broadscale Resolving Power Performance of a High Precision Uniform Field Ion Mobility-Mass Spectrometer. *Analyst* **2015**, *140*, 6824-6833.

38. Mason, E. A.; Schamp, H. W. Mobility of Gaseous Ions in Weak Electric Fields. *Ann. Phys.* **1958**, *4*, 233-270.

39. Mason, E. A.; McDaniel, E. W. *Transport Properties of Ions in Gases*; John Wiley & Sons: New York, **1988**, p 560.

40. Moseley, J. T.; Gatland, I. R.; Martin, D. W.; McDaniel, E. W. Measurements of Transport Properties of Ions in Gases; Results for K^+ Ions in N_2. *Phys. Rev.* **1969**, *178*, 234-239.

41. Rokushika, S.; Hatano, H.; Baim, M. A.; Hill, H. H. Jr. Resolution Measurement for Ion Mobility Spectrometry. *Anal. Chem.* **1985**, *57*, 1902-1907.

42. Watts, P.; Wilders, A., On the Resolution Obtainable in Practical Ion Mobility Systems. *Int. J. Mass Spectrom. Ion Processes* **1992**, *112*, 179-190.

43. Siems, W. F.; Wu, C.; Tarver, E. E.; Hill, H. H.; Larsen, P. R.; McMinn, D. G. Measuring the Resolving Power of Ion Mobility Spectrometers. *Anal. Chem.* **1994**, *66*, 4195-4201.

44. Marshall, A.G.; Hendrickson, C.L.; Shi S.D. Peer Reviewed: Scaling MS Plateaus with High Resolution FT-ICRMS. A Guide to Increasing Resolution and Higher Masses by MS. *Anal. Chem.* **2002**, *74*, 252-259.

45. Groessl M.; Graf, S.; Lisa, M. Holcapek, M.; Sampaio, J.; Dick, B.; Vogt, B.; Knochenmuss, R.; 63rd Annual Conference on Mass Spectrometry and Allied Topics **2015**.

46. Asbury, G. R.; Hill, H. H., Jr. Evaluation of Ultrahigh Resolution Ion Mobility Spectrometry as an Analytical Separation Device in Chromatographic Terms. *J. Micro. Sep.* **2000**, *12*, 172-178.

47. Tabrizchi, M.; Rouholahnejad, F. Pressure Effects on Resolution in Ion Mobility Spectrometery. *Talanta* **2006**, *69*, 87-90.

48. Silveira, J. A.; Ridgeway, M. E.; Park, M. A. High Resolution Trapped Ion Mobility Spectrometry of Peptides. *Anal. Chem.* **2014**, *86*, 5624-5627.

49. Deng, L.; Ibrahim, Y. M.; Baker, E. S.; Aly, N. A.; Hamid, A. M.; Zhang, X.; Zheng, X.; Garimella, S. V. B.; Webb, I. K.; Prost, S. A. Sandoval, J. A.; Norheim, R. V.; Anderson, G. A.; Tolmachev, A. V.; Smith, R. D. Ion Mobility Separations of Isomers Based Upon Long Path Length Structures for Lossless Ion Manipulations Combined with Mass Spectrometry. *ChemistrySelect* **2016**, *1*, 2396-2399.

50. Groessl, M.; Graf, S.; Knochenmuss, R. High Resolution Ion Mobility-Mass Spectrometry for Separation and Identification of Isomeric Lipids. *Analyst* **2015**, *140*, 6904-6911.

51. Dwivedi, P.; Wu, C.; Matz, L. M.; Clowers, B. H.; Siems, W. F.; Hill, H. H., Gas-Phase Chiral Separations by Ion Mobility Spectrometry. *Anal. Chem.* **2006,** *78*, 8200-8206.

CHAPTER 5

CORRELATING RESOLVING POWER, RESOLUTION, AND COLLISION CROSS SECTION: UNIFYING CROSS-PLATFORM ASSESSMENT OF SEPARATION EFFICIENCY IN ION MOBILITY SPECTROMETRY

5.1. Introduction

Ion mobility combined with mass spectrometry (IM-MS) is now an important and established analytical technique for characterizing chemical compounds simultaneously by molecular size (collision cross section, CCS) and molecular weight (mass-to-charge ratio, m/z).[1-4] In the past decade, a myriad of ion mobility technologies have been developed and interfaced with MS (Table 5.1), including traveling wave drift cells (TWIMS),[5,6] uniform field and confining RF drift tubes (DTIMS and rf-DTIMS),[7,8] mobility separators (FAIMS/DMS),[9,10] field-flow dispersive devices (DMA TIMS, and Transversal Modulation IMS, TMIMS),[11-14] and confining 2-dimensional ion conveyors (SLIM),[15,16] among others. While each of these IM technologies utilize different mobility dispersive fields to generate an ion mobility spectrum, all operate on a common basis of separating molecules based upon differences in their gas-phase ion mobility behavior. Thus, it should be possible to relate the separation efficiency of all IM techniques to a common, normalized parameter such as the reduced ion mobility coefficient (K_0), or the gas-specific CCS value.

In ion mobility and mass spectrometry, the resolving power (R_p) is defined quantitatively from a single peak as a ratio of the location of the peak divided by its width (eqn. 1).[17]

$$R_p = \frac{x}{\Delta x} \quad (1)$$

IM Technique	Abbreviation	Dispersion Dimension
Drift Tube Ion Mobility Spectrometry	DTIMS	Time
Confining RF DTIMS	rf-DTIMS	Time
Ambient Pressure DTIMS	ap-DTIMS	Time
Traveling Wave Ion Mobility Spectrometry	TWIMS	Time
Cyclic Traveling Wave Ion Mobility Spectrometry	Cyclic TWIMS	Time
Trapped Ion Mobility Spectrometry	TIMS	Time
Structures for Lossless Ion Manipulations	SLIM (DTIMS and TWIMS)	Time
Asymmetric Field Ion Mobility Spectrometry	FAIMS	Voltage
Differential Mobility Spectrometry	DMS	Voltage
Differential Mobility Analyzer	DMA	Voltage
Overtone Mobility Spectrometry	OMS	Frequency
Cyclic Ion Mobility Spectrometry	Cyclic IMS	Frequency

Table 5.1. Various IM techniques and the respective dispersion dimension commonly reported for each technique.

Here, x is the dimensional location of the measurement, which is technique-specific, and Δx is commonly defined as the full width of the peak at half its maximum height (fwhm). In mass spectrometry, the dimension of x is mass-to-charge (m/z) which is an intrinsic property of the ion. As all mass spectrometers report separations in m/z space, mass resolving power provides a convenient and reliable common basis for comparing results from different MS techniques (*e.g.*, quadrupole, time-of-flight, and Fourier transform ion trap instruments). For modern mass spectrometers, mass separation efficiency can range from a few thousand (quadrupoles and electrodynamic ion traps), to tens of thousands (time-of-flight), to upwards of one million resolving power (Fourier transform MS). In contrast, IM resolving power is commonly calculated from the technique-specific mobility dispersion dimension (*e.g.*, drift time or dispersion voltage) and resolving powers are rarely reported above 100.

While the time-based definition of resolving power ($t/\Delta t$) has been utilized for over two decades to report the separation efficiency of DTIMS instruments, the emergence of other IM techniques has complicated the interpretation of the time-based IM resolving power. For example, TWIMS ion mobility dispersion occurs on a timescale that is about an order of magnitude faster than many DTIMS platforms, resulting in erroneously low resolving power value when the time-based definition is utilized. The shortcomings of a time-based resolving power definition led Giles and coworkers to report a CCS-based resolving power (CCS/ΔCCS) when quantifying the separation efficiency of a second-generation TWIMS device.[6] For some IM techniques, mobility separations do not directly occur in the time domain, such as with TIMS and FAIMS/DMS where a scanned electric field is utilized to generate a time-dependent IM spectrum. As recently underscored by Glish and coworkers, FAIMS/DMS is capable of achieving very high resolving power numbers (*e.g.*, 7903), however, the corresponding 2-peak separation is lower than this high

resolving power suggested.[18] Hence, a technique-specific resolving power definition cannot give a comparable description of the analytical selectivity of different IM instruments.

While a single peak resolving power definition is a convenient metric for assessing IM instrument performance, practical separation efficiency is also often defined in terms of two-peak resolution (R_{pp}), which is a definition commonly used in condensed phase chromatography to quantify separation efficiency. IM shares similarities with chromatography, namely that analyte separations in both techniques are based on an extrinsic property (retention time and CCS, respectively) which can be altered to enhance the analytical selectivity of the separation. Two-peak resolution in IM is defined as separation of two closely-spaced Gaussian peaks (*e.g.* compounds A and B) via equation 2.[19,20]

$$R_{pp}(\text{experiment}) = 1.18 \text{ x} \frac{X_B - X_A}{\Delta x_B + \Delta x_A} \quad (2)$$

Conventionally for IM, equation 2 is defined in the time-domain (drift time for x) and the fwhm of each peak is used. Our previous study indicated a direct relationship between two-peak resolution (R_{pp}), single-peak resolving power (R_p) and the ion's gas-phase collision cross section (CCS), through equation 3.[21]

$$R_{pp}\ (\text{predicted}) = 0.00589 \text{ x } R_p \text{x } \Delta\text{CCS\%} \quad (3)$$

Here the resolution is denoted as "predicted" to indicate that this value can be obtained theoretically. For a mobility separation of two analytes, R_p should be calculated as the average resolving power of both peaks, whereas the percent difference in cross section (ΔCCS%) is based on the average CCS, as defined in equation 4.

$$\Delta CCS\% = \frac{(CCS_B - CCS_A)}{\text{avgerage } CCS_{A,B}} \text{ x } 100\% \quad (4)$$

We emphasize here that the ΔCCS% is a measure of how different two compounds are in cross section space, calculated as a percentage, and in this manner ΔCCS% is size-independent. For example, two molecules with CCS measurements of 100 and 101 $Å^2$ (Δ 1 $Å^2$) have the same ΔCCS% (1.0% difference) as a separate pair of compounds measuring 200 and 202 $Å^2$ (Δ 2 $Å^2$). These two separations should be equally challenging, and hence require the same measure of resolving power to separate as their percent difference in CCS space is equal. It is also important to note that when resolving power is measured as CCS/ΔCCS, that ΔCCS is the FWHM of a given IMS peak, and is not related to the percent difference in cross section of two peaks (ΔCCS%).

The validity of equation 4 was previously established based on a Gaussian fit to uniform field IM data and provided the basis for predicting the IM separation of two analytes in a hypothetical mixture given that both their CCS values and the instrument resolving power was known.[21]

In this present study, we attempt to ascertain whether the relationship in equation 3 reflects a general observation of mobility behavior across various instrumentation and techniques. Thus this work endeavors to unify the various methods of mobility separation under a single descriptor of analytical efficiency in order to predict analyte separation for cross systems assessment.

5.2. Experimental Methods

5.2.1. Chemical Standards

L-leucine (61819) and L-isoleucine (I2752) were obtained from Sigma-Aldrich (St. Louis, MO, USA). The protein digest standard (MassPrep Mix 1) was obtained from Waters Co. (Milford, MA, USA) and consists of four tryptically-digested proteins (yeast enolase, rabbit phophorylase b, yeast alcohol dehydrogenase, and bovine serum albumin). The L-leucine and L-isoleucine standards were reconstituted to a final concentration of 10 μg/mL in high purity water (18 MΩ, Milli-Q, EMD Millipore, Billerica, MA, USA) buffered with 10 mM ammonium acetate (Sigma-Aldrich) to a pH of 6.5 (SevenEasy pH Meter, Mettler-Toledo, Columbus, OH, USA).

5.2.2. Instrumentation and Methods

A commercial DTIMS instrument (6560, Agilent Technologies) was used for all empirical CCS measurements performed in this study. Details of the instrumentation and CCS method have been previously described.[7,19,22] Briefly, chemical standards were directly infused into the electrospray ionization source (Jet Stream, Agilent) at a flow rate of 5 μL/min using a syringe pump (KDS 101, KD Scientific, Inc.). Ion mobility separations were conducted in a uniform field drift tube operated with high purity nitrogen drift gas at 3.95 Torr and room temperature (*ca.* 298 K). A seven-frame stepped electric field method was utilized in the range of 10.9 to 18.5 V/cm, which provided the necessary data to perform a linear regression analysis used to determine the non-mobility ion transit times. This DTIMS CCS method was previously optimized based on the results of an interlaboratory study.[23]

5.2.3. Selection of Published Spectra

Previously published IM spectra were selected for this current study based on the quality of the published spectra, the inclusion of two well-defined ion mobility distributions (either partially or fully resolved), and the requirement that measurements were obtained from pure chemical standards. A diverse set of spectra were selected representing different IM instrumentation and techniques. The applicability of a Gaussian-based model for separation was assessed using a protocol described in the Supporting Information (Figure E.1). Briefly, theoretical Gaussian distributions were generated and overlaid onto IM spectra obtained from the literature (see Figure 5.1 A-F). The important assumption made here is that the published IM spectra represent near optimal separations for each IM technique, as these spectra were obtained from experts in their respective fields. While not comprehensive, the spectra chosen here are representative of many well-conducted studies across the field. A comprehensive and annotated list of references to each spectrum used in this assessment is provided in the Supporting Information (Appendix E.1).

5.2.4. Evaluation of Separation Efficiency

A total of 22 published ion mobility separations were examined from multiple sources including peer-reviewed literature, conference posters, and instrument vendor white papers, which represent various IM techniques and platforms (Table E.2) and a broad range of analyte masses (131 to 8566 Da). For each separation, CCS values were used as reported from the cited source and the percent difference in CCS was calculated through equation 4. Average resolving power and resolution were calculated via equations 1 and 2, respectively, using the dimension of the reported separation. Utilizing the average resolving power and the calculated percent difference in CCS, the predicted resolution (R_{pp}) is subsequently calculated via equation 3. In order to compare

the theoretical resolution predicted by equation 4 to the observed experimental two-peak resolution, we calculate the percent error in our prediction through equation 5.

$$\text{Percent Error} = \frac{\text{Experimental } R_{\text{pp}} - \text{Predicted } R_{\text{pp}}}{\text{Experimental } R_{\text{pp}}} \text{ x } 100\% \quad (5)$$

5.3. Results and Discussion

5.3.1. Gaussian Distributions

While the mechanics of ion diffusion in drift tube instruments are well characterized and can be described as Gaussian to a good approximation,[24-26] the band-broadening mechanisms for other IM separation methods cannot be easily described by the first principles established in the kinetic theory of gases. To determine if other mobility techniques exhibit peak shapes that can modeled with a normal distribution, the IM spectra selected for this study were examined using a protocol described in the Supporting Information (Figure E.1). Based on the quality of correlation observed between the published IM spectra and the theoretical Gaussian distributions, it was concluded here that the spectra from a wide distribution of IM techniques exhibit peak shapes accurately described by a normal distribution in standard operating conditions (*e.g.* no secondary conformers or peak saturation is observed (Figure 5.1 A-F). This observation, in turn, justifies the use of a Gaussian-based mathematical description of ion mobility separation efficiency.

5.3.2. CCS-Based Resolving Power

Obtaining CCS from different IM experiments can be challenging as the fundamental ion mobility equation is only applicable for uniform field instruments with well-characterized gas

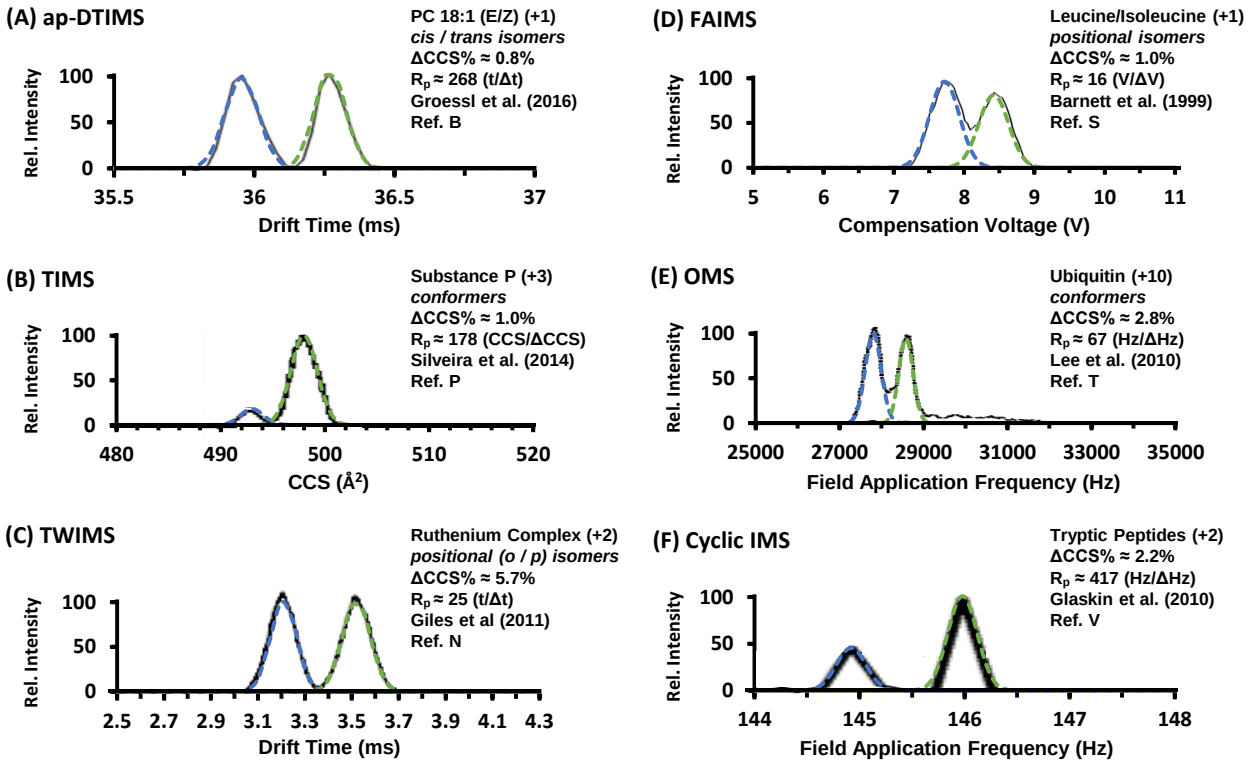

Figure 5.1. Selected IM spectra obtained from the literature representing challenging analyte separations using various IM techniques and instrumentation. Gaussian distribution overlays are shown as dotted traces. The corresponding single-peak resolving powers and percent differences in CCS as determined in the current analysis are provided for each example. **(A)** Reproduced/Adapted with permission from Groessl and coworkers, 2016 (see Supporting Information). **(B)** Reproduced/Adapted with permission from Ref. 30. American Chemical Society, 2014. **(C)** Reproduced/Adapted with permission from Ref. 6. Wiley and Sons, 2011. (D) Reproduced/Adapted with permission from Ref. 52. Elsevier, 1999. **(E)** Reproduced/Adapted with permission from Ref. 32. American Chemical Society, 2010. **(F)** Reproduced/Adapted with permission from Ref. 36. American Chemical Society, 2010.

compositions, *e.g.*, DTIMS and DMA. Other IM techniques, namely TWIMS, OMS[27-29] and TIMS[12,30,31] have established protocols for converting the corresponding transmission frequency of analytes into CCS or K_o,[31,32] which is of particular utility in relation to equations 3 and 4. Defining the FAIMS and DMS separations in terms of CCS is more challenging as the mobility spectra are reported in terms of the compensation voltage that transmits the ion of interest. Depending on the particular experiment setup, nominal resolving power in FAIMS ($V/\Delta V$) can be artificially low (Figure 5.1 D), or uncharacteristically high, as noted by a recent report.[18] It is not currently possible to translate FAIMS or DMS measurements directly into cross section space using a fundamental relationship. In addition, many FAIMS and DMS experiments are carried out in a mixture of drift gases in order to enhance selectivity,[33,34] making comparisons to published CCS values (which are gas-specific) challenging.[35] For the purposes of this study, chemical systems with known CCS values are selected, which allows each chosen spectra to be evaluated in terms of the percent difference in CCS.

5.3.3. Cross-Platform Assessment

For the 22 ion mobility separations surveyed in this study, both the observed experimental resolution (equation 2) and predicted resolution (equation 3), were calculated and the corresponding percent error between these calculations was determined via equation 5. The percent error is a reflection of the ability of equation 3 to predict the level of separation efficiency for two analytes possessing a characterized difference in cross section at a given level of resolving power. Results are summarized in Table 5.2. Mobility separations for DTIMS, TIMS, and OMS instruments[32,36-41] (Data Points A to J, and T) show sufficient agreement with equation 3, with typically less than 10% error between the experimental and predicted resolution. We consider this

	First Author	Ref. Point	Percent Difference in CCS (%)[1]	Reported Resolving Power (R_p)[2]	Calculated Resolving Power (R_p)[3]	Experimental Resolution (R_{pp})[4]	Predicted Resolution (R_{pp})[5]	Percent Error in Resolution (%)[6]	Dispersion Axis Projected in IM Spectra
DTIMS	Groessl, M.	A	0.4	>250	332	0.84	0.78	7.3	t_d (ms)
	Groessl, M.	B	0.8	250	268	1.38	1.26	8.3	t_d (ms)
	Groessl, M.	C	[1.2]	[251]	251	1.77	1.77	-0.3	t_d (ms)
	Asbury, G. R.	D	[1.2]	[130]	131	0.76	0.93	-22.2	t_d (ms)
	Groessl, M.	E	1.3	[187]	187	1.31	1.46	-11.8	t_d (ms)
	Pierson, G. U.	F	1.7	[66]	66	0.65	0.65	0.1	CCS (Å^2)
	Tang , G. R.	G	1.7	[62]	63	0.58	0.63	-8.0	t_d (ms)
	Dodds, J. N.	H	2.3	58	58	0.79	0.79	0.1	CCS (Å^2)
	Gaye, M. M.	I	2.6	[83]	83	1.26	1.26	0.0	CCS (Å^2)
	Adamov, A.	J	3.2	77	72	1.46	1.46	-0.2	K_0 (cm^2/Vs)
TWIMS	Deng, L.	K	0.4	124	342	0.71	0.26	63.1	t_d (ms)
	Giles, K.	L	1.5	--	[208]	4.34	1.90	56.3	t_d (ms)
	Giles, K.	M	5.1	18	40	1.21	0.55	55.0	t_d (ms)
	Giles, K.	N	5.7	25	41	1.36	0.83	38.7	t_d (ms)
	Hofmann, J.	O	5.9	26	43	1.51	0.88	41.4	t_d (ms)
TIMS	Silveira, J. A.	P	1.0	154-183	178	1.05	1.06	-0.3	CCS (Å^2)
	Bruker	Q	1.0	[113]	113	0.68	0.69	-0.6	K_0 (cm^2/Vs)
	Bruker	R	1.7	185	177	1.74	1.74	0.1	K_0 (cm^2/Vs)
OTHER	Barnett, D. A.	S	[1.0]	--	130	0.83	--	--	Voltage (V)
	Lee, S.	T	2.8	[66]	67	1.09	1.09	0.1	Frequency (Hz)
	Glaskin, R. S.	U	2.7	121	85	1.42	1.33	6.3	Frequency (Hz)
	Glaskin, R. S.	V	2.2	417	145	1.90	5.72	185	Frequency (Hz)

1. Calculated from equation 4. Bracketed values were determined using CCS values obtained in the PI's laboratory
2. Bracketed values were calculated from equation 1 using the dispersion axis provided.
3. Calculated from equation 1 using the CCS-based definition for R_p.
4. Calculated from equation 2 using the dispersion axis provided.
5. Calculated from equation 3 using the dispersion axis provided.
6. Calculated from equation 5.

Table 5.2. Separation parameters reported for various ion mobility platforms. The "Reference Point" column references the annotations in Figure 4 and in Appendix S1 of the supporting information.

good agreement as experimental single-peak resolving power can vary by as much as 11% between consecutive measurements on a DTIMS instrument.[22] This good correlation suggests for DTIMS, TIMS, and OMS, the separation efficiency as determined from each corresponding dispersion dimension correlate to their respective CCS-based resolving powers. In some cases, for FAIMS/DMS, the (time and frequency, respectively) correlate closely with the CCS-based R_p definition developed in this work. However, FAIMS/DMS and cyclic IMS separations are currently reported based on dispersion voltages or field application frequency, respectively, which yield R_p values that do not dispersion axis is reported with negative values which cannot be used to determine resolving power. For cyclic IMS, the frequency based R_p values are higher than the CCS-based R_p, whereas utilizing the voltage axis in FAIMS yields R_p values that are lower than their corresponding CCS-based R_p. An erroneously low R_p was also found for TWIMS when using the time-domain definition of resolving power, and this result is discussed in detail in the following section.

5.3.4. Traveling Wave Resolving Power

Large deviations from equation 4 in terms of percent error (typically 40% or larger) were found for traveling wave instruments, which are utilized extensively by the IM-MS community. This limitation in time-based R_p calculations for TWIMS has been previously reported. For example, in their well-documented separation of reverse peptides (SDGRG and GRGDS, point M) Giles and coworkers were able to separate these two sequence isomers with *ca.* 5.1% difference in CCS to near baseline resolution using a second generation TWIMS geometry (Synapt G2).[6] Using their experimental time-based resolving power of *ca.* 18 ($t_d/\Delta t_d$) results in *ca.* 55% error through the prediction given by equation 4 (Figure D.2 A). The interpretation of this discrepancy is that

although both drift tube and traveling wave experiments are time-dispersive separations, traveling wave devices operate at a higher level of selectivity than would be expected for their corresponding time based resolving power.[6,42,43] Interestingly, using the established protocols for converting analyte drift time to CCS in TWIMS,[44,45] Giles and coworkers also calculated resolving power in cross section space (CCS/ΔCCS). Their resulting experimental CCS-based R_p are nearly identical to what is found in this current work (*ca.* 40 CCS/ΔCCS) and show much more agreement to the predicted R_p (equation 3) than the time-based R_p, with 1% versus 55% error, respectively, based on equation 5 (Figure E.2 B). Following this example, we converted TWIMS resolving power from the time domain ($t_d/\Delta t_d$) to CCS space (CCS/ΔCCS) for five different TWIMS separations reported in the literature, and the results are summarized in Table E.1 (also Figures E.3, E.4, and Table E.1). The five selected TWIMS separations include 3 studies of isomer separations obtained on the Synapt G2 (Points M, N, and O) where time based R_p is *ca*. 20-25,[6,46] however once the CCS-based definition of equation 1 is used, the R_p is approximately doubled (*ca.* 40 CCS/ΔCCS). These larger R_p values better-reflect the analytical selectivity of TWIMS, with a corresponding low percent error predicted by equation 5. Conversion to CCS-based R_p is also necessary for the recently developed cyclic TWIMS[4,47] (Point L) which indicates that this device operates with a resolving power of *ca.* 480 for 50 cycles (*c.f.*, Table E.1). Additionally, the SLIM-based TWIMS instrument currently being developed by Smith and coworkers at Pacific Northwest National Laboratory (Point K),[48] has shown very high analytical separation capabilities, and using the CCS-based definition, we can quantify for the first time the resolving power of current SLIM-based TWIMS devices as benchmarking around 340 (Figure E.4). We note that the SLIM technology was initially developed for DTIMS-based separations.[49,50] The discrepancy between CCS and time

based R_p in TWIMS is related to the nonlinear relationship between voltage and analyte drift time in these devices, which has been discussed previously.[42,43,51]

5.3.5. Cross-Platform Assessment of Separation Capabilities

Unlike the TWIMS instruments, both time and CCS based R_p are nominally very similar for drift tube instruments. For example, in our previous work the separations related to isomers of leucine/isoleucine indicate the same level of nominal resolving power in both the time dimension and CCS space (*ca.* 60 $t_d/\Delta t_d$ and CCS/ΔCCS).[21] Other DTIMS conversions from time to CCS-based R_p also indicated negligible differences in resolving power, typically less than 5%. This correlation of R_p in both the time and CCS dimension is a result of the linear relationship between drift time and CCS in uniform field instruments. Other IM techniques in Figure 5.1 measure R_p in terms of reduced mobility ($K_o/\Delta K_o$) and also exhibit low percent error. As FAIMS is not able to empirically measure CCS, the only FAIMS spectrum used in this work (Point S, Table 5.2),[52] is included for comparison using previously measured nitrogen-based CCS values in our laboratory. Also, it should be noted that Barnett *et. al.* utilized ambient air (compressed) as the buffer gas instead of pure nitrogen, which will yield a slightly different CCS than what is used in this comparison.[52]

With a common frame of reference, we can compare the separation abilities of various IM techniques. The plot in Figure 2 depicts boundary regions representing various levels of separation efficiency calculated through equation 3 covering a wide range of percent difference in CCS and resolving power. Numerical relationships between R_p and $\Delta CCS\%$ are tabulated in Tables 5.2 and E.1. The location of a given data point in Figure 5.2 corresponds to the percent difference in CCS

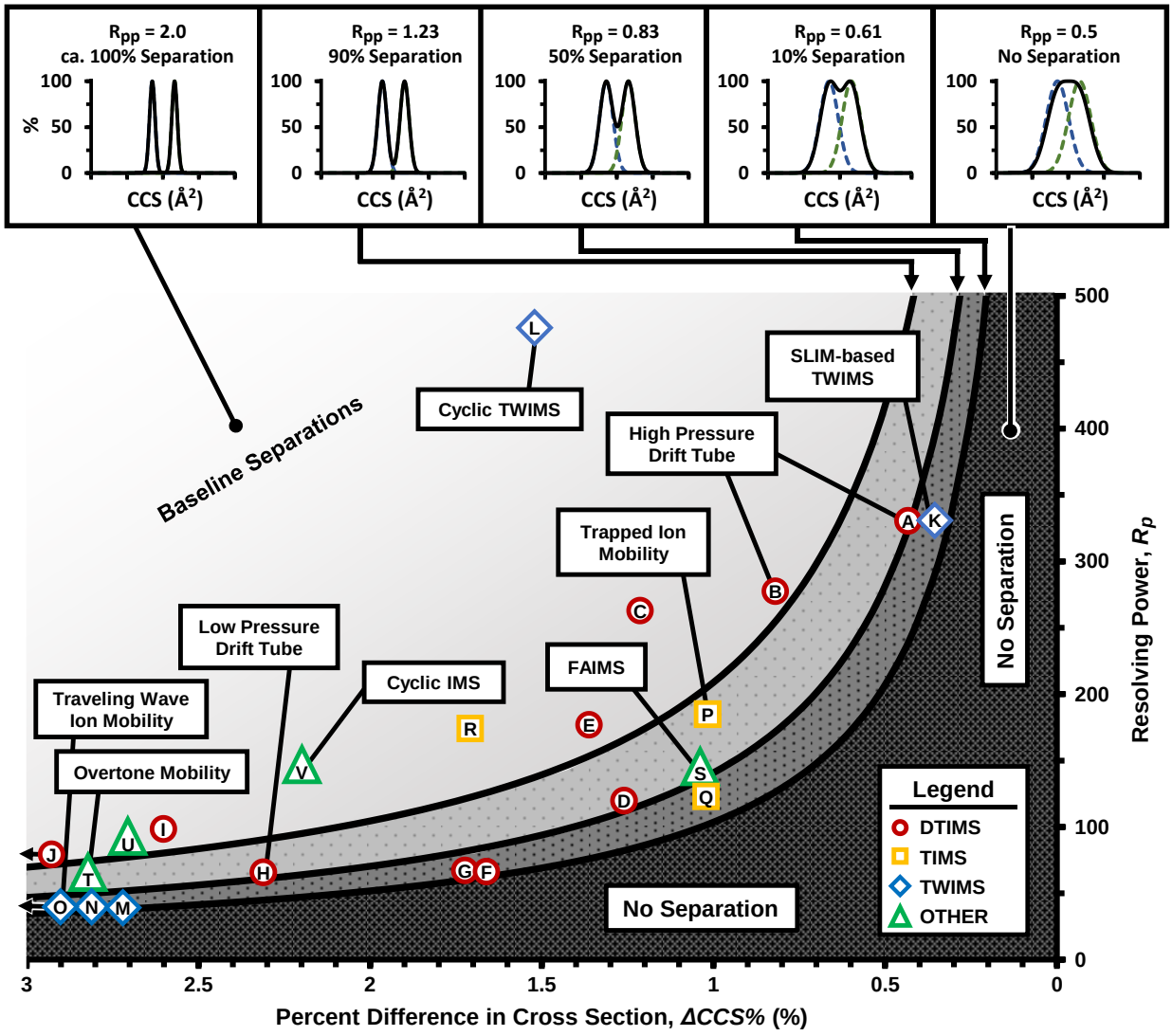

Figure 5.2. Plot depicting the required resolving power to separate two compounds in ion mobility with a known percent difference in cross section. Various levels of separation efficiency are indicated along the top panels both in terms of two-peak resolution (R_{pp}) and visually by means of percent separation. Previously published ion mobility separations (c.f., Table 2) are referenced in the plot and represent various ion mobility techniques. The techniques labeled "Other" (green triangles) include FAIMS, OMS, and cyclic IMS. Resolving powers for traveling wave and cyclic IMS instruments are reported here in the ion cross section domain (CCS/ΔCCS).

of the specific compounds analyzed, the experimental resolving power (determined as described previously), and the calculated two-peak resolution of the published separation. The light shaded region at the top left section of the graph corresponds to all combinations of ΔCCS% and R_p which will yield baseline or greater separation ($R_{pp} \geq 1.23$). For example, reverse peptides (SDGRG/GRGDS (+1), ΔCCS = 1.5%) were baseline separated by Giles *et. al.* using a prototype cyclic TWIMS instrument with *ca.* 480 resolving power (CCS/ΔCCS) (Point L, $R_{pp} = 4.34$).[53] The darker shaded regions at the bottom right of Figure 2 indicate regions of greater than half-height separation ($R_{pp} \geq 1.23$), equal to half height separation ($R_{pp} = 0.83$) and minimum resolution ($R_{p\text{-}p} \leq 0.61$, or 10% separation), respectively. Note the current state-of-the art in IM performs with R_p over 300, which enables separation of ions differing by as little as ca. 0.5% in CCS (*e.g.*, 1 Å^2 at 200 Å^2).[54,55] In the ap-DTIMS examples chosen for this work, high resolution is achieved by operating the instrument at greater than atmospheric pressures (*ca.* 1050 Torr) and utilizing Hadamard transform multiplexing.[56,57]

Figure 5.2 reveals several important analytical trends for the field of ion mobility. First, despite the wide range of CCS values represented here (ca. 100 to 500 Å^2), the percent difference in CCS and the CCS-based R_p represents robust parameters for comparing the relative separation capabilities of different IM instrumentation. Second, various IM instruments operate across a very wide range of separation efficiencies, with the majority of commercially-available IM-MS platforms accessing IM resolving powers of 80 or less. The highest separation efficiencies represent ap-DTIMS and long path length TWIMS devices (both cyclic and serpentine), which have demonstrated resolving powers (CCS/ΔCCS) in excess of 300.

5.3.6. How Much Resolving Power is Necessary

In order to assess the amount of resolving power required for routine ion mobility separation in biological applications, a protein digest was evaluated, which yielded a total of 100 CCS measurements for +1 and +2 protonated tryptic peptides. Identifications were made on the basis of mass measurement accuracy, which was less than 5 ppm for all peptides used in the subsequent analysis.

5.3.6.1. Mass Analysis

In order to describe the separation of the digested peptides by IM-MS, first we examine the mass dimension of the separation (Figure 3A). Of the 204 possible peptides (no missed cleavages), 10 peptides (*ca.* 5%) are constituents of isomeric pairs generated by permuted amino acid sequences (*e.g.*, LAK and ALK) or isomeric amino acid substitutions (*e.g.* leucine/isoleucine) and hence are not resolvable by single-dimensional MS alone. To separate all 204 possible peptides in the digest (excluding the 5 isomer pairs) from the nearest neighboring peak (*i.e.* 203 separations) would require *ca.* 100,000 mass resolving power (Figure 3A and 3C), which is currently obtainable by FTMS (Orbitraps and ion cyclotron resonance).[58-60] The smallest observable difference in the mass dimension was 0.062 Δm/z, which requires greater than 10,000 mass R_p to separate at half height. Interestingly, by noting all of the possible peptides produced in the digest, Figure 3A shows that a mass resolving power of 10,000 should be able to resolve *ca.* 95% of the possible peptides in the mixture at half height. If the mass R_p was increased by an order of magnitude to 100,000 (*e.g.*, an Orbitrap mass analyzer) peptide coverage only increases by 3% (198/203 peptide pairs

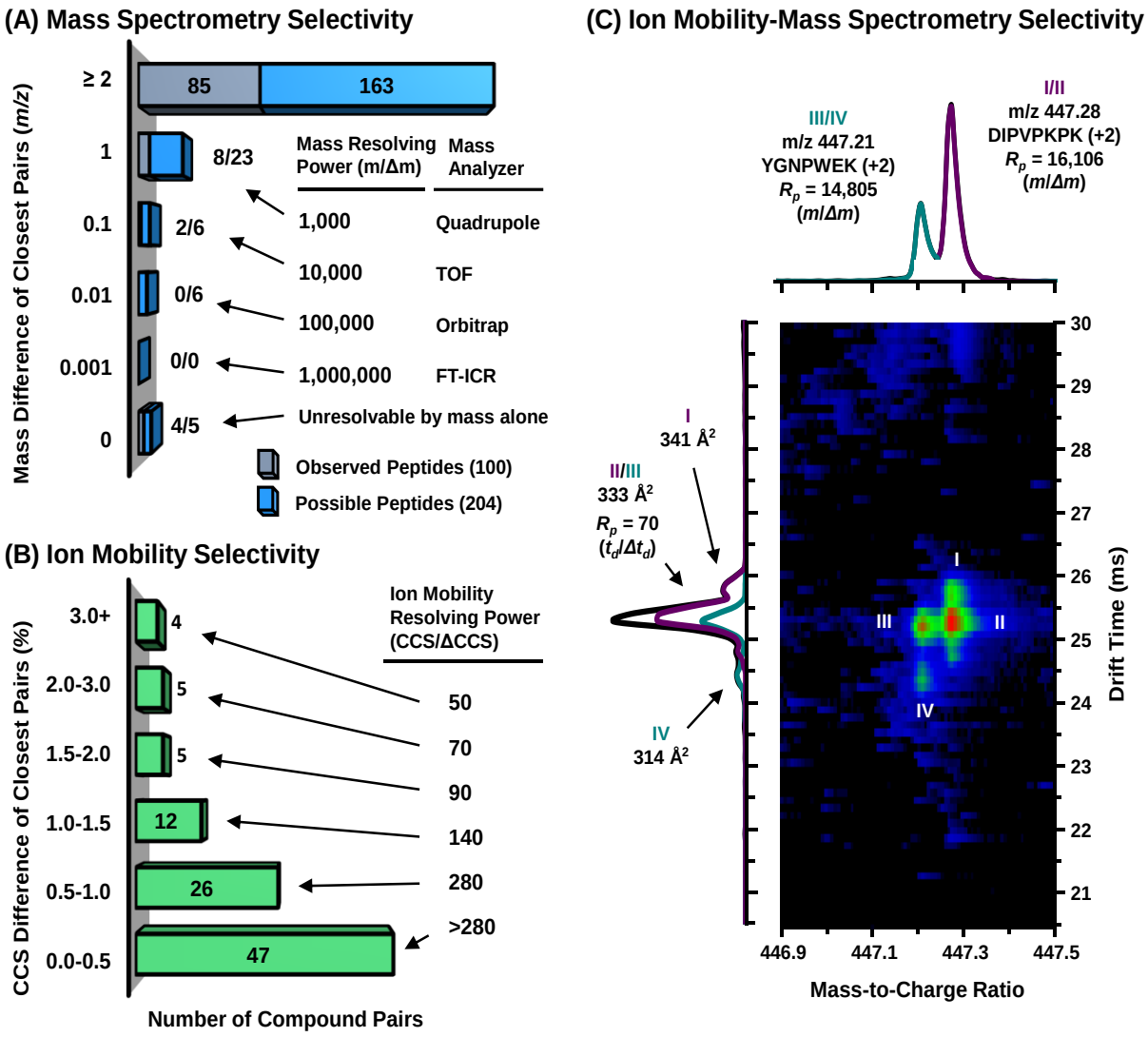

Figure 5.3. Comparison of mass spectrometry and ion mobility data collected from a tryptic peptide mixture originating from four proteins. **(A)** Difference in m/z between nearest neighbors for all possible peptides in the digest mixture (light blue) and from those peptides observed experimentally in this study (gray). **(B)** Bar graph of the percent difference in CCS between nearest-neighboring peptides for the 99 analyte pairs observed. **(C)** Separation of two doubly charged peptides by mass spectrometry and suspected conformers of each peptide noted through ion mobility.

separable). Thus, for this proteomics example, high resolution MS is the primary analytical dimension in which most analytes are resolved.

5.3.6.2. Ion Mobility Analysis

To examine the potential of separating the peptides based on differences in mobility, the 100 observed analytes were sorted in order of increasing CCS and the percent difference in CCS from the nearest neighbor peak was calculated (Figure 5.3 B). The results of this pair-wise CCS analysis indicate that more than half of the compound pairs analyzed (*ca.* 53%) have a percent difference in CCS of at least 0.5% from their nearest neighbor. Separating these compounds based purely on mobility alone would require 280 resolving power or less, which is currently obtainable (Table S2). [30,57,61] To separate *ca.* 95% (CCS $\geq$ 0.02%) of the peptides by IM alone would require about 7,000 mobility resolving power. Interestingly, this level of mobility resolving power is on the same order of magnitude as a moderate resolution mass analyzer (*c.f.*, Figure 3 A). However, this magnitude of resolving power is far beyond the capabilities of current IM instrumentation. Also, if the sample size was increased (*i.e.* N>100 compounds), the probability of concomitant IM peaks would be high and thus decreases the likelihood of discrete analytes being resolved. This indicates that IM selectivity is supplemental to the superior separation capabilities of MS and the best analytical performance is achieved when both techniques are used in concert (IM-MS).

5.3.7. Ion Mobility-Mass Spectrometry

Clearly, the full analytical utility of ion mobility is accessible only when directly coupled to a mass spectrometer.[4,62,63] Current mass analyzers are highly selective (R_p > 100,000), and, in

many cases, accurate mass measurement when combined with tandem MS/MS capabilities can elucidate an analyte identification. However, when investigating analytical mixtures that possess isomers or investigating proteins which often express many conformers, ion mobility analysis is chemically insightful. For example, Figure 5.3 C illustrates a closer examination of two peaks noted in the IM-MS experiment for the protein digest. Two different peptides (from two different protein precursors) have an exact mass difference of 0.063 m/z and are resolvable by TOF mass analysis (features I/II and III/IV). However, the mass spectrometer cannot distinguish that DIPVPKPK (+2) has two distinct isobaric features (I and II) that are discernible in the ion mobility dimension at 70 resolving power ($t_d/\Delta t_d$) for this +2 ion. Likewise, YGNPWEK (+2) also possesses secondary features when observed in the IM dimension (III/IV). However, the primary features (II and III) possess near identical CCS values and are unresolvable by ion mobility alone whereas the mass spectrometer resolves these features as two distinct peaks. Hence, the utility of IM-MS is evident in the analysis of complex samples that require identification of both distinct molecules (MS) and potential isomers, conformers or multimeric species of these compounds (IM), illustrating the well-known advantages of hyphenated separations.[64,65]

5.4. Conclusions

Here we develop a straightforward theoretical framework for comparing the separation efficiency of different IM techniques by defining the instrument resolving power in terms of the gas-phase CCS. We note that defining resolving power in this manner is particularly critical for obtaining meaningful metrics of separation capabilities for TWIMS techniques. Based on the analysis developed in this work, the separation capabilities of various IM instrumentation can, for the first time, be compared relative to differences in the gas-phase CCS. The results of this study

indicate that current ion mobility instruments operate across a broad range of separation efficiencies between 50 and 300 resolving power (CCS/ΔCCS) and the current state-of-the-art IM instruments are now demonstrating R_p in excess of 300 and thus are capable of separating compounds with CCS differences as low as 0.5% (c.f., Table 2). While this high level of structural selectivity enables IM to resolve constitutional isomers and conformers (typically 0.5% difference in CCS or greater), we hypothesize to resolve the majority of the components in a biological mixture using ion mobility alone would require resolving powers on the order of several thousand, which is far beyond the capabilities of current instrumentation and may not be achievable due to fundamental peak broadening limits imposed by ion diffusion. Ion mobility experiments therefore provide the greatest analytical benefits when combined with mass spectrometry, as well as other analytical dimensions (*e.g.* LC-IM-MS), which collectively function to broaden the analytical selectivity of the chemical separation. Nevertheless, routine ion mobility resolving powers in excess of 300 which are now being demonstrated will be essential to addressing chemical separations in highly challenging studies, such as in synthetic biology, medicine, and the omics sciences.

Finally, the guidance as illustrated in this manuscript suggest a potential criterion for reporting ion mobility resolving power in the future, similar to guidelines also reported in other scientific contexts, such as standards set forth for microarray (MIAME)",[66] proteomics (MIAPE)",[67] and glycomics experiments (MIRAGE).[68]

5.5. Acknowledgements

This chapter contains the published research article: James N. Dodds, Jody C. May, and John A. McLean, "Correlating Resolving Power, Resolution and Collision Cross Section: Unifying Cross Platform Assessment of Separation Efficiency in Ion Mobility Spectrometry," *Analytical Chemistry* **2017,** *89*, 12176-12184.

Financial support for aspects of this research was provided by The National Institutes of Health (NIH Grant R01GM099218) and under Assistance Agreement No. 83573601 awarded by the U. S. Environmental Protection Agency. This work has not been formally reviewed by EPA. The views expressed in this document are solely those of the authors and do not necessarily reflect those of the Agency. EPA does not endorse any products or commercial services mentioned in this publication. Furthermore, the content is solely the responsibility of the authors and does not necessarily represent the official views of the funding agencies and organizations.

5.6. References

1. Zhong, Y.; Hyung, S.-J.; Ruotolo, B. T., Ion Mobility-Mass Spectrometry for Structural Proteomics. *Expert Rev Proteomic* **2012**, *9*, 47-58.

2. Lapthorn, C.; Pullen, F.; Chowdhry, B. Z., Ion Mobility Spectrometry-Mass Spectrometry (IM-MS) of Small Molecules: Separating and Assigning Structures to Ions. *Mass Spectrom. Rev.* **2012**, *32*, 43-71.

3. Maurer, M. M.; Donohoe, G. C.; Valentine, S. J., Advances in Ion Mobility-Mass Spectrometry Instrumentation and Techniques for Characterizing Structural Heterogeneity. *Analyst* **2015**, *140*, 6782-6798.

4. May, J. C.; McLean, J. A., Ion Mobility-Mass Spectrometry: Time-Dispersive Instrumentation. *Anal. Chem.* **2015**, *87*, 1422-1436.

5. Giles, K.; Pringle, S. D.; Worthington, K. R.; Little, D.; L., W. J.; Bateman, R. H., Applications of a Travelling Wave-Based Radio-Frequency-Only Stacked Ring Ion Guide. *Rapid Commun. Mass Spectrom.* **2004**, *18*, 2401-2414.

6. Giles, K.; Williams, J. P.; Campuzano, I., Enhancements in Travelling Wave Ion Mobility Resolution. *Rapid Commun. Mass Spectrom.* **2011**, *25*, 1559-1566.

7. May, J. C.; Goodwin, C. R.; Lareau, N. M.; Leaptrot, K. L.; Morris, C. B.; Kurulugama, R. T.; Mordehai, A.; Klein, C.; Barry, W.; Darland, E.; Overney, G.; Imatani, K.; Stafford, G. C.; Fjeldsted, J. C.; McLean, J. A., Conformational Ordering of Biomolecules in the Gas Phase: Nitrogen Collision Cross Sections Measured on a Prototype High Resolution Drift Tube Ion Mobility-Mass Spectrometer. *Anal. Chem.* **2014**, *86*, 2107-2116.

8. Allen, S. J.; Giles, K.; Gilbert, T.; Bush, M. F., Ion Mobility Mass Spectrometry of Peptide, Protein, and Protein Complex Ions Using a Radio-Frequency Confining Drift Cell. *Analyst* **2016**, *141*, 884-891.

9. Shvartsburg, A. A., *Differential Ion Mobility Spectrometry: Nonlinear Ion Transport and Fundamentals of FAIMS*; CRC Press: Boca Raton, FL, 2009.

10. Purves, R. W., Enhancement of Biological Mass Spectrometry by Using Separations Based on Changes in Ion Mobility (FAIMS and DMS). *Anal. Bioanal. Chem.* **2013**, *405*, 35-42.

11. Amo-Gonzalez, M.; Fernandez de la Mora, J., Mobility Peak Tailing Reduction in a Differential Mobility Analyzer (DMA) Coupled with a Mass Spectrometer and Several Ionization Sources. *J. Am. Soc. Mass Spectrom.* **2017**, *8*, 1506-1517.

12. Fernandez-Lima, F. A.; Kaplan, D. A.; Suetering, J.; Park, M. A., Trapped Ion Mobility Spectrometry: Past, Present and Future Trends. *Int. J. Ion Mobil. Spectrom.* **2011**, *14*, 93-98.

13. Michelmann, K.; Silveira, J. A.; Ridgeway, M. E.; Park, M. A., Fundamentals of Trapped Ion Mobility Spectrometry. *J. Am. Soc. Mass Spectrom.* **2015**, *26*, 14-24.

14. Vidal-de-Miguel, G.; Macía, M.; Cuevas, J., Transversal Modulation Ion Mobility Spectrometry (TM-IMS), A New Mobility Filter Overcoming Turbulence Related Limitations. *Anal. Chem.* **2012**, *84*, 7831-7837.

15. Deng, L.; Ibrahim, Y. M.; Hamid, A. M.; Garimella, S. V.; Webb, I. K.; Zheng, X.; Prost, S. A.; Sandoval, J. A.; Norheim, R. V.; Anderson, G. A.; Tolmachev, A. V.; Baker, E. S.; Ibrahim, Y. M.; Smith, R. D., Ultra-High Resolution Ion Mobility Separations Utilizing Traveling Waves in a 13m Serpentine Path Length Structures for Lossless Ion Manipulations Module. *Anal. Chem.* **2016**, *88*, 8957-8964.

16. Deng, L.; Webb, I. K.; Garimella, S. V.; Hamid, A. M.; Zheng, X.; Norheim, R. V.; Prost, S. A.; Anderson, G. A.; Sandoval, J. A.; Baker, E. S. Ibrahim, Y. M.; Smith, R. D., Serpentine Ultralong Path with Extended Routing (SUPER) High Resolution Traveling

Wave Ion Mobility-MS Using Structures for Lossless Ion Manipulations. *Anal. Chem.* **2017**, *89*, 4628-4634.

17. Siems, W. F.; Wu, C.; Tarver, E. E.; Hill, H. H., Jr.; Larsen, P. R.; McMinn, D. G., Measuring the Resolving Power of Ion Mobility Spectrometers. *Anal. Chem.* **1994**, *66*, 4195-4201.

18. Santiago, B. G.; Harris, R. A.; Isenberg, S. L.; Glish, G. L., Resolving Powers of >7900 Using Linked Scans: How Well Does Resolving Power Describe the Separation Capability of Differential Ion Mobility Spectrometry. *Analyst* **2015**, *140*, 6871-6878.

19. Kurulugama, R. T.; Darland, E.; Kuhlmann, F.; Stafford, G.; Fjeldsted, J., Evaluation of Drift Gas Selection in Complex Sample Analyses Using a High Performance Drift Tube Ion Mobility-QTOF Mass Spectrometer. *Analyst* **2015**, *14*, 6834-6844.

20. Tabrizchi, M.; Rouholahnejad, F., Pressure Effects on Resolution in Ion Mobility Spectrometry. *Talanta* **2006**, *69*, 87-90.

21. Dodds, J. N.; May, J. C.; McLean, J. A., Investigation of the Complete Suite of Leucine and Isoleucine Isomers: Toward Prediction of Ion Mobility Separation Capabilities. *Anal. Chem.* **2016**, *89*, 952-959.

22. May, J. C.; Dodds, J. N.; Kurulugama, R. T.; Stafford, G. C.; Fjeldsted, J. C.; McLean, J. A., Broadscale Resolving Power Performance of a High Precision Uniform Field Ion Mobility-Mass Spectrometer. *Analyst* **2015**, *140*, 6824-6833.

23. Stow, S. M.; Causon, T. J.; Zheng, X.; Kurulugama, R. T.; Mairinger, T.; May, J. C.; Rennie, E. E.; Baker, E. S.; Smith, R. D.; McLean, J. A.; Hann, S.; Fjeldsted, J. C., An Interlaboratory Evaluation of Drift Tube Ion Mobility-Mass Spectrometry Collision Cross Section Measurements. *Anal. Chem.* **2017**, *89*, 9048-9055.

24. Spangler, G. E.; Collins, C. I., Peak Shape Analysis and Plate Theory for Plasma Chromatography. *Anal. Chem.* **1975**, *47*, 403-407.

25. Edelson, D.; Morrison, J.; McKnight, L.; Sipler, D., Interpretation of Ion-Mobility Experiments in Reacting Systems. *Phys. Rev.* **1967**, *164*, 71-75.

26. Revercomb, H. E.; Mason, E. A., Theory of Plasma Chromatography/Gaseous Electrophoresis. Review. *Anal. Chem.* **1975**, *47*, 970-983.

27. Kurulugama, R. T.; Nachtigall, F. M.; Lee, S.; Valentine, S. J.; Clemmer, D. E., Overtone Mobility Spectrometry: Part 1. Experimental Observations. *J. Am. Soc. Mass Spectrom.* **2009**, *20*, 729-737.

28. Valentine, S. J.; Stokes, S. T.; Kurulugama, R. T.; Nachtigall, F. M.; Clemmer, D. E., Overtone Mobility Spectrometry: Part 2. Theoretical Considerations of Resolving Power. *J. Am. Soc. Mass Spectrom.* **2008**, *20*, 738-750.

29. Valentine, S. J.; Kurulugama, R. T.; Clemmer, D. E., Overtone Mobility Spectrometry: Part 3. On the Origin of Peaks. *J. Am. Soc. Mass Spectrom.* **2011**, *22*, 804-816.

30. Silveira, J. A.; Ridgeway, M. E.; Park, M. A., High Resolution Trapped Ion Mobility Spectrometry of Peptides. *Anal. Chem.* **2014**, *86*, 5624-5627.

31. Hernandez, D. R.; DeBord, J. D.; Ridgeway, M. E.; Kaplan, D. A.; Park, M. A.; Fernandez-Lima, F. A., Ion Dynamics in a Trapped Ion Mobility Spectrometer. *Analyst* **2014**, *139*, 1913-1921.

32. Lee, S.; Ewing, M. A.; Nachtigall, F. M.; Kurulugama, R. T.; Valentine, S. J.; Clemmer, D. E., Determination of Cross Sections by Overtone Mobility Spectrometry: Evidence for Loss of Unstable Structures at Higher Overtones. *J Phys. Chem. B* **2010**, *114*, 12406-12415.

33. Shvartsburg, A. A.; Tang, K.; Smith, R. D., Understanding and Designing Field Asymmetric Waveform Ion Mobility Spectrometry Separations in Gas Mixtures. *Anal. Chem.* **2004**, *76*, 7366-7374.

34. Santiago, B. G.; Harris, R. A.; Isenberg, S. L.; Ridgeway, M. E.; Pilo, A. L.; Kaplan, D. A.; Glish, G. L., Improved Differential Ion Mobility Separations Using Linked Scans of Carrier Gas Composition and Compensation Field. *J. Am. Soc. Mass Spectrom.* **2015**, *26*, 1746-1753.

35. May, J. C.; Morris, C. B.; McLean, J. A., Ion Mobility Collision Cross Section Compendium. *Anal. Chem.* **2017**, *89*, 1032-1044.

36. Glaskin, R. S.; Valentine, S. J.; Clemmer, D. E., A Scanning Frequency Mode for Ion Cyclotron Mobility Spectrometry. *Anal. Chem.* **2010**, *82*, 8266-8271.

37. Reid Asbury, G.; Hill, H. H., Jr., Evaluation of Ultrahigh Resolution Ion Mobility Spectrometry as an Analytical Separation Device in Chromatographic Terms. *J. Microcolumn Sep.* **2000**, *12*, 172-178.

38. Pierson, N. A.; Chen, L.; Valentine, S. J.; Russell, D. H.; Clemmer, D. E., Number of Solution States of Bradykinin from Ion Mobility Spectrometry Measurements. *J. Am. Chem. Soc.* **2011**, *133*, 13810-13813.

39. Tang, X.; Bruce, J. E.; Hill, H. H., Jr., Design and Performance of an Atmospheric Pressure Ion Mobility Fourier Transform Ion Cyclotron Resonance Mass Spectrometer. *Rapid Commun. Mass Spectrom.* **2007**, *21*, 1115-1122.

40. Gaye, M.; Nagy, G.; Clemmer, D.; Pohl, N., Multidimensional Analysis of 16 Glucose Isomers by Ion Mobility Spectrometry. *Anal. Chem.* **2016**, *88*, 2335-2344.

41. Adamov, A.; Mauriala, T.; Teplov, V.; Laakia, J.; Pedersen, C. S.; Kotiaho, T.; Sysoev, A. A., Characterization of a High Resolution Drift Tube Ion Mobility Spectrometer With a Multi-Ion Source Platform. *Int. J. Mass Spectrom.* **2010**, *298*, 24-29.

42. Shvartsburg, A. A.; Smith, R. D., Fundamentals of Traveling Wave Ion Mobility Spectrometry. *Anal. Chem.* **2008**, *80*, 9689-9699.

43. May, J. C.; McLean, J. A., The Influence of Drift Gas Composition on the Separation Mechanism in Traveling Wave Ion Mobility Spectrometry: Insight from Electrodynamic Simulations. *Int. J. Ion Mobil. Spectrom.* **2013**, *16*, 85-94.

44. Ruotolo, B. T.; Giles, K.; Campuzano, I.; Sandercock, A. M.; Bateman, R. H.; Robinson, C. V., Evidence for Macromolecular Protein Rings in the Absence of Bulk Water. *Science* **2005**, *310*, 1658-1661.

45. Bush, M. F.; Hall, Z.; Giles, K.; Hoyes, J.; Robinson, C. V.; Ruotolo, B. T., Collision Cross Sections of Proteins and Their Complexes: A Calibration Framework and Database for Gas-Phase Structural Biology. *Anal. Chem.* **2010**, *82*, 9557-9565.

46. Hofmann, J.; Hahm, H. S.; Seeberger, P. H.; Pagel, K., Identification of Carbohydrate Anomers Using Ion Mobility-Mass Spectrometry. *Nature* **2015**, *526*, 241-244.

47. Giles, K.; Ujma, J.; Wildgoose, J. L.; Green, M. R.; Richardson, K.; Langridge, D. J.; Tomczyk, N., A High Performance OA-ToF Mass Spectrometer for Accurate Mass Measuremnet of Mobility Separated Ions. In *65th Annual American Society for Mass Spectrometry Conference*: Indianapolis, IN, 2017.

48. Deng, L.; Ibrahim, Y. M.; Baker, E. S.; Aly, N. A.; Hamid, A. M.; Zhang, X.; Zheng, X.; Garimella, S. V.; Webb, I. K.; Prost, S. A., Ion Mobility Separations of Isomers Based Upon Long Path Length Structures for Lossless Ion Manipulations Combined with Mass Spectrometry. *ChemistrySelect* **2016**, *1*, 2396-2399.

49. Webb, I. K.; Garimella, S. V. B.; Tolmachev, A. V.; Chen, T.-C.; Zhang, X.; Norheim, R. V.; Prost, S. A.; LaMarche, B.; Anderson, G. A.; Ibrahim, Y. M.; Smith, R. D., Experimental Evaluation and Optimization of Structures for Lossless Ion Manipulations

for Ion Mobility Spectrometry with Time-of-Flight Mass Spectrometry. *Anal. Chem.* **2014**, *86*, 9169-9176.

50. Tolmachev, A. V.; Webb, I. K.; Ibrahim, Y. M.; Garimella, S. V. B.; Zhang, X.; Anderson, G. A.; Smith, R. D., Characterization of Ion Dynamics in Structures for Lossless Ion Manipulations. *Anal. Chem.* **2014**, *86*, 9162-9168.

51. Zhong, Y.; Hyung, S.-J.; Ruotolo, B. T., Characterizing the Resolution and Accuracy of a Second-Generation Traveling-Wave Ion Mobility Separator for Biomolecular Ions. *Analyst* **2011**, *136*, 3534-3541.

52. Barnett, D. A.; Ells, B.; Guevremont, R.; Purves, R. W., Separation of Leucine and Isoleucine by Electrospray Ionization-High Field Asymmetric Waveform Ion Mobility Spectrometry-Mass Spectrometry. *J. Am. Soc. Mass Spectrom.* **1999**, *10*, 1279-1284.

53. Giles, K.; Wildgoose, J. L.; Pringle, S.; Langridge, D. J.; Nixon, P.; Garside, J.; Carney, P., Characterising a T-Wave Enabled Multi-Pass Cyclic Ion Mobility Separator. In *63rd Annual American Society for Mass Spectrometry Conference*: St. Louis, MO, 2015.

54. Kirk, A. T.; Zimmermann, S., Pushing a Compact 15cm Long Ultra-High Resolution Drift Tube Ion Mobility Spectrometer with R=250 to R=425 Using Peak Deconvolution. *Int. J. Ion Mobil. Spectrom.* **2015**, *18*, 17-22.

55. Kirk, A. T.; Raddatz, C.-R.; Zimmermann, S., Separation of Isotopologues in Ultra-High-Resolution Ion Mobility Spectrometry. *Anal. Chem.* **2017**, *89*, 1509-1515.

56. Zhang, X.; Knochenmuss, R.; Siems, W. F.; Liu, W.; Graf, S.; Hill, H. H., Jr., Evaluation of Hadamard Transform Atmospheric Pressure Ion Mobility Time-of-Flight Mass Spectrometry for Complex Mixture Analysis. *Anal. Chem.* **2013**, *86*, 1661-1670.

57. Groessl, M.; Graf, S.; Knochenmuss, R., High Resolution Ion Mobility-Mass Spectrometry for Separation and Identification of Isomeric Lipids. *Analyst* **2015**, *140*, 6904-6911.

58. Scheltema, R. A.; Hauschild, J.-P.; Lange, O.; Hornburg, D.; Denisov, E.; Damoc, E.; Kuehn, A.; Makarov, A.; Mann, M., The Q Exactive HF, A Benchtop Mass Spectrometer with a Pre-Filter, High-Performance Quadrupole and an Ultra-High-Field Orbitrap Analyzer. *Mol. Cell. Proteomics* **2014**, *13*, 3698-3708.

59. Nagornov, K. O.; Gorshkov, M. V.; Kozhinov, A. N.; Tsybin, Y. O., High-Resolution Fourier Transform Ion Cyclotron Resonance Mass Spectrometry with Increased Throughput for Biomolecular Analysis. *Anal. Chem.* **2014**, *86*, 9020-9028.

60. Shaw, J. B.; Lin, T.-Y.; Leach, F. E.; Tolmachev, A. V.; Tolić, N.; Robinson, E. W.; Koppenaal, D. W.; Paša-Tolić, L., 21 Tesla Fourier Transform Ion Cyclotron Resonance Mass Spectrometer Greatly Expands Mass Spectrometry Toolbox. *J. Am. Soc. Mass Spectrom.* **2016**, *27*, 1929-1936.

61. Hamid, A. M.; Garimella, S. V. B.; Ibrahim, Y. M.; Deng, L.; Zheng, X.; Webb, I. K.; Anderson, G. A.; Prost, S. A.; Norheim, R. V.; Tolmachev, A. V.; Baker, E. S.; Smith, R. D., Achieving High Resolution Ion Mobility Separations Using Traveling Waves in Compact Multiturn Structures for Losslesss Ion Manipulations. *Anal. Chem.* **2016**, *88*, 8949-8956.

62. Hoaglund, C. S.; Valentine, S. J.; Sporleder, C. R.; Reilly, J. P.; Clemmer, D. E., Three-Dimensional Ion Mobility/TOFMS Analysis of Electrosprayed Biomolecules. *Anal. Chem.* **1998**, *70*, 2236-2242.

63. McLean, J. A., The Mass-Mobility Correlation Redux: The Conformational Landscape of Anhydrous Biomolecules. *J. Am. Soc. Mass Spectrom.* **2009**, *20*, 1775-1781.

64. Giddings, J. C., Two-Dimensional Separations: Concept and Promise. *Anal. Chem.* **1984**, *56*, 1258A-1270A.

65. May, J. C.; McLean, J. A., Advanced Multidimensional Separations in Mass Spectrometry: Navigating the Big Data Deluge. *Ann. Rev. Anal. Chem.* **2016**, *9, 387-409*.

66. Brazma, A.; Hingamp, P.; Quackenbush, J.; Sherlock, G.; Spellman, P.; Stoeckert, C.; Aach, J.; Ansorge, W.; Ball, C. A.; Causton, H. C.; Gaasterland, T.; Glenisson, P.; Holstege, F. C. P.; Kim, I. F.; Markowitz, V.; Matese, J. C.; Parkinson, H.; Robinson, A.; Sarkans, U.; Schulze-Kremer, S.; Stewart, J.; Taylor, R.; Vilo, J.; Vingron, M., Minimum Information About a Microarry Experiment (MIAME)-Toward Standards for Microarry Data. *Nat Genet* **2001**, *29*, 365-371.

67. Taylor, C. F.; Paton, N. W.; Lilley, K. S.; Binz, P.-A.; Julian, R. K.; Jones, A. R.; Zhu, W.; Apweiler, R.; Aebersold, R.; Deutsch, E. W.; Dunn, M. J.; Heck, A. J. R.; Leitner, A.; Macht, M.; Mann, M.; Martens, L.; Neubert, T. A.; Patterson, S. D.; Ping, P.; Seymour, S. L.; Souda, P.; Tsugita, A.; Vandekerckhove, J.; Vondriska, T. M.; Whitelegge, J. P.; Wilkins, M. R.; Xenarios, I.; Yates, J. R.; Hermjakob, H., The Minimum Information About a Proteomics Experiment (MIAPE). *Nat Biotech* **2007**, *25*, 887-893.

68. Kolarich, D.; Rapp, E.; Struwe, W. B.; Haslam, S. M.; Zaia, J.; McBride, R.; Agravat, S.; Campbell, M. P.; Kato, M.; Ranzinger, R., The Minimum Information Required for a Glycomics Experiment (MIRAGE) Project: Improving the Standards for Resporting Mass-Spectrometry-Based Glycoanalytic Data. *Mol. Cell. Proteomics* **2013**, *12*, 991-995.

APPENDIX A

REFERENCES OF ADAPTATION FOR CHAPTERS

Chapter I. **James N. Dodds**, Jody C. May, John A. McLean, "Chiral Analysis in Mass Spectrometry: Applications of Chromatography and Ion Mobility," Invited chapter for inclusion in "Chiral Analysis: Advances in Spectroscopy, Chromatography, and Emerging Methods," 2nd Ed. Prasad Polavarapu, Ed., Elsevier (to be published in 2018).

Chapter II. Shawn T. Phillips, **James N. Dodds,** Jody C. May, and John A. McLean, "Isomeric and Conformational Analysis of Small Drug and Drug-Like Molecules by Ion Mobility-Mass Spectrometry (IM-MS)," Invited Chapter for inclusion in "Bioinformatics and Drug Delivery: Methods and Protocols," 3rd Ed. Richard S. Larson and Tudor Oprea, Eds. Springer (to be published in 2018).

Chapter III. **James N. Dodds,** Jody C. May, John A. McLean, ""Broadscale Resolving Power Performance of a High Precision Uniform Field Ion Mobility-Mass Spectrometer," *Analyst,* **2015,** *140,* 6824-6833.

Chapter IV. **James N. Dodds,*** Jody C. May,* and John A. McLean, "Investigation of the Complete Suite of the Leucine and Isoleucine Isomers: Towards Prediction of Ion Mobility Separation Capabilities," *Analytical Chemistry* **2017,** *89,* 952-959. (*Co-first authors)

Chapter V. **James N. Dodds,*** Jody C. May,* and John A. McLean, "Correlating Resolving Power, Resolution and Collision Cross Section: Unifying Cross Platform Assessment of Separation Efficiency in Ion Mobility Spectrometry," *Analytical Chemistry* **2017,** *89,* 12176-12184. (*Co-first authors)

APPENDIX B

SUPPLEMENTARY MATERIALS FOR CHAPTER II

B.1. Supplemental Materials for Acquiring Spectra from IMS Browser

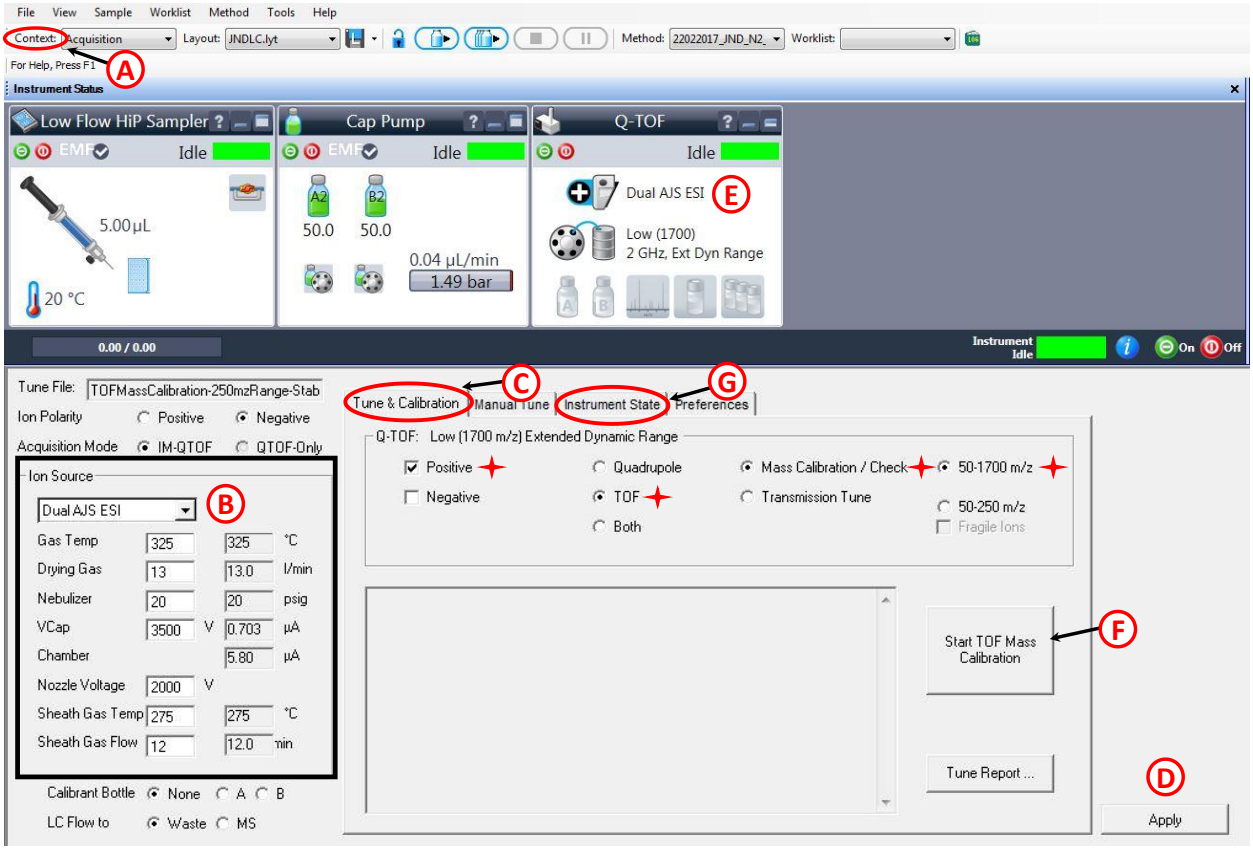

Figure B.1. Agilent Mass Hunter Work Station Data Acquisition Program tune page with callouts for various commands.

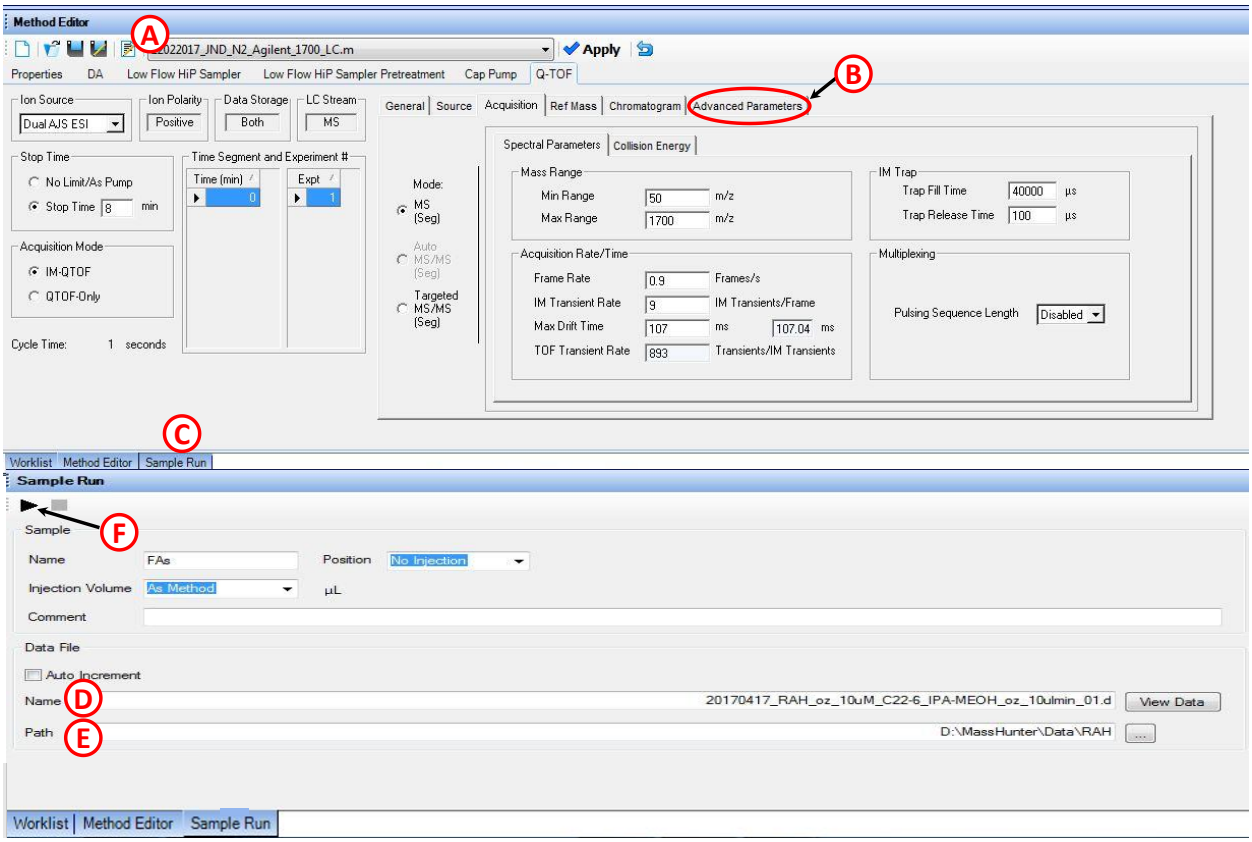

Figure B.2. Sample run dialogue box including file directory information and sample name.

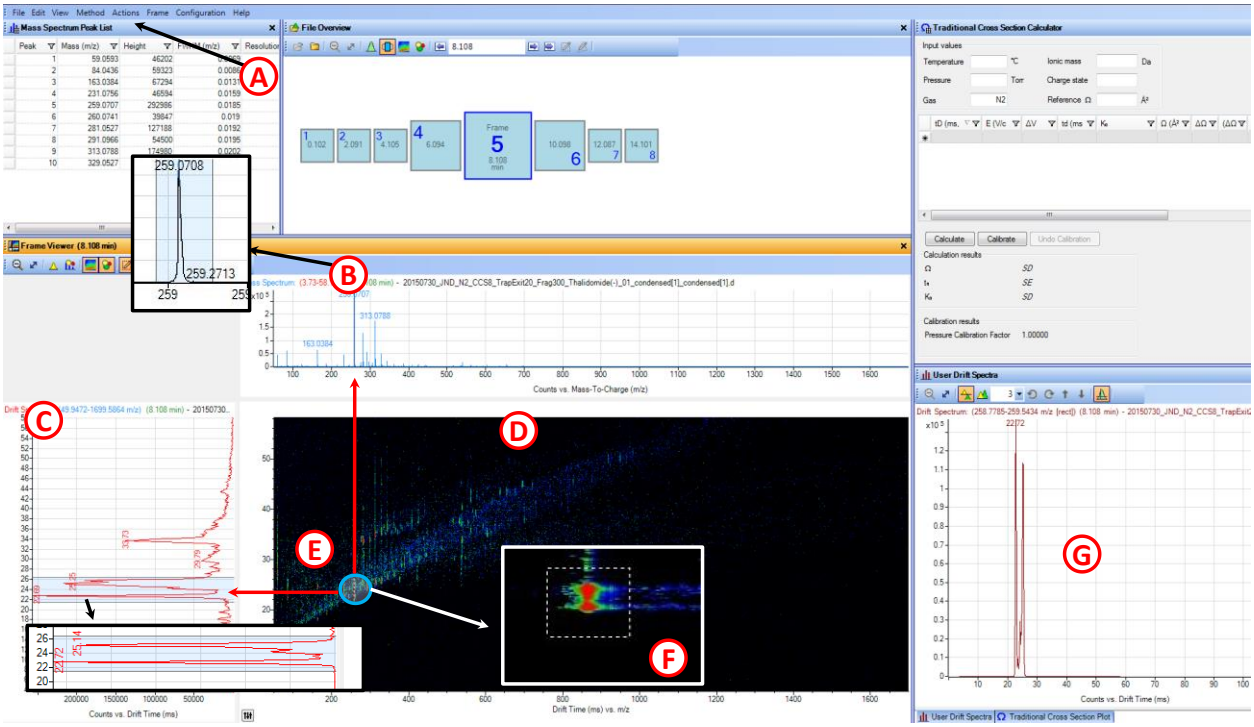

Figure B.3. Agilent Mass Hunter IM-MS Browser interface. **(A)** Mass spectrum of thalidomide, **(B)** drift spectra window with expanded window for thalidomide drift profile, and **(C)** 2-D IM-MS window with call out of the thalidomide $[M+H]^+$ ion species.

C.1. Supplemental Materials for Theoretical and Experimental Resolving Power

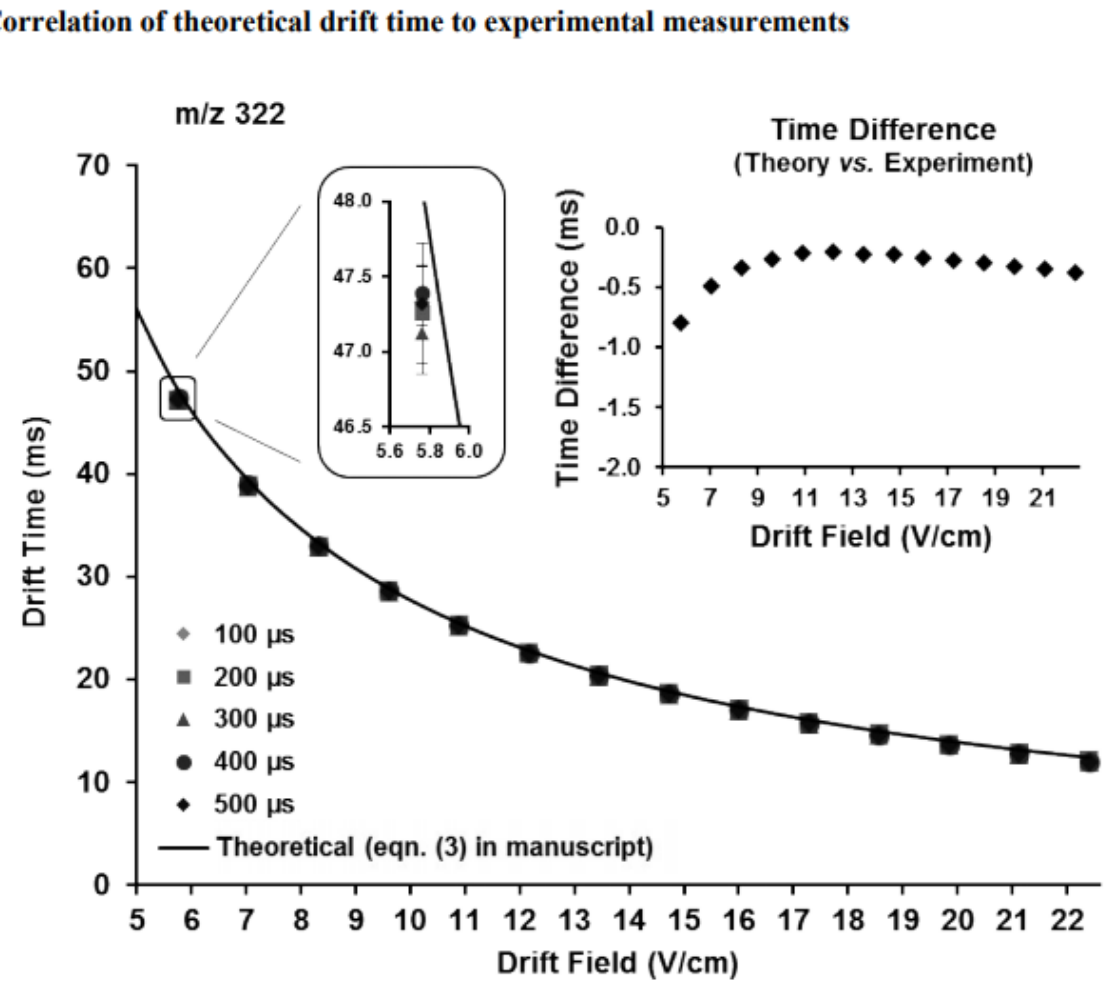

Figure C.1. Correlation of theoretical drift time values obtained from equation 3 (in manuscript) to experimental drift times for the m/z 322 ion. Each point represents 4 replicate measurements. For drift time, theory accurately predicts the experimental results. The expanded region at low drift field where error is highest (left inset) illustrates that the gate width contribution is within experimental error. The right inset demonstrates the difference between experimental and theoretical drift times, while not zero, is systematically reproducible at the higher drift fields (beyond 8 V/cm). The higher error at low drift field is reproducible for the other ions and we infer that this represents error associated with the extrapolation procedure used to correct the drift time for the non-mobility component. Note here that in order to utilize the IMS drift length (78.1 cm) in equation 3, the experimental drift times are corrected by subtracting the non-mobility time component, as obtained by conducting the stepped drift field linear regression analysis used in determining ion transport data [1]. The low drift field values (below 8 V/cm) are not utilized in this linear regression analysis.

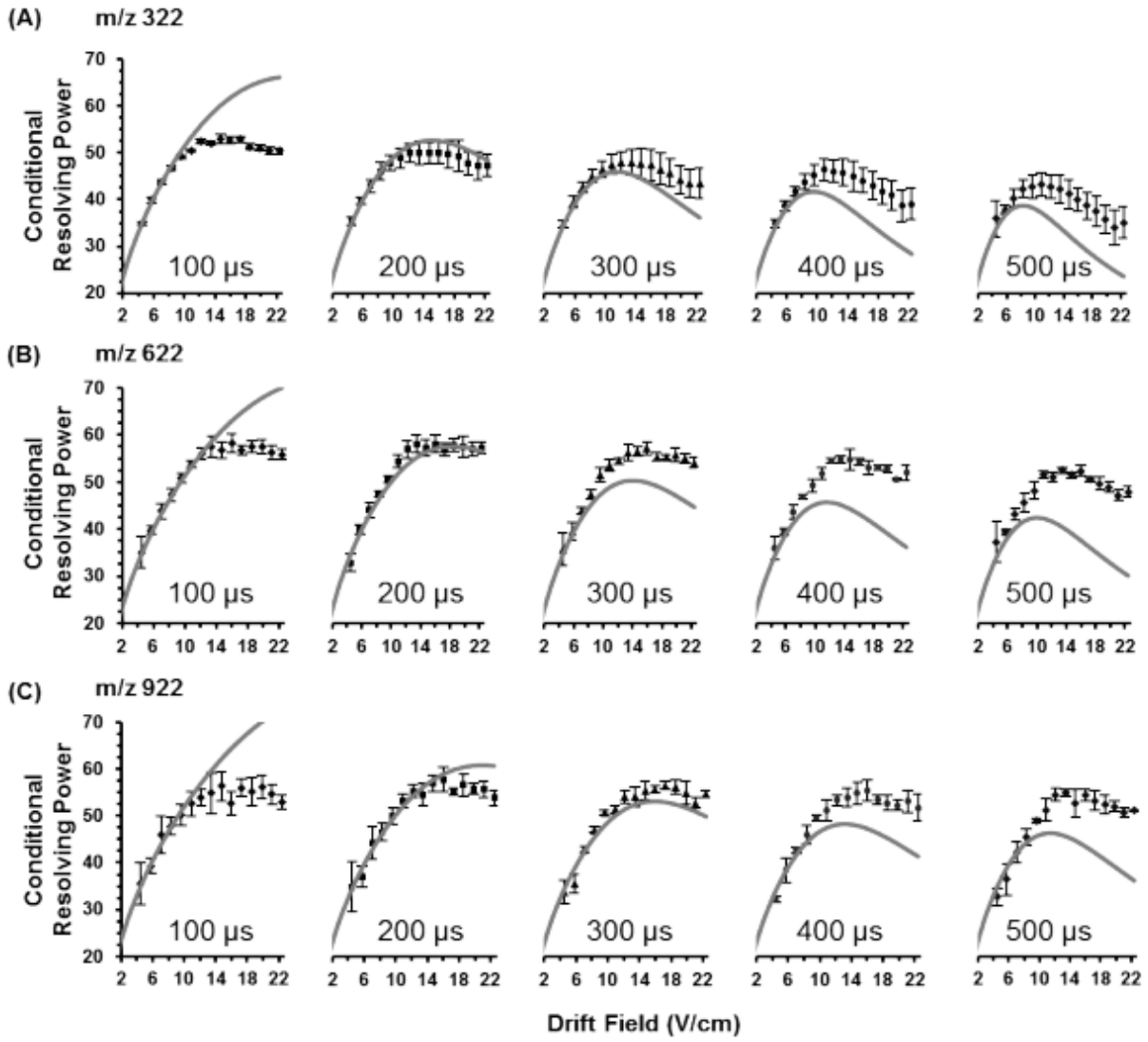

Figure C.2. Comparison of the conditional resolving power theory (equation 5) in manuscript, solid lines) with empirical results for each of the five gate widths investigated, for **(A)** m/z 322, **(B)** m/z 622, and **(C)** m/z 922. While conditional resolving power predicts the qualitative shape of the resolving power curves, a notable deviation is observed between experiment and theory for high and low gate widths, with the most favorable correlation occurring at *ca.* 200 µs (second plot in each panel).

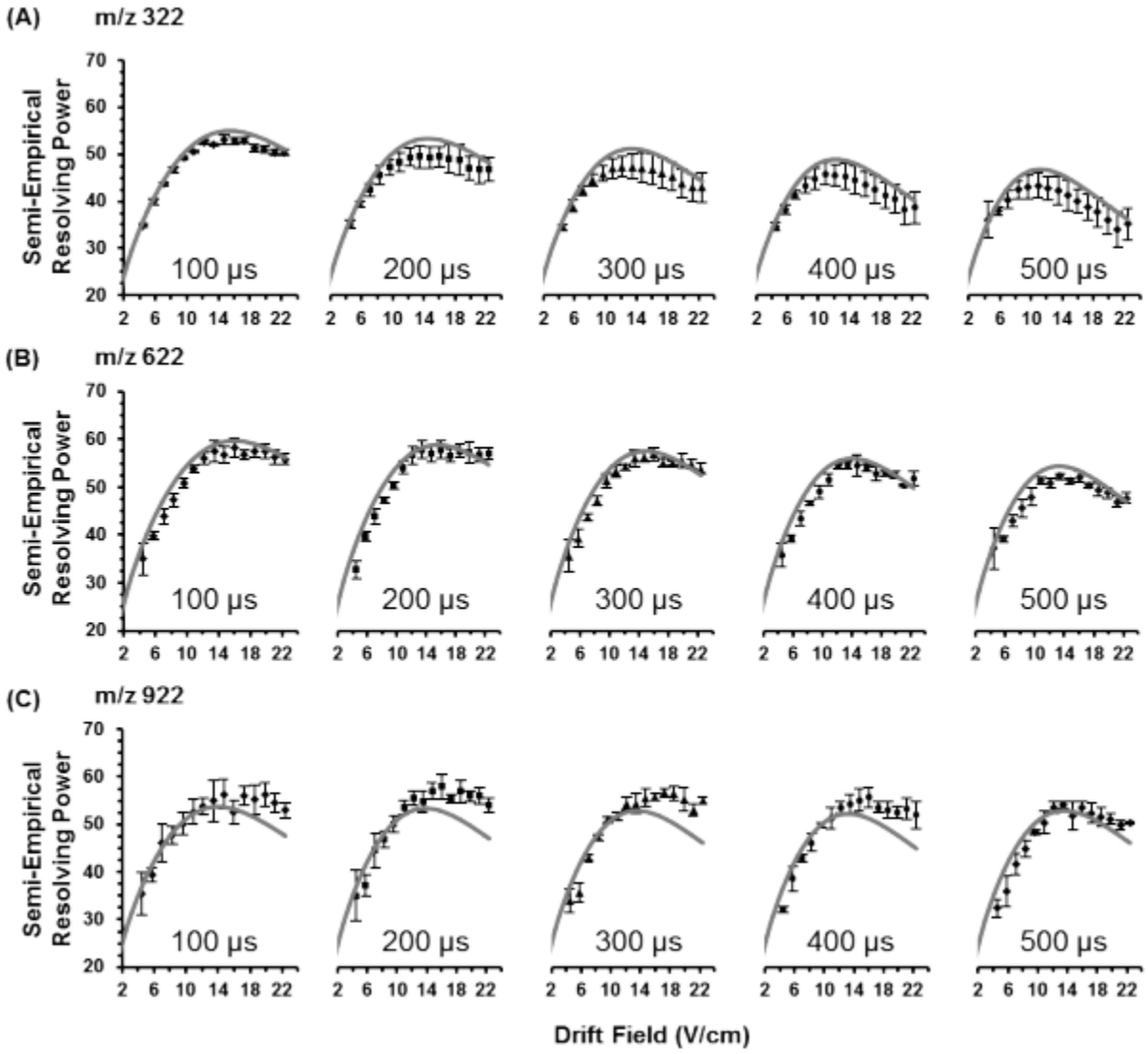

Figure C.3. Comparison of the semi-empirical resolving power theory (equation 7 in manuscript) to experimental results using the coefficients determined for the current instrumentation used in this study. Empirical results are the same as shown in Figure C.2. Good quantitative correlation is observed for these three ions across all gate widths investigated.

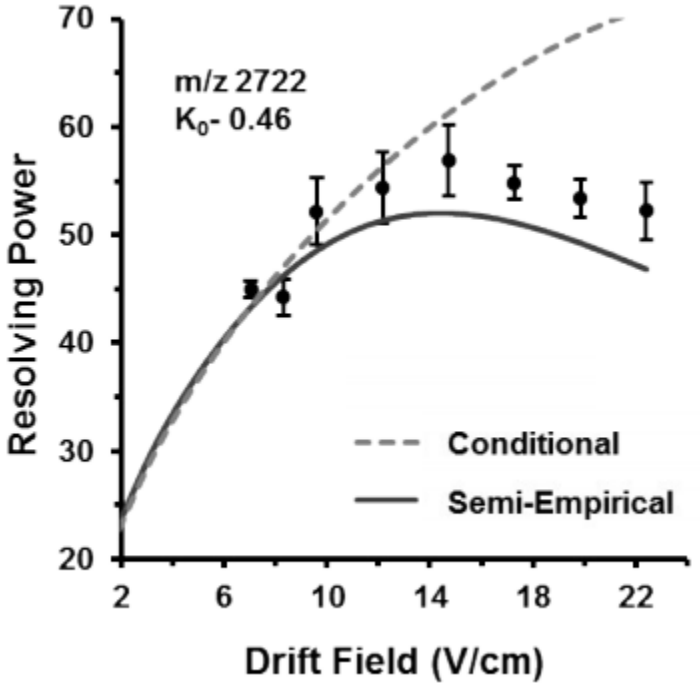

Figure C.4. Comparison of the conditional resolving power formula with the derived semiempirical method for a low mobility ion (ATM m/z 2722) at an applied gate width of 200 μs. Conditional resolving power theory significantly over-predicts the resolving power at this low mobility, which is consistent with the trend observed for the other ATM ions (Figure C.2). Semiempirical resolving power is closer to experimental measurements, with a slight under-prediction of the resolving power, which is similar to the correlation observed for the m/z 922 system (Figure C.3).

Details of the procedure for determining the semi-empirical coefficients

The procedure used in this work to derive the semi-empirical coefficients is based on the same linear regression analysis first outlined by Siems *et al.* [2], but differs slightly in how the coefficients are determined from the least-squares fitting. The expression for peak width derived from first-principles kinetic theory by Revercomb and Mason (equation 4 in manuscript) [3] is as follows:

$$\Delta t = \left({t_g}^2 + \frac{16 ln2 \cdot k_B T}{V \cdot z \cdot e} \cdot {t_d}^2 \right)^{\frac{1}{2}} \tag{S1}$$

The semi-empirical resolving power expression introduces three additional terms to equation S1:

$$\Delta t = \left(\gamma + \beta \cdot {t_g}^2 + \alpha \cdot \frac{T}{V} \cdot {t_d}^2 \right)^{\frac{1}{2}} \tag{S2}$$

Where the "α" and "β" coefficients are multipliers to the diffusion and gate width terms, respectively, and the "γ" coefficient is introduced as an added source of variance within the square root. Comparing the diffusion term on the RHS of eqn. (S1) to eqn. (S2), we obtain the following correspondence to "α":

$$\alpha = \frac{16 ln2 \cdot k_B}{z \cdot e} \tag{S3}$$

Which for singly-charged ions (z = 1) gives the "ideal" value of $\alpha = 0.957 \times 10^3$ V/K. Likewise, "ideal" values for the other coefficients are $\beta = 1$ and $\gamma = 0$ s^2.

Determination of the "α" coefficient

Equation S1 can be rearranged to yield the following expression:

$$\Delta t^2 = \alpha \cdot \left(\frac{T}{V} \cdot {t_d}^2 \right) + \left(\beta \cdot {t_g}^2 + \gamma \right) \tag{S4}$$

The "α" coefficient is then determined by plotting the square of the experimental peak width (Δt^2) as a function of the diffusion term ($\frac{T}{V} \cdot {t_d}^2$). A slope-intercept analysis of the least-squares linear fit to the data is then used to obtain the following for the slope (m):

$$m = \alpha \tag{S5}$$

and the y-intercept (y_0):

$$y_0 = \beta \cdot {t_d}^2 + \gamma \tag{S6}$$

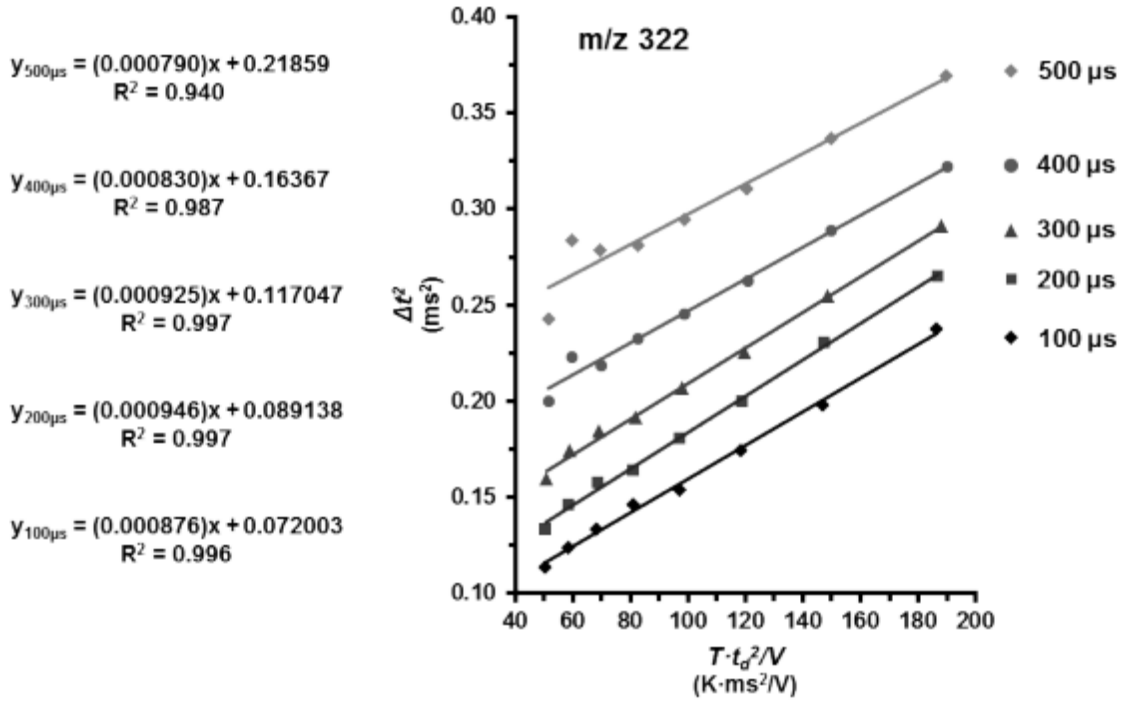

Figure C.5. Linear regression analysis used to determine the "α" coefficient, shown here for the m/z 322 ion. Each line represents a different dataset obtained using one of five different initial ion gate widths (100, 200, 300, 400, and 500 µs); data within each gate width is measured for eight separate drift fields (13.4, 14.7, 16.0, 17.3, 18.6, 19.9, 21.1, and 22.4 V/cm). Note that this analysis was conducted for nine components of the ATM solution (m/z 322, 622, 922, 1222, 1522, 1822, 2122, 2422, and 2722) and the slopes obtained from each linear fit was averaged to obtain the "α" used in the manuscript.

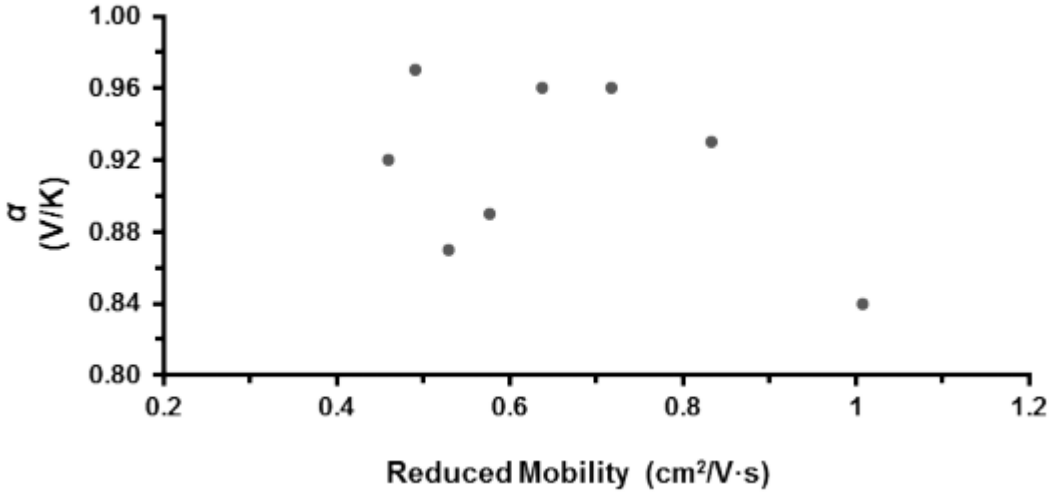

Figure C.6. Variation of all "α" values obtained from eight different ions as a function of the ion's reduced mobility value (K_0). No strong correlation between "α" and K_0 was observed, and so the average "α" (0.000910 ± 0.00005 V/K) was utilized in all subsequent analysis.

Determination of the "β" coefficient

As was done previously, equation (S1) can be rearranged to yield the following expression:

$$\Delta \boldsymbol{t}^2 = \boldsymbol{\beta} \cdot \left(\boldsymbol{t_g}^2\right) + \left(\boldsymbol{\alpha} \cdot \frac{T}{V} \cdot \boldsymbol{t_d}^2 + \boldsymbol{\gamma}\right) \quad \text{(S7)}$$

The "β" coefficient is determined here by plotting the square of the experimental peak width ($\Delta \boldsymbol{t}^2$) as a function of the square of the gate width ($\boldsymbol{t_g}^2$). A slope-intercept analysis of the least-squares linear fit to the data is then used to obtain the following for the slope (m):

$$m = \beta \quad \text{(S8)}$$

and the y-intercept ($\boldsymbol{y_0}$):

$$y_0 =\cdot \alpha \cdot \frac{T}{V} \cdot t_d{}^2 + \gamma \quad \text{(S9)}$$

The slope corresponding to the highest field (22.4 V/cm) is used as the "β" coefficient in subsequent analyses as this represents the situation in which ions spend the least amount of time in the drift tube, and thus would exhibit the strongest "memory" of the initial gating event.

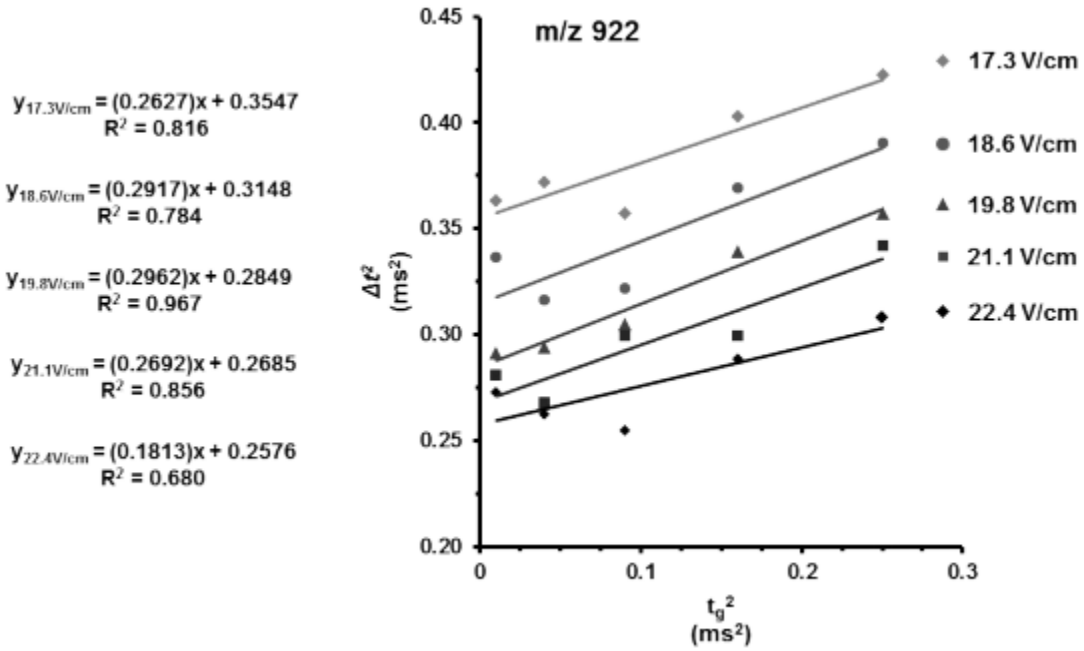

Figure C.7. Linear regression analysis used to determine the "β" coefficient, shown here for the m/z 922 ion. A best fit line was plotted for data from each of five field strengths (17.3, 18.6, 19.8, 21.1, and 22.4 V/cm) with each data set representing measurements obtained from the five gate widths evaluated (100, 200, 300, 400, and 500 μs). While additional data was obtained at lower drift fields, the higher fields represent conditions in which ions transit the drift region faster and thus would retain more memory of the influence of the initial gating event. This also introduces some additional variability in the data, as noted by the inconsistent slope at the highest field investigated (22.4 V/cm).

Determination of the "γ" coefficient

The determination of "γ" described here deviates slightly from the original work by Siems *et al*. In the original work, "γ" was determined by performing a linear regression analysis on all y-intercept values obtained from the "α" and "β" plots to generate new datasets which represent hypothetical data in the limits of zero gate width, and infinite voltage, respectively. The y-intercepts obtained from these hypothetical datasets is "γ" [2]

Here, we utilize the values obtained for "α" and "β" directly into the y-intercept expressions (equation (C.6) and equation (C.9) and solve for "γ" directly for each linear fit. This results in a tabulated set of "γ" values for each ion investigated. To obtain "γ" from the "α" expression *via.* equation (C.6), the "β" obtained at the highest drift field is utilized, which represents the case where ions spend the least amount of time in the drift region. This also simplifies the analysis since only a single "α" value is evaluated for each data series. Obtaining "γ" from the "β" expression *via.* equation (C.9) is more straightforward and involves solving for "β" by utilizing the average "α" obtained for each ion. The average is rationalized here since "α" does not exhibit a strong dependence on the specific ion utilized in the analysis (Figure C.6).

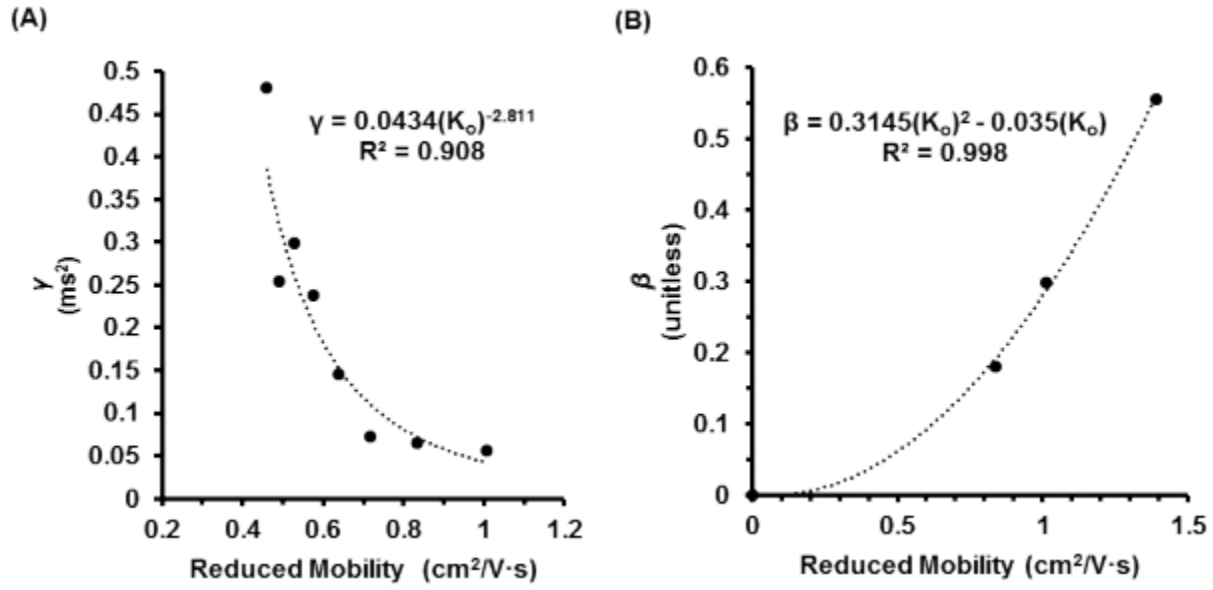

Figure C.8. Regression analysis used to determine the function which relates the semi-empirical coefficients (β and γ) to the ion's reduced mobility, K_0. **(A)** The curve best fitting the data is a power fit based on eight high mass ions in the ATM solution (m/z 622, 922, 1222, 1522, 1822, 2122, 2422, and 2722). **(B)** Fitting parameters for the "β" term as a function of mobility for the m/z 322, 622, and 922 ions. These equations are reintroduced into the semi-empirical resolving power expression (equation 7 in the manuscript) in order to introduce the ion-specific contribution to each of these terms.

Using the coefficients and coefficient expressions summarized in Table 1 in the manuscript, the semi-empirical resolving power equation is expanded to the following functional form:

$$\boldsymbol{R_{SE}} = \frac{\frac{\boldsymbol{L}}{\boldsymbol{K_0 \cdot E_0}} \cdot \left(\frac{\boldsymbol{273.15}}{\boldsymbol{T}} \cdot \frac{\boldsymbol{P}}{\boldsymbol{760}}\right) \cdot \boldsymbol{1000}}{\left[(\boldsymbol{0.0434} \cdot \boldsymbol{K_0}^{\boldsymbol{-2.811}}) + (\boldsymbol{0.3145} \cdot \boldsymbol{K_0}^{\boldsymbol{2}} - \boldsymbol{0.035} \cdot \boldsymbol{K_0}) \cdot \boldsymbol{t_g}^{\boldsymbol{2}} + (\boldsymbol{0.00091}) \cdot \frac{\boldsymbol{T}}{\boldsymbol{V}} \cdot \left(\frac{\boldsymbol{L}}{\boldsymbol{K_0 \cdot E_0}} \cdot \left(\frac{\boldsymbol{273.15}}{\boldsymbol{T}} \cdot \frac{\boldsymbol{P}}{\boldsymbol{760}}\right) \cdot \boldsymbol{1000}\right)^{\boldsymbol{2}}\right]^{\boldsymbol{0.5}}} \quad \text{(S10)}$$

The 10^3 multipliers in the numerator and the RHS of the denominator within the square root term is necessary to convert drift time to milliseconds, which is the unit used in the semi-empirical expressions. Note also that the gate time (t_g) term is in milliseconds (whereas conventionally this is reported in microseconds).

References

1. May, JC; Goodwin, CR; Lareau, NM; Leaptrot, KL; Morris, CB; Kurulugama, RT; Mordehai, A; Klein, C; Barry, W; Darland, E; Overney, G; Imatani, K; Stafford, GC; Fjeldsted, JC; McLean, JA; "Conformational Ordering of Biomolecules in the Gas Phase: Nitrogen Collision Cross Sections Measured on a Prototype High Resolution Drift Tube Ion Mobility-Mass Spectrometer", *Analytical Chemistry* 86, 2107-2116 (2014).

2. Siems, WF; Wu, C; Tarver, EE; Hill Jr., HH; Larsen, PR; McMinn, DG; "Measuring the Resolving Power of Ion Mobility Spectrometers" *Analytical Chemistry* 66, 4195-4201 (1994).

3. Revercomb, HE; Mason, EA; "Theory of Plasma Chromatography/Gaseous Electrophoresis— A Review" *Analytical Chemistry* 47(7), 970-983 (1975).

SUPPLEMENTARY MATERIALS FOR CHAPTER IV

D.1. Supplemental Materials for Investigation of Leucine and Isoleucine Isomers

D.1.1. Comments on measuring CCS and Ion Mobility Distributions Presented in this Work

All IM-MS measurements in this study were obtained in positive ionization mode utilizing incremental steps of increasing drift field in the mobility portion of the Agilent 6560 IM-MS with nitrogen as the drift gas. After the non-mobility flight times (*i.e.* dead times) were subtracted at each voltage and the collision cross section for each analyte was calculated, the equation shown in Figure C.3 was used to convert the time component of the experiment (x axis) to CCS. The optimal drift field occurs at 14.7 V/cm for the analytes examined in this study (see Figure C.2), and hence the distributions at this drift field are presented in Figures C.4 and C.5. All theoretical (modeled) spectra are generated using Equation 4 of the main text.

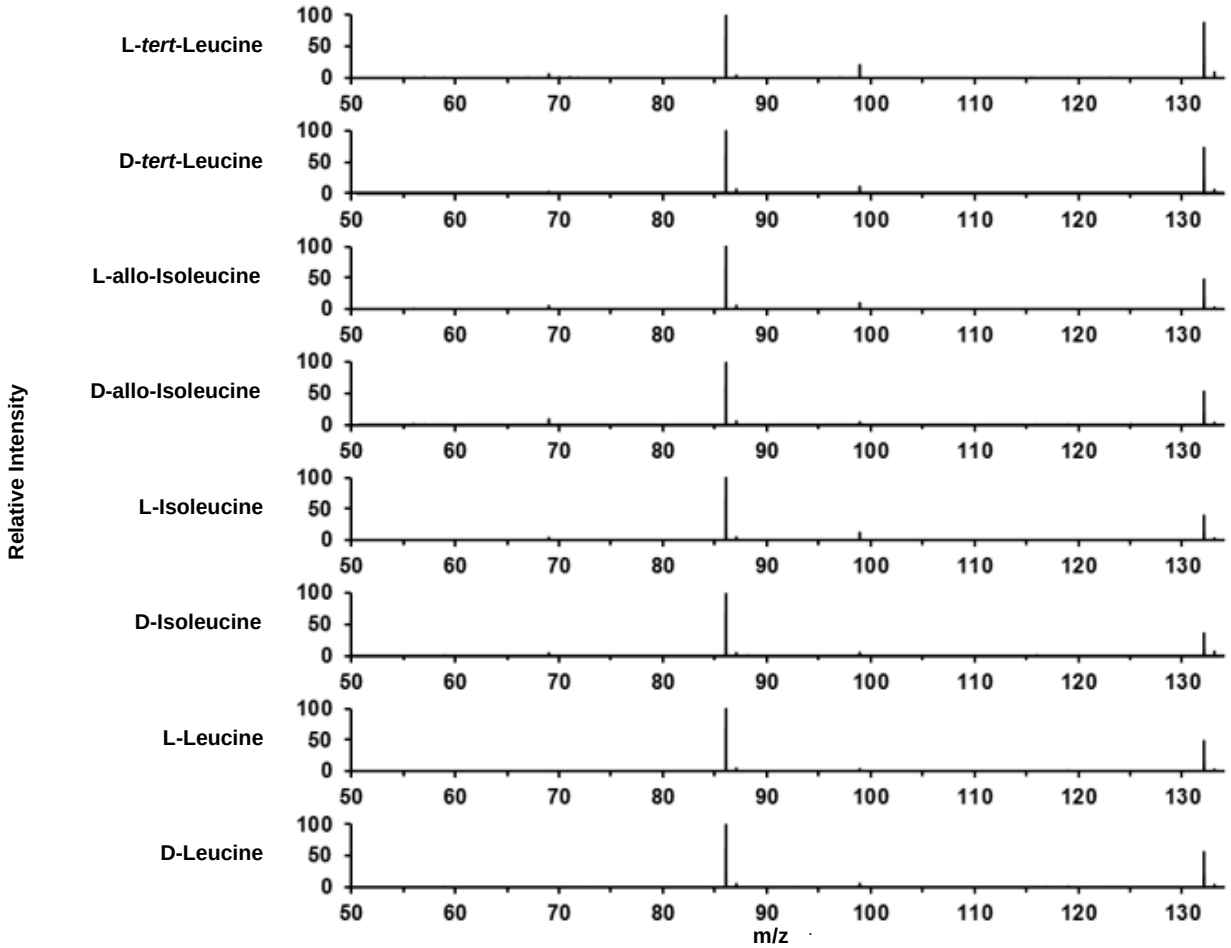

Figure D.1. CID fragmentation spectra for the leucine/isoleucine isomers investigated in this work. Fragmentation data was obtained using the QTOF stage of the IM-MS instrument after extracting the mobility of the precursor ion (m/z 132.1). Fragmentation energy was kept constant at 20 eV (laboratory frame).

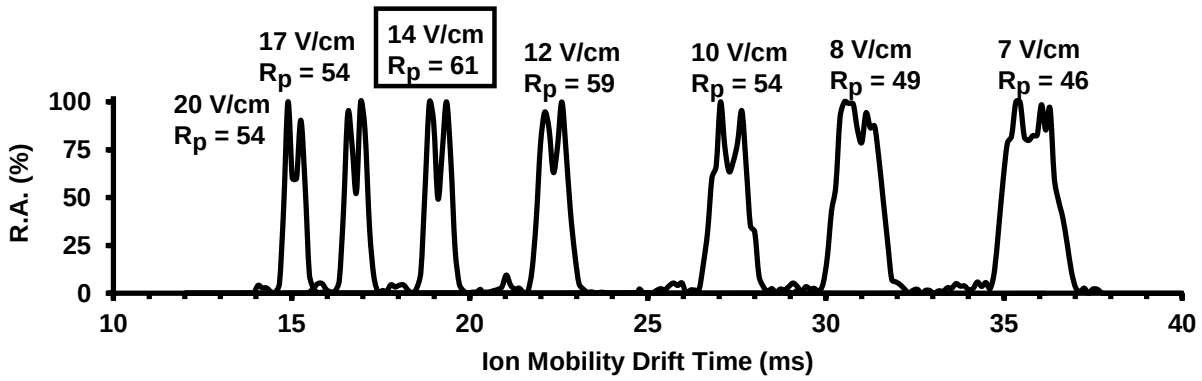

Figure D.2. An overlaid IM spectrum obtained at different drift fields which demonstrates the separation of a mixture of L-norleucine and L-isoleucine for various applied drift fields. The optimal separation occurs at the maximum observed resolving power, here 61 resolving power at 14.7 V/cm, which results in a *ca.* 50% valley for this isomer pair.

Molecule	CCS ($Å^2$)	σ CCS ($Å^2$)	t_d (14.7 V/cm)	FWHM (ms)	K_O (cm^2/V s)	R_P
D-Leucine	135.2	0.3	19.14	0.32	1.634	59.8
L-Leucine	135.1	0.3	19.1	0.34	1.635	56.2
D-Isoleucine	133.3	0.3	18.9	0.33	1.658	57.3
L-Isoleucine	133.5	0.3	18.89	0.32	1.655	59.0
D-allo-Isoleucine	133.1	0.3	18.87	0.30	1.66	62.9
L-allo-Isolecuine	132.9	0.2	18.87	0.32	1.663	59.0
D-tert-Leucine	132.5	0.2	18.76	0.34	1.668	55.2
L-tert-Leucine	132.4	0.3	18.77	0.33	1.669	56.9
L-Norleucine	136.6	0.3	19.35	0.32	1.617	60.5
6-Aminocaproic Acid	129.3	0.2	18.27	0.30	1.709	60.9
N-N-Dimethylglycine	127.5	0.3	18.15	0.32	1.732	56.7

Table D.1. Cross section data for each isomer of $C_6H_{13}NO_2$ investigated in this work. The standard deviation of the CCS for each measurement (RSD *ca.* 0.2%) is included in addition to the corresponding reduced mobility (k_o), drift time, FWHM, and resolving power.

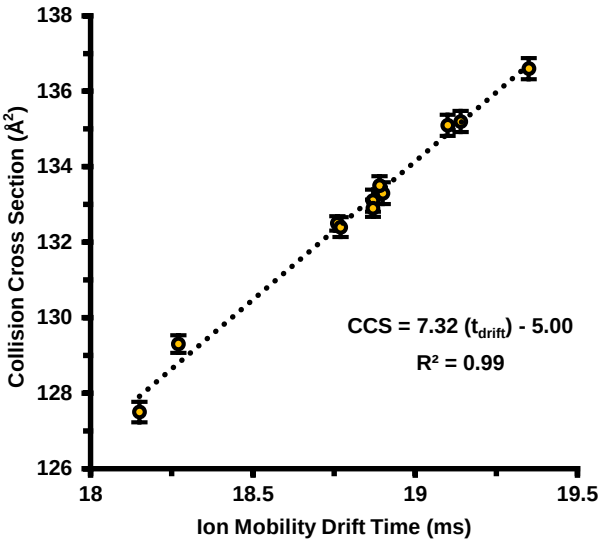

Figure D.3. Linear correlation between drift time and collision cross section obtained from the Mason-Schamp equation (below) for isomers analyzed in this study. Drift times correlate to peak centroids at 14.7 V/cm in a uniform field instrument. Error bars indicate the uncertainty in the CCS measurement.

$$\Omega = \frac{3Ze_c}{16N} * \left(\frac{2\pi}{k_b T}\right)^{\frac{1}{2}} * \left(\frac{m_{ion}+m_{gas}}{m_{ion}*m_{gas}}\right)^{\frac{1}{2}} * \left(\frac{V*t_d}{L^2} * \frac{273.15℃}{T} * \frac{P}{760\ torr}\right)$$

Cross sections were obtained by calculating the corrected drift time and incorporating various laboratory parameters of the experiment including ion mass (m_{ion}), gas mass (m_{gas}), drift voltage (V), drift tube length (L), temperature (T) and pressure (P).

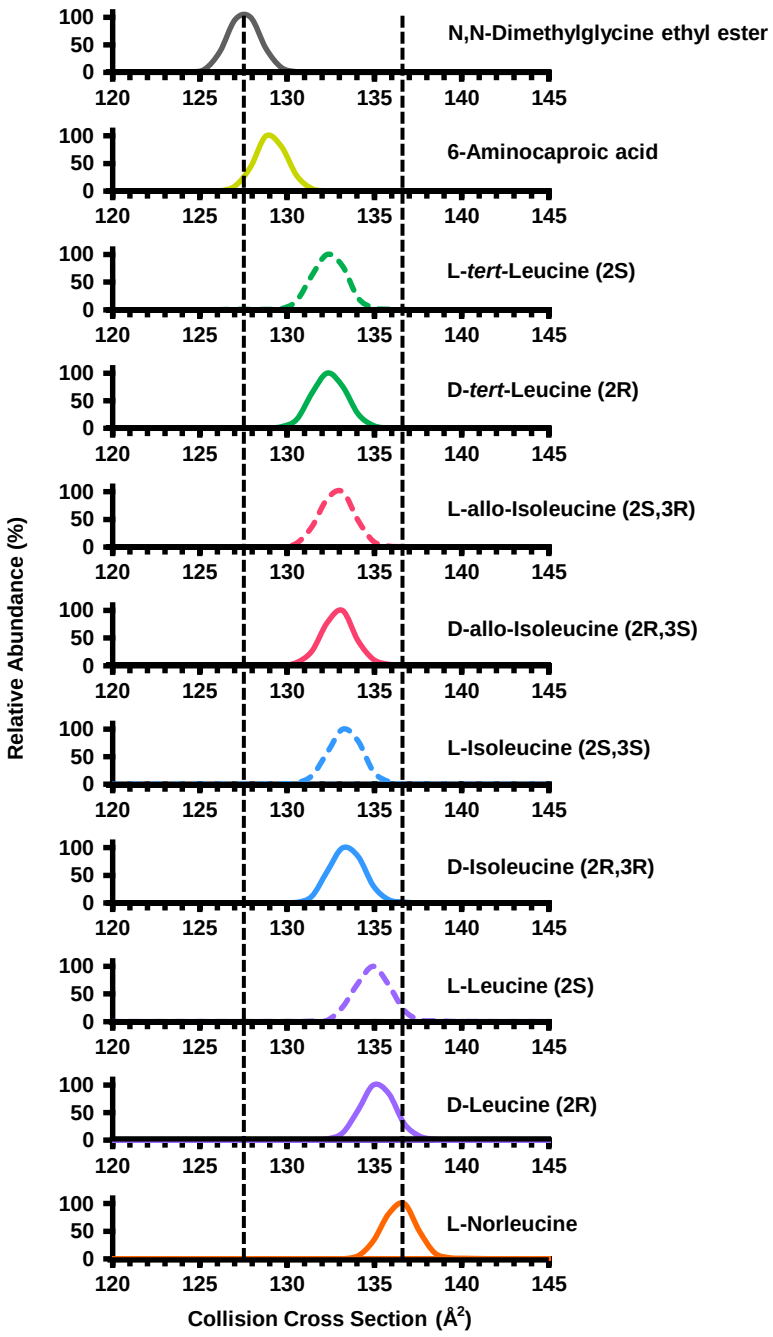

Figure D.4. Individual drift spectra from Figure 4.2 B with dotted lines to indicate the range of CCS data.

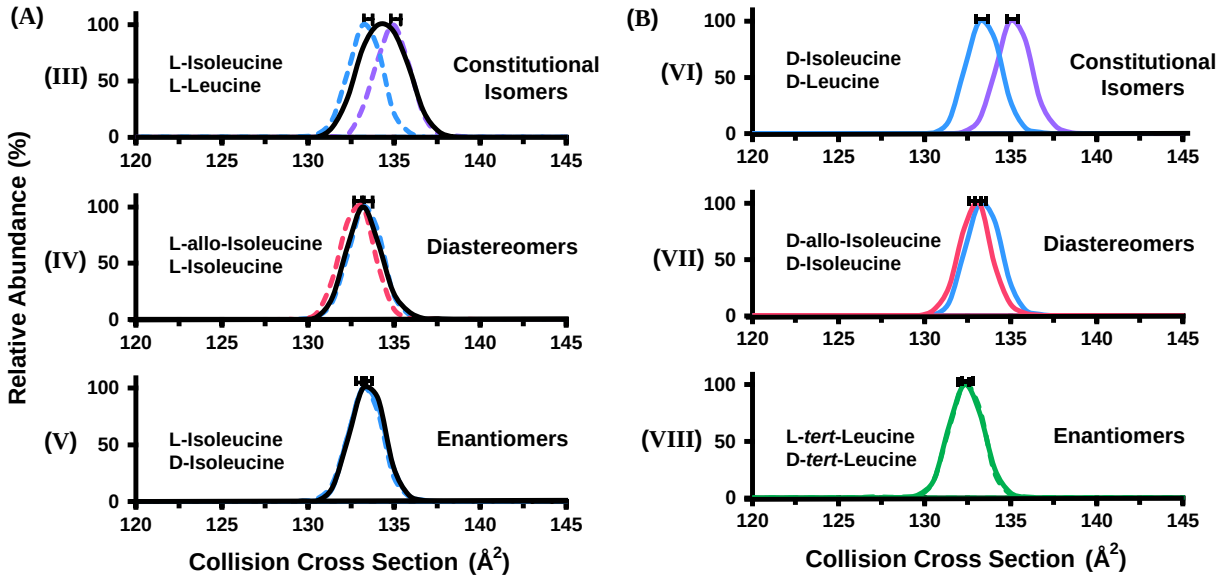

Figure D.5. (A) Individual overlays and mixtures for panels B-IV and B-V from Figure 2. Note the discrepancy between separations of overlays (colored spectra) and analytical mixtures (black traces). **(B)** For comparison, panels VI and VII represent the enantiomer pairs for the other isomers overlaid to the left in **(A)**. Another representative enantiomer comparison is depicted in VIII for reference.

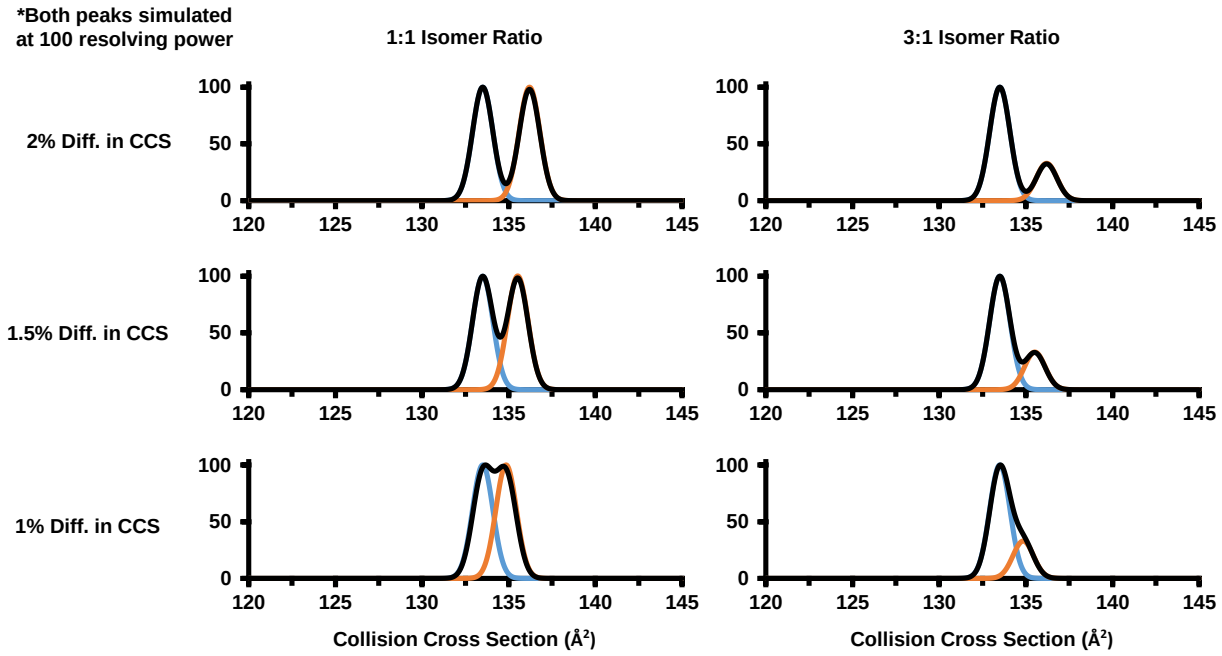

Figure D.6. Comparison highlighting the effect of isomer abundance ratios on separation efficiency. Abundance ratios have significantly more of an impact on separation efficiency for more difficult separations (*i.e.* lower percent difference in CCS). For isomers that are 2-1.5% different in CCS both compounds are distinguishable in a 3:1 ratio at 100 resolving power. As the molecules become more structurally similar (similar cross sections, and hence lower percent difference) the isomer ratio becomes increasingly more important in order to observe both species in a mixture.

SUPPLEMENTARY MATERIALS FOR CHAPTER V

E.1. Supporting Information for Ion Mobility Cross Section, Resolving Power and Resolution Comments on Modeling Ion Mobility Distributions Presented in this Work

In this Supporting Information we describe each step in the process to fit Gaussian distributions to existing publication data (see Figure C.1). We also include additional figures related to IM separations in TWIMS related to the discrepancy between reporting time based resolving power versus CCS based R_p (see Figures C.2 and C.3). Lastly we include descriptive citations for the 22 sources examined in this work and provide links to the non-peer reviewed sources. Finally, we discuss each previously reported IM separation in detail and any pertinent information that provides context for the empirical measurements (*e.g.* cited resolving power, CCS, and chemical identity of molecules/isomers that are separated).

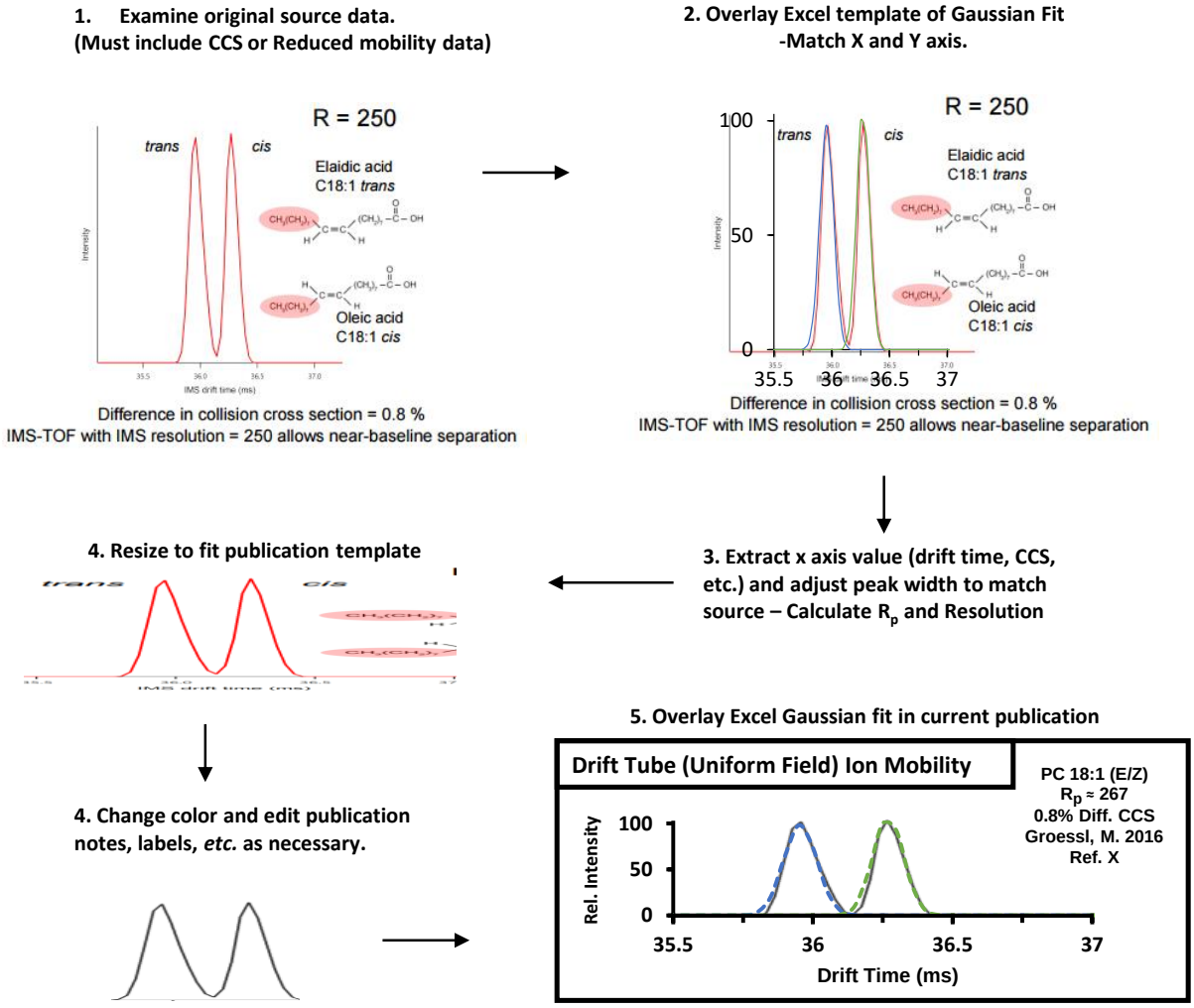

Figure E.1. Workflow for overlaying Gaussian fits to published spectra. This method was applied for all sources referenced in Figures 2, 3, and 4. Two-peak resolution values (R_{pp}) were calculated by using equation 7 in the manuscript along with relevant information noted from the source publication (*i.e.* drift time, CCS, and FWHM). Letter abbreviations added to delinate figures in caption (here **A**). Reproduced/Adapted with permission from Ref. A with permission from Michael Groessl, primary author (ASMS 2016, see Ref. A).

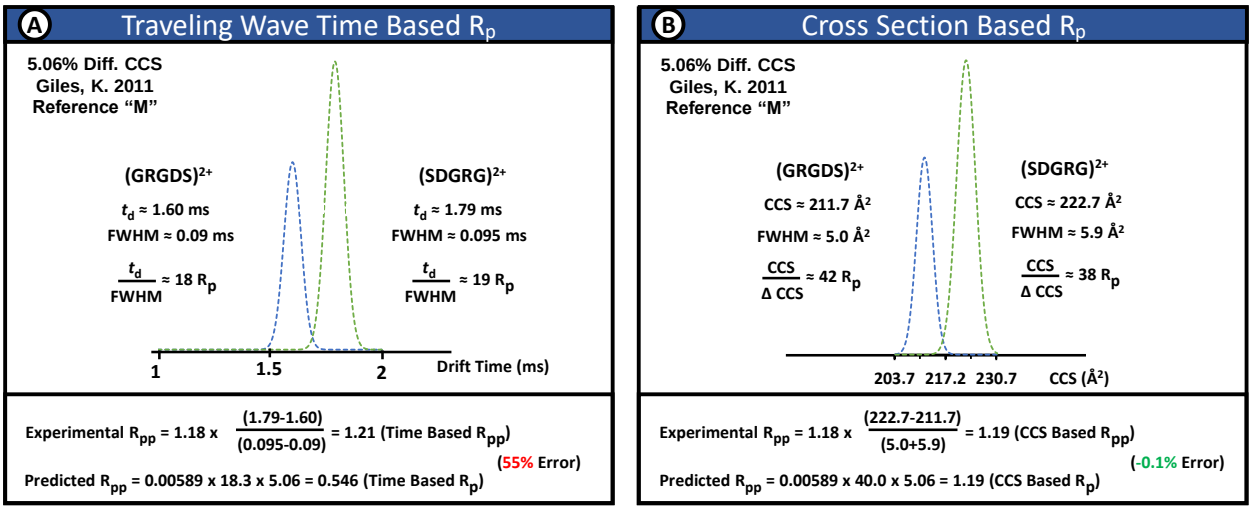

Figure E.2. Comparison of resolving power in both the **(A)** time based dimension (t_d/fwhm) and **(B)** cross section space (CCS/ΔCCS) for traveling wave instruments as noted in Reference M. Giles and coworker's experimental results ($R_{pp} \approx 1.21$) have much closer agreement with R_p calculated in the CCS domain as opposed to R_p determined from the time domain.

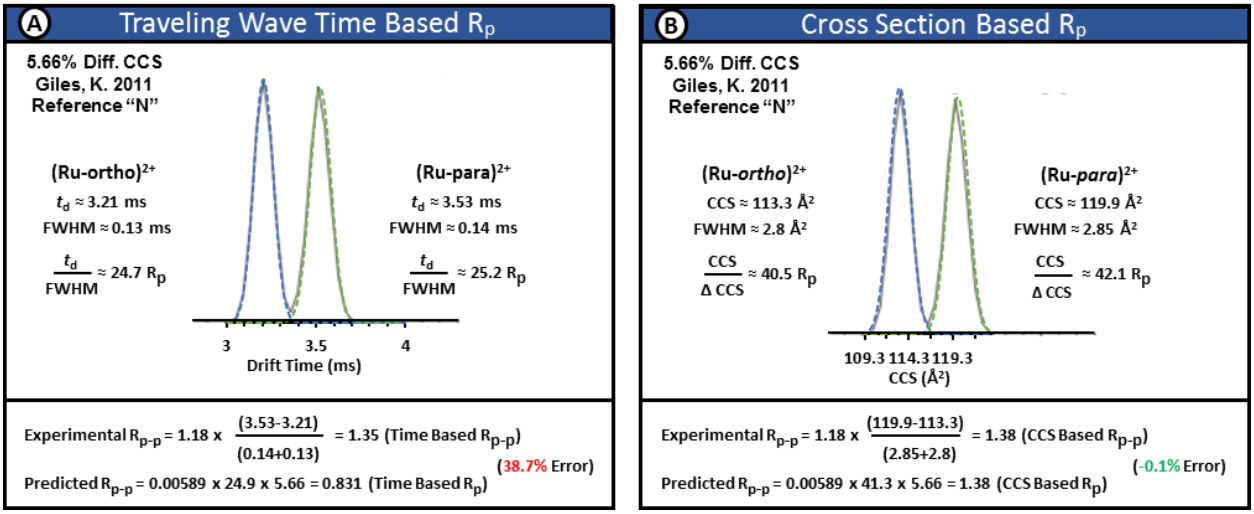

Figure E.3. Separation of Ruthenium complexes (*ortho*/*para* isomers) as described in reference "N". **(A)** Time based resolving power, which does not accurately reflect the separation efficiency of the device. **(B)** Cross section based R_p is a more accurate depiction of TWIMS selectivity. Reproduced/Adapted with permission from Ref. 6. Wiley and Sons, 2011.

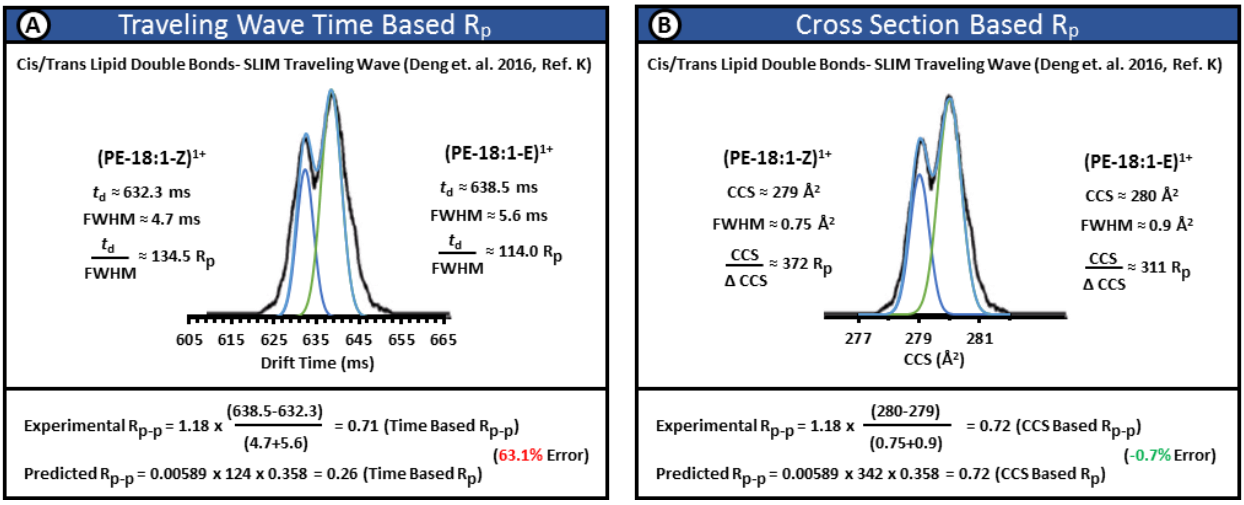

Figure E.4. Separation of *cis/trans* lipid isomers in the SLIM traveling wave currently undergoing development by Smith and coworkers at PNNL. As with the commercial TWIMS devices, time based resolving power is not an accurate descriptor of separation efficiency **(A)**. Conversion to CCS based R_p **(B)** is more reflective of the analytical selectivity of this device. Reproduced/Adapted with permission from Ref. 48 in main text, Wiley and Sons, 2016.

	First Author	Reference Point	Percent Difference in CCS (%)[1]	Experimental Resolving Power (R_p)[2]	Experimental Resolution (R_{pp})[3]	Predicted Resolution (R_{pp})[4]	Percent Error in Resolution (%)[5]	Dispersion Axis Used in the Calculations
TWIMS	Deng, L.	K	0.4	342	0.72	0.72	-0.7	$t_d \rightarrow$ CCS
	Giles, K.	L	1.5	476	4.34	4.34	0.1	$t_d \rightarrow$ CCS
	Giles, K.	M	5.1	40	1.19	1.19	-0.1	$t_d \rightarrow$ CCS
	Giles, K.	N	5.7	41	1.38	1.38	0.1	$t_d \rightarrow$ CCS
	Hofmann, J.	O	5.9	43	1.49	1.49	0.0	$t_d \rightarrow$ CCS

1. Calculated from equation 4.
2. Calculated from equation 1 using the CCS.
3. Calculated from equation 2 using the CCS as the dispersion axis.
4. Calculated from equation 3 using the CCS-based definition for R_p.
5. Calculated from equation 5.

Table E.1. TWIMS separation parameters calculated by defining the separation equations in terms of the CCS.

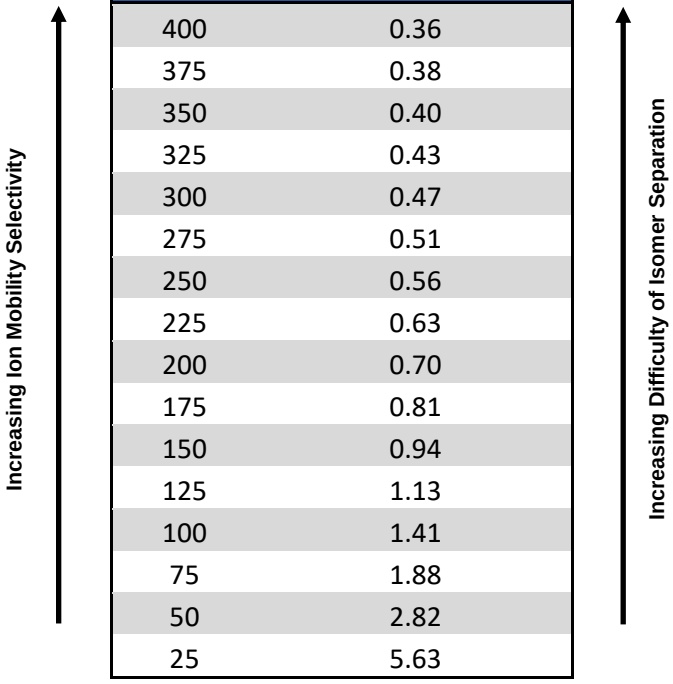

Resolving Power	% Difference in CCS resolvable at Half Height
400	0.36
375	0.38
350	0.40
325	0.43
300	0.47
275	0.51
250	0.56
225	0.63
200	0.70
175	0.81
150	0.94
125	1.13
100	1.41
75	1.88
50	2.82
25	5.63

Table E.2. Tabulated relationship between CCS-based resolving power and the percent difference in collision cross section.

Supplemental References for Chapter 5.

(A) Groessl, M.; Graf, S.; Lisa, M.; Holcapek, M.; Sampaio, J.; Dick, B.; Vogt, B.; Knochenmuss, R. "Analysis of Isomeric Lipids by High Resolution Ion Mobility Mass Spectrometry". *63rd Annual ASMS Conference on Mass Spectrometry and Allied Topics*, St. Louis, MO (2015) - Poster.

Link: http://www.tofwerk.com/wp-content/uploads/2015/06/Tofwerk_WP262_asms2015.pdf (accessed March 1, 2017)

(B) Groessl, M.; Graf, S. "Separation of Isomers in Lipidomics and Metabolomics Experiments by High Resolution Ion Mobility Spectrometry-Mass Spectrometry (IMS-MS)" *64th Annual ASMS Conference on Mass Spectrometry and Allied Topics*, San Antonio, TX (2016) - Poster.

Link: http://www.tofwerk.com/wp-content/uploads/2016/06/TOFWERK_ASMS2016_TP469.pdf (accessed March 1, 2017)

(C) Groessl, M.; Graf, S. "Separation of Isomers in Lipidomics and Metabolomics Experiments by High Resolution Ion Mobility Spectrometry-Mass Spectrometry (IMS-MS)" *64th Annual ASMS Conference on Mass Spectrometry and Allied Topics*, San Antonio, TX (2016) - Poster.

Link: http://www.tofwerk.com/wp-content/uploads/2016/06/TOFWERK_ASMS2016_TP469.pdf (accessed March 1, 2017)

(D) Asbury, G. R.; Hill, H.H.; J. "Evaluation of Ultrahigh Resolution Ion Mobility Spectrometry as an Analytical Separation Device in Chromatographic Terms" *Journal of Microcolumn Separations 12*, 172-178 (2000). Figure 5, middle panel.

(E) Groessl, M.; Klee, S.; Graf, S.; "High Resolution Ion Mobility Spectrometry-Mass Spectrometry (IMS-MS) for Separation of Isomers in Natural Products and Complex Mixtures" *64th Annual ASMS Conference on Mass Spectrometry and Allied Topics*, San Antonio, TX (2016) - Poster.

(F) Pierson, N.A.; Chen L.; Valentine, S. J.; Russell, D. H.; Clemmer, D. E. "Number of Solution States of Bradykinin from Ion Mobility And Mass Spectrometry Measurements" *Journal of the American Chemical Society 133*, 13810-13813 (2011). Figure 2, 90:10 dioxane:water spectrum.

(G) Tang, X.; Bruce, J. E.; Hill, H. H. "Design and Performance of an Atmospheric Pressure Ion Mobility Fourier Transform Ion Cyclotron Resonance Mass Spectrometer" *Rapid Communications in Mass Spectrometry 21*, 1115-1122 (2007). Figure 6, mixture.

(H) Dodds, J. N.; May, J. C.; McLean, J. A. "Investigation of the Complete Suite of Leucine and Isoleucine Isomers: Toward Prediction of Ion Mobility Separation Capabilities" *Analytical Chemistry 89*, 952-959 (2016). Figure 3B.

(I) Gaye, M. M.; Nagy, G.; Clemmer, D. E.; Pohl, N. L. B. "Multidimensional Analysis of 16 Glucose Isomers by Ion Mobility Spectrometry" *Analytical Chemistry 88*, 2335-2344 (2016). Figure 2.

(J) Adamov, A.; Mauriala, T.; Teplov, V.; Laakia, J.; Pedersen, C. S.; Kotiaho, T.; Sysoev, A. A. "Characterization of a High Resolution Drift Tube Ion Mobility Spectrometer with a Multi-Ion Source Platform" *International Journal of Mass Spectrometry 298,* 24-29 (2010). Figure 4B.

(K) Deng, L.; Ibrahim, Y. M.; Baker, E. S.; Aly, N. A.; Hamid A. M.; Zhang, X.; Zheng, X.; Garimella, S. V. B.; Webb, I. K.; Prost, S. A.; Sandoval, J. A.; Norheim, R. V.; Anderson, G. A.; Tolmachev, A. V.; Smith, R. D. "Ion Mobility Separations of Isomers based upon Long Path Length Structures for Lossless Ion Manipulations Combined with Mass Spectrometry" *ChemistrySelect 1,* 2396-2399 (2016). Figure 2C.

(L) Giles, K.; Ujma, J.; Wildgoose, J.; Green, M. R.; Richardson, K.; Langridge, D.; Tomczyk, N. "Design and Performance of a Second-Generation Cyclic Ion Mobility Enabled Q-TOF" *65th Annual ASMS Conference on Mass Spectrometry and Allied Topics*, Indianapolis, IN (2017) – Poster.

Link: http://www.waters.com/webassets/cms/library/docs/2017asms_giles_cyclic.pdf (Accessed August 29, 2017)

(M) Giles, K.; Williams J. P.; Campuzano, J. "Enhancements in Travelling Wave Ion Mobility Resolution" *Rapid Communications in Mass Spectrometry 25*, 1559-1566 (2011). Figure 2, bottom panel.

(N) Giles, K.; Williams J. P.; Campuzano, J. "Enhancements in Travelling Wave Ion Mobility Resolution" *Rapid Communications in Mass Spectrometry 25*, 1559-1566 (2011). Figure 3.

(O) Hofmann, J.; Hahm, H. S.; Seeberger, P. H.; Pagel, K. "Identification of Carbohydrate Anomers using Ion Mobility-Mass Spectrometry" *Nature 526,* 241-244 (2015). Figure 2C, third panel (isomers 6 and 3).

(P) Silveira, J. A.; Ridgeway, M. E.; Park, M. A. "High Resolution Trapped Ion Mobility Spectrometry of Peptides" *Analytical Chemistry 86,* 5624-5627 (2014). Figure 2B.

(Q) Commercial vendor (Bruker) brochure for the timsTOF™ instrument, "1844502 – timsTOF™. Flexibility to Empower Your Ideas" (2016). Figure 4C.

Link: https://www.bruker.com/fileadmin/user_upload/8-PDF-Docs/Separations_MassSpectrometry/Literature/Brochures/1844502_timsTOF_brochure_05-2016_ebook.pdf (Accessed March 1, 2017)

(R) Commercial vendor (Bruker) brochure for the timsTOF™ instrument, "1844502 – timsTOF™. Flexibility to Empower Your Ideas" (2016). Figure 2.

Link: https://www.bruker.com/fileadmin/user_upload/8-PDF-Docs/Separations_MassSpectrometry/Literature/Brochures/1844502_timsTOF_brochure_05-2016_ebook.pdf (Accessed March 1, 2017)

(S) Barnett, D. A.; Ells, B.; Guevremont, R.; Purves, R. W. "Separation of Leucine and Isoleucine by Electrospray Ionization-High Field Asymmetric Waveform Ion Mobility Spectrometry-Mass

Spectrometry" *Journal of the American Society for Mass Spectrometry 10*, 1279-1284 (1999). Figure 4, lower trace.

(T) Lee, S.; Ewing, M. A.; Nachtingall, F. M.; Kurulgama, R. T.; Valentine, S. J.; Clemmer, D. E. "Determination of Cross Sections by Overtone Mobility Spectrometry: Evidence for Loss of Unstable Structures at Higher Overtones" *Journal of Physical Chemistry B 114*, 12406-12415 (2010). Figure 2, panel 2 (21^{st} harmonic frequency number).

(U) Glaskin, R. S.; Valentine, S. J.; Clemmer, D. E. "A Scanning Frequency Mode for Ion Cyclotron Mobility Spectrometry" *Analytical Chemistry 82*, 8266-8271 (2010). Figure 4, third inset.

(V) Glaskin, R. S.; Valentine, S. J.; Clemmer, D. E. "A Scanning Frequency Mode for Ion Cyclotron Mobility Spectrometry" *Analytical Chemistry 82*, 8266-8271 (2010). Figure 4, first inset.

APPENDIX E

CURRICULUM VITAE

James N. Dodds, Ph.D.

Vanderbilt University Department of Chemistry
7330 Stevenson Center, Station B 35-1822
Nashville, TN 37235
Lab: (615)-343-4563
james.n.dodds@vanderbilt.edu

EDUCATION

Vanderbilt University Nashville, TN
Ph.D. in Chemistry Expected May 2018

Dissertation: Investigation Of Separation Strategies for Bioanalytical Methods: Chromatography, Ion Mobility, and Mass Spectrometry
Advisor: Dr. John A. McLean

University of North Georgia Dahlonega, GA
Advisor: Dr. Dan Thompson May 2013

RESEARCH EXPERIENCE

Graduate Research Assistant Aug 2013-May 2018

Vanderbilt University, Nashville, TN

Advisor: Dr. John A. McLean

Development of separation strategies for the characterization of complex biological matrices using chromatography, ion mobility, and mass spectrometry.

Independent Undergraduate Research Aug 2012-Dec 2012

University of North Georgia, Dahlonega, GA

Advisor: Dr. Dan Thompson

Designed an interface between a thermogravimetric analyzer and a single quadrupole mass spectrometer to analyzer pyrolysis byproducts of analytical standards.

PUBLICATIONS

1. **Dodds, J. N.**; May, J. C.; McLean, J. A. "Correlating Resolving Power, Resolution, and Collision Cross Section: Unifying Cross-Platform Assessment of Separation Efficiency in Ion Mobility Spectrometry." *Anal. Chem.* **2017**, *89*, 12176-12184.

2. **Dodds, J. N.**; May, J. C.; McLean, J. A. "Investigation of the Complete Suite of Leucine and Isoleucine Isomers: Toward Prediction of Ion Mobility Separation Capabilities." *Anal. Chem.* **2017**, *89*, 952-959.

3. May, J. C.; **Dodds, J. N.**; Kurulugama, R. T.; Stafford, G. C.; Fjeldsted, J. C.; McLean, J. A. "Broadscale Resolving Power Performance of a High Precision Uniform Field Ion Mobility-Mass Spectrometer. *Analyst* **2015**, *140*, 6824-6833.

4. **Dodds, J. N.**; May, J. C.; McLean, J. A. "Chiral Strategies in Mass Spectrometry: Integration of Chromatography, Electrophoresis, and Gas-Phase Mobility." Book Chapter in *Chiral Analysis: Advances in Spectroscopy, Chromatography, and Emerging Methods.* **2017**.

5. Phillips, S. T.; **Dodds, J. N.**; May, J. C.; McLean, J. A. "Isomeric and Conformational Analysis of Small Drug and Drug-Like Molecules by Ion Mobility-Mass Spectrometry (IM-MS)." Book Chapter in *Methods in Molecular Biology Series.* 3rd Ed. **2017**

PRESENTATIONS

1. **Dodds, J. N.**; May, J. C.; McLean, J. A. "A Theoretical and Empirical Approach to Separating Isomer Classes in Uniform Field Ion Mobility." 65th ASMS, San Antonio, TX (Spring 2016) **ORAL**.

2. **Dodds, J. N.**; May, J. C.; McLean, J. A. "Ion Mobility and the Omics: The Challenge of Separating Isomeric Systems." SciX 2017, Reno, NV (Fall 2017) **ORAL.**

3. **Dodds, J. N.**; May, J. C.; McLean, J. A. "Correlating Resolving Power, Resolution, and Collision Cross Section: Broadscale Depiction of Separation Efficiency in Ion Mobility Spectrometry." 66th ASMS, Indianapolis, IN (Spring 2017) **POSTER**.

4. **Dodds, J. N.**; May, J. C.; McLean, J. A. "Correlating Resolving Power, Resolution, and Collision Cross Section: Broadscale Depiction of Separation Efficiency in Ion Mobility Spectrometry." 66th ASMS, Indianapolis, IN (Spring 2017) **POSTER**.

5. **Dodds, J. N.**; May, J. C.; McLean, J. A. "Improving the Separation of Isomers in Ion Mobility-Mass Spectrometry." Quantitative Chemical Biology Conference, Nashville, TN (Fall 2016) **POSTER**.

6. **Dodds, J. N.**; Leaptrot, K. L.; May, J. C.; McLean, J. A. "Resolution and Resolving Power Studies Investigating the Separation Capabilities of Drift Tube and Traveling Wave Ion Mobility-Mass Spectrometers." 64th ASMS, St. Louis, MO (Spring 2015) **POSTER**.

7. **Dodds, J. N.**; May, J. C.; McLean, J. A. "Investigating the Ion Mobility Resolving Power of a Commercially Available Uniform Ion Mobility-Mass Spectrometer." Southeastern Region Meeting of the American Chemical Society, Nashville, TN (Fall 2014) **POSTER**.

TEACHING EXPERIENCE

1. Head Teaching Assistant for General Chemistry Laboratory Courses (Spring 2016).
2. Teaching Assistant for General Chemistry Laboratory Course (104 A/B) – Assisted instructor in laboratory practicals and weekly study sessions (Fall 2013 – Fall 2015).
3. Teaching Assistant for General Chemistry for Non-Science Majors Laboratory Course (101) – Assisted instructor in laboratory practicals and preparation of chemical reagents (Spring 2016).

Perspectives and Outlooks

With the state of the ion mobility community expanding so rapidly, the future directions of the research provided in this document allow for multiple paths of expansion related to this work. Using the higher resolution instruments described in Chapter 5 illustrates the bright future of separation in store for ion mobility. For example, a new professor coming into the field would have several distinct directions for research topics in the near future. Provided sufficient funding, a new professor could theoretically use the relationships described in this work to study previously-inseparable species in complex mixtures. As a concrete example, the diastereomers of L-*allo*-isoleucine and L-isoleucine described in Chapter 4 have yet to be separated by ion mobility analysis alone. In this work we illustrated that these two diastereomers possess collision cross section values which are about 0.4% different in size. While this difference is not large enough to separate using the instrumentation currently available in our laboratory (*ca.* 60 R_p), the new instruments (*e.g.* TofWerk HP-Drift Tube and Bruker's timsTOF) have sufficient resolving power (*ca.* 300+ R_p) to separate these compounds. The physical analysis of this specific experiment would unambiguously demonstrate the predictive ability of the equations described in this work to model ion mobility separations prior to an empirical experiment. It is also very plausible that the level of selectivity provided with access to the newest instrumentation in ion mobility spectrometry would provide further separation across a host of biological classes (*e.g.* cis/trans lipids and α/β linkages in carbohydrate chemistry). While often only a sole stereoisomer is responsible for biological activity (*e.g.* L- specific amino acids), the additional selectivity of ion mobility could highlight uncommon instances when the least-preferred chiral variant is included in a sample, potentially highlighting specific bioanalytical activity that might not have been otherwise characterized. Furthermore, without limited funding it would be possible to purchase each high

resolution ion mobility platform variant (TofWerk HP-Drift Tube, timsTOF, and Water's Cyclic TWIMS G2S after commercialization) and this process would provide a unifying experimental separation group for an established set of ion mobility separations. The principle shortcoming of Chapter 5 in this work is that most research into ion mobility separations is spread across a wide host of compounds, and very rarely are two or more identical mixtures ever examined across platforms. Provided unlimited funding, if each of the above instruments were centralized in one research facility translational experiments across platforms would highlight the intricacies of separation specific to each device (*i.e.* TWIMS, DTIMS, TIMS, etc.).

While these ideas are very achievable in terms of purchasing analytical standards and subsequent analysis by each instrument type, the monetary investment of each platform is around $1,000,000 USD. Also, while the studies described would be very exciting, they would probably only be highlighted in a single publication, which is not an ideal return on investment. Towards this directive in a realistic setting, a new P.I. in the field who would like to examine this hypothesis would be better served by forming collaborations with the research groups who currently house each type of high resolution instrument. Also, it is often imperative to have a long working history with each specific platform in order to gain the highest separation capability possible for each device (see Chapter 3). With these practical concerns, it seems having a central scientist travel to each research group along with the samples of interest could follow the experiment within each group under the supervision of the local instrument expert, ensuring that each IM-MS separation is operated at peak capacity.

The other major area of interest in ion mobility spectrometry described in this work is related to developing CCS libraries as an addition identifier of chemical composition. Towards this end, without financial restrictions it would be a herculean undertaking to purchase every analytical

standard related to primary metabolism and collect CCS information for future compilation in future repositories. This work would be monumental in paving the way for untargeted analysis by IM-MS for analytes across a wide range of biological classes, including carbohydrates, lipids, peptides and amino acids. While this effort would require large sums of time, money, and effort, the results produced by such an endeavor would be translational across the ion mobility field. However, the data analysis of such an effort would be incredibly time consuming, all financial concerns aside. For example, a recent work in our laboratory examined the factors related to CCS measurement for 700 primary metabolites purchased as analytical standards. While the actual data acquisition only required a week of instrument time, the data analysis has currently taken several months. As such, running every analytical standard with biological relevance is probably unrealistic, even if the standards do exist.

While the current investigation of primary metabolites by IM-MS is rapidly concluding, if a new researcher was entering the ion mobility field another area in dire need of research would be the rapid screening of designer drugs by portable ion mobility spectrometers. Commercial instruments are often utilized in airport security screens, and increased levels of resolving power for new devices are directly reflected from advancements in larger IM-MS platforms. Roadside screening of drugs by ion mobility analysis would require analytical standards for comparison to ensure instrument reproducibility, and small concentrations (*ca.* 1 mg/mL) of these narcotics are available from commercial vendors without requiring DEA approval. Studies related to rapid drug testing would expand the current realm of ion mobility research from academic institutions into more broadscale forensic analysis. The devices that are currently available also represent a modest financial acquisition (*ca.* $20,000-40,000) and are well within the confines of procurement for a new faculty member at a small state university.